AN INVESTIGATION INTO FLOW OVER RIGID ELEMENTS SIMULATING BED FORMATIONS IN ERODIBLE CHANNELS

A Thesis submitted to the University of Southampton

for the degree of

Doctor of Philosophy in the Faculty of Engineering

(Civil Engineering Department)

by

Mahmoud Faisal Rifai

August 1969

ABSTRACT

An investigation was made of flow characteristics over a rigid bed that simulates bed formations in alluvial rivers. The detailed study of separated flow geometry over one element showed that the position of re-attachment point depends strongly on the geometry of the body that produces separation.

In alluvial rivers it was found that the form drag friction factor as partly dependent on the particle Froude number for a variety of flow conditions and in one case the Von Karman constant, deduced from the average slope of the velocity distribution over the depth, was found to vary with flow conditions and with a value different from 0.4.

The study of turbulence characteristics showed that the vertical distribution of turbulence intensity is slightly affected by the presence of bed formations. The spectral analysis of velocity fluctuations showed that frequency spectrum has a consistent shape in the longitudinal direction of flow. The contribution of the low frequency to the turbulent energy was found to be dominant. In water flows with depths of about $\frac{1}{2}$ - 1 ft and velocities less than 2ft/sec frequencies above 25 Hz do not contribute much to the total energy.

In the re-attached part of the flow over the triangular elements the ratio of the R.M.S. pressure fluctuations to the local shear was similar to that for a turbulent boundary layer reported by Aki (1967).

A comparison between the flow in water and in air showed that air can be used as a medium for scale model investigation.

ACKNOWLEDGEMENTS

The research work presented in this thesis was carried out in the Civil Engineering Department of the University of Southampton.

I wish to record my indebtedness to Mr. K.V.H. Smith, M.Sc., M.I.C.E., M.I.Struct.E., M.I.P.H.E. for his active supervision and invaluable suggestions throughout the course of this study.

Thanks are also due to the following members of the staff of the Institute of Sound and Vibration, the University of Southampton for general assistance in instrumentation and computation: Drs. P.O.A.L. Davies, C. Mercer, and Messrs. R.E. Pacifico, I. Wold and J. Mason.

All gratitude is due to my wife Maha for her care and forbearance, which helped me a great deal throughout the course of this work.

CONTENTS

LIST OF TABLES

LIST OF PLATES

LIST OF FIGURES

LIST OF SYMBOLS

A	Constant
$\vec{A}$	Expression for a vector
A_1	Cross sectional area of inlet pipe
A_1''	Constant
A'	Constant
A''	Constant
a'	Radius of diaphragm
B	Constant
B_1	Constant
B'	Constant
B''	Constant
B_e	Band width
$\bar{C}$	Chezy constant
C	Constant
C'	Constant
C''	Thermal capacity
D	Constant
d_1	Reference depth
d	Depth of flow
D_{50}	Representative size of bed material
D'	Fluxural rigidity
d_o	Outside diameter of Preston tube
$\bar{e}_1$	Roughness concentration
e	Fluctuating voltage
e'	Voltage error
E	Total voltage
E_o	Voltage for zero velocity
E'	Elasticity modulus
Eb	Bridge voltage
$\bar{f}$	D'Arcy friction factor
f_b	Bed Friction factor
f_b''	Form drag friction factor
F_D	Form drag
F_S	Surface drag
f	Frequency
f_m	Cut-off frequency
$F_{11}(f)$, $F(f)$	Normalized frequency spectrum

f'	Resonant frequency
FL	Flatness
$f(x)$	Probability of the event (x)
G	Length of increments
g	Gravitational acceleration
G'	Gain
h	Element height
H, H_o	Heat transfer coefficients
$\bar{H}$	Representative height
j,i	Dummy variables
I	Representative value for integration
I'	Current
k	Dummy variable
K	Von Karman constant
K'	Strain-gauge constant
l	Length of element
l'	Length of wake
L_x	Macroscal of turbulence
L	Representative length
ℓ_1	Mixing length
L_1	Length of inlet pipe
m	Dummy variable
M	Maximum number of lags
n	Variable in the normal direction
$\bar{n}$	Manning friction factor
OR	Overheat ratio
P_t	Dynamic Pressure
P_o	Static Pressure
P	Pressure
P_1	Fluctuating pressure
p'	Pressure on diaphragm
$\bar{p}$	Unit normal pressure on element
Q	Discharge
r	Hydraulic radius
r_b	Bed hydraulic radius
R_{oij}	Correlation function

$R(\tau)$	Normalized auto-correlation function
$R(s)$	Spatial correlation function
R	Operating resistance of hot film
R_a	Resistance of hot-film at ambient temperature
R_1	Resistance in Wheatston bridge
R_r	Reference resistance
R_B, R_{CO}, R_D, R_L, R_p	Resistances in the temperature compensating system
R'	Resistance of strain gauge
$\overline{S}$	Slope
s	Separation distance
$\vec{S}$	Vector which represents surface
SK	Skewness
t	Time
t'	Thickness of diaphragm
T	Integration time
T_1	Hot-film operating temperature
T_a	Ambient temperature for hot film
U	Temporal mean velocity
$\overline{U}$	Average velocity
u	Fluctuating velocity in the x direction
u_1	End value of fluctuating velocity
U^*	Shear velocity
U_x	Velocity at x
$\vec{V}$	Velocity vector
v	Fluctuating velocity in the y direction
$\forall$	Volume
X	Body force
x	Co-ordinate in the longitudianl direction
$\overline{X}$	Variable
X'	Variable
y	Co-ordinate in the vertical direction
Y_1	Representative length of roughness
Y_1	Reference co-ordinate in the vertical direction
z	Co-ordinate in the transverse direction

α	Coefficient that relates shear to pressure
$\bar{\alpha}$	Angle of upstream face of element
β	Coefficient that relates velocity to pressure
β'	Coefficient that relates stress to size of diaphragm
β''	Coefficient in temperature compensating system
γ	Specific weight of fluid
γ'	Specific weight of material used
Δ	Representative length for roughness
δ	Voltage from which time constant can be deduced
ρ	Density of fluid
τ_o	Mean shear on the bed
τ'	Time constant
τ_s	Unit surface shear
τ_F	Unit from drag reduced to surface shear
τ	Time lag in correlation calculation
τ_2	Tension on diaphragm
λ	Microscale of turbulence
σ	Standard deviation
$\bar{\sigma}^2$	Mean square value
σ'	Stress on diaphragm
η	Mean deviation
μ	Dynamic viscosity of fluid
ν	Kinematic viscosity of fluid
ν'	Poisson's ratio
ε	Voltage difference
ε'	Strain in diaphragm

CHAPTER ONE

GENERAL

"If you have to do with water,
perform your experiments first,
and ponder things afterwards"
(Leonardo da Vinci)

1.1 INTRODUCTION

In order to determine the variations of the resistance to flow, which is empirically known, with changing flow characteristics and surface roughness, consideration of the internal flow structure is necessary. The degree of turbulence was always associated with systematic studies on the mean velocity profiles for a large range of surface roughness. This approach gave the well known semi-logarithmic expression for velocity profiles and resistance to flow as functions of the Reynolds number and the relative roughness. In their theoretical approach, pr and tl and Von Karman based their universal resistance expression on the hypothesis that turbulent velocity fluctuation parallel and transverse to the mean flow are functions of the distance from the wall and of velocity gradients.

The general relations for mean velocity distribution and resistance to flow as functions of the Reynolds number and relative roughness have been consistently confirmed by numerous investigators. It remained, however, to check on the validity of introducing a factor to allow for the turbulence in the stream, which was obviously empirical. In this connection, the study of the actual distribution of the components of turbulent velocity fluctuations and of their cross-products,

of the spectral distrubution of turbulent energy, and of the turbulent pressure fluctuations is necessary.

1.2 THE PROBLEM

1.2.1 The resistance to flow in open channels has for some time been the subject of an extensive study. In alluvial channels, however, the problem is considerably complicated by the looseness of beds and the interaction between bed forms and the flow structure. A simple study of the various well known resistance coefficients does not seem to offer an acceptable answer. A number of investigators have derived different formulae from the same basic data to describe bed forms and resistance to flow. It is very difficult and almost impossible to find a common formula which describes the bed forms and the resistance to flow for any bed material and flow conditions.

A detailed investigation of the flow structure near the boundary of bed formations is relevant to the variation in the resistance to flow and the interaction of the flow with the bed formation. Artificial triangular elements similar in shape to the most common bed forms (mild slope with long face upstream and steep slope with short face downstream) were used to simulate a bed of an alluvial channel.

1.2.2 First the problem was looked at in a general way. The flow over the triangular elements was studied in a wind tunnel. With the hot wire anemometer, information about the conditions in the flow field was obtained. In this connection, turbulence structure and statistical characteristics of the fluctuating component of longitudinal velocity were obtained for different positions of the triangular elements.

1.2.3 Instrumentation

The problem was transferred into water as a medium for detailed investigation. Available devices to measure turbulence were not as well developed in water as they were in air. For this reason the development of suitable transducers was necessary. Commercial hot-films were matched with an anemometer for aerodynamic measurements which had been made at the Institute of Sound and Vibration, University of Southampton. Development work was also needed for a detecting device for pressure fluctuations. A pressure transducer of resistive type was developed and made in collaboration with the same Institute and satisfactory performance was obtained.

1.2.4 Detailed investigation in flume

The triangular elements were placed in the bottom of an open channel. The variation of form resistance with change in flow conditions was investigated. Depth of flow and discharge were considered as independent variables to describe the flow. With change in depth, the elements were looked at in a fundamentally different manner. Therefore, the change in depth was not merely a parameter in an equation but an important factor which is reflected in the velocity distribution and the flow structure as a whole.

The component of the friction resistance was estimated from direct measurements of shear stress on the surface, making use of a Preston tube, but no attempt was made to correlate the total resistance of the artificial elements with that of bed forms in alluvial channels.

The characteristics of the fluctuating motion were clarified by a thorough study of the flow pattern over the element for various flow conditions. Some statistical functions such as the time correlation, frequency spectra and probability density functions were evaluated.

The distribution of turbulence level was compared with other investigators' results.

1.3 AIM OF THE PRESENT INVESTIGATION

Measurements of turbulence have been made previously by many investigators, but the present investigation represents an attempt to extend this work with a view to obtaining a better understanding of the detailed structure of the velocity field and of the way in which the turbulent motion in various regions close to the boundary contributes to it.

In the present experiments the first aim was to make an attempt to assess the relative order of magnitude of quantities which appear in the momentum equation. The second objective was to investigate in more detail the behaviour of various frequency components that make up the velocity field in relation to change in flow conditions and location along the triangular elements. Thirdly, detailed investigation of the form resistance of the triangular elements under different conditions of depth and average velocity was made.

Finally, a qualitative interpretation was made of the mechanism of resistance to flow in connection with turbulent flow structure.

CHAPTER TWO

THEORETICAL ANALYSIS AND REVIEW OF PREVIOUS WORK

2.1 TURBULENT MOTION

Turbulence in air flow has been for some time successfully studied by numerous investigators. The study of turbulence in Aerodynamics has greatly increased the basic knowledge and understanding of Hydrodynamics. Not until the past few decades has turbulence attracted the attention of hydraulicians. Although there are many problems that would be better understood if the mechanism of turbulence in water were known in more details; nevertheless it has not been possible to study the characteristics of turbulent flow in water with the same precision and ease as in air, due to difficulty in the development of suitable transducers.

Turbulence is a very complicated physical phenomenon. Basically, it may be said that turbulence is present at any point in a fluid if the velocity vector at this point shows a random variation, in direction and magnitude, with time. As the fluctuations are very rapid, only in a statistical sense can turbulence be described.

What causes turbulence to occur ?

In the case of laminar flow, the forces which cause the flow are completely balanced by the work of viscous resistance alone, that is the molecular exchange between adjacent layers of the stream lying parallel to the boundary. When the flow power exceeds a certain critical limit the total slip area in a volume element must be increased in order to develop more work from the viscous resistance. As a consequence the flow assumes a more complicated character, in which a mass exchange resistance is produced which is sufficient to bring the total level of the resistance work up to that of the forces causing the flow.

Turbulence could also be caused by obstructions in the path of fluid, by passing a fluid through a mesh or by some other means such as mechanical stirring.

2.2 THE EQUATIONS OF MOTION

2.2.1 The turbulent motion can be decomposed into a mean motion with velocity components U_i parallel to the x_i axis, and superimposed fluctuation components u_i. The velocity components of the total motion will be

$$V_i = U_i + u_i \tag{1}$$

The equations that describe the conservation of mass and momentum in a viscous incompressible fluid are :

The continuity equation

$$\frac{\partial V_i}{\partial x_i} = 0 \tag{2}$$

and the Navier-Stokes equations

$$V_j \frac{\partial V_i}{\partial x_j} = X_i - \frac{1}{\rho} \frac{\partial P}{\partial x_i} + \nu \frac{\partial^2 V_i}{\partial x_j \partial x_j} \tag{3}$$

where ρ is the density and ν the kinematic viscosity of the fluid. Substituting for V_i and averaging, the Navier-Stokes equation can be expressed as

$$\rho U_j \frac{\partial U_i}{\partial x_j} = \rho X_i - \frac{\partial P}{\partial x_i} + \frac{\partial}{\partial x_j} \left[\mu \frac{\partial U_i}{\partial x_j} - \rho \overline{u_i u_j} \right] \tag{4}$$

where $$\bar{u}_i = 0 \tag{5}$$

The difference between Eq. (3) and Eq. (4) is that there are additional stresses $\rho \overline{u_i u_j}$ which represent the mean rate of transfer of momentum across a surface due to the velocity fluctuations. These stresses were first introduced by Reynolds and are known by his name.

2.2.2. There are two basically different kinds of turbulence; homogeneous isotropic and non-isotropic turbulence. Homogeneity means that the statistical properties of a fluid are independent of the particular position in the field and isotropy means that they are independent of direction. In homogeneous isotropic turbulence the mean square value of the three fluctuation components are equal to each other and are the same throughout the field $\bar{u}_i^2 = \bar{u}.^2$ Also, quantities of the type $\overline{u_i\, u_j}$ are zero. In non isotropic turbulence or shear flow, the three components of velocity fluctuation are different from each other and $\overline{u_i\, u_j}$ are different from zero.

There are two distinct kinds of non-isotropic turbulence. Wall turbulence, as it is called, is usually generated by the friction forces at fixed walls, and free turbulence which is generated by the flow of layers of fluid with different velocities past or over each other.

2.2.3. In two dimensional turbulent shear flow, where no external forces are present and the rate of pressure drop in the direction of flow is constant we have

$$U_i = f(x_2)$$
$$U_2 = U_3 = 0 \quad \text{and} \quad \frac{\partial P}{\partial x_1} = \text{constant}$$

If we designate x, y, z for x_1, x_2, x_3 and U, V, W for U_1, U_2, U_3 respectively, we can write Eq. (4) in the x direction

$$\frac{\rho \partial uv}{\partial y} - \frac{\mu \partial^2 U}{\partial y^2} = \text{constant} \qquad (6)$$

Thus

$$\mu \frac{dU}{dy} - \rho\overline{uv} = \tau_o - cy \qquad (7)$$

Here τ_o is the shear stress at the wall where y = o and u = v = o. This equation states that the sum of the mean viscous stresses $\mu \frac{dU}{dy}$ and Reynolds shear stresses $-\rho\overline{uv}$ is balanced by the wall shear τ_o and the

pressure gradient ($\frac{\partial P}{\partial x}$ = constant), and that this sum varies linearily with y. Equation 7 is represented graphically in Fig. 1.

The absence of any average shear stress and velocity gradient in isotropic turbulence makes it a very rare case in Hydraulics. It is only approached in the centre of large conduits or behind screens or grids in wind tunnels or after a hydraulic jump, and it is never present near a boundary.

Many basic principles put forward in the study of isotropic turbulence, which have been confirmed experimentally, gradually find their way into the study of shear flow.

2.2.4. Pressure fluctuations

The Navier-Stokes equation contains terms which are very difficult to measure. Although terms involving pressure appear in the equation, the pressure is not an independent quantity, being determined by the velocity field. The pressure at a point is influenced by the velocity field so the relation between pressure and velocity is not a simple one and there are therefore many cases in which it would be very valuable if pressure fluctuations were measured directly. Taking the divergence of the Navier-Stokes equations yields

$$\frac{\partial^2 P}{\partial x_j \, x_i} = \rho \frac{\partial V_i}{\partial x_j} \frac{\partial V_j}{\partial x_i} \qquad (8)$$

which is Poisson's equation (which could be written in terms of the fluctuating components as well)that relates pressure to velocity. It might be expected that in the same way as experimental work on velocity fluctuations has provided the progress in understanding the turbulent motion, the measurement of an additional and not simply related quantity such as pressure might lead to a further improvement in understanding.

The theory that has been developed by aerodynamicists concerning the characteristics of pressure fluctuations in turbulent boundary layers has been successfully applied to turbulent boundary layers as encountered in Hydraulics.

What interests the hydraulic engineer from the aerodynamic theory of pressure fluctuations is that pressure fluctuations may be expressed in terms of wall shear stress τ_o as

$$\sqrt{\bar{p}^2} = \alpha\tau_o \tag{8a}$$

where α is a coefficient which varies between 3 and 6 depending on the diameter of the transducer used and on the displacement thickness of the boundary layer.

In addition, pressure fluctuations may be related to velocity fluctuations as

$$\sqrt{\bar{p}^2} = \beta\rho\bar{u}^2 \tag{8b}$$

where u is the longitudinal component of the fluctuating velocity, ρ the fluid density and β a coefficient reported by some investigators to have values ranging from 0.35 to 0.72

2.3 THE RESISTANCE TO FLOW

The d'Arcy-Weisbach equation which expresses the resistance to steady fully developed uniform flow in terms of the friction factor is

$$\bar{S} = \frac{\bar{f}}{4r}\frac{\bar{U}^2}{2g} \tag{9}$$

$\bar{f}$ is the friction factor and is related to Chezy's $\bar{C}$ and Manning's $\bar{n}$ by the following relationships

$$\bar{C} = \sqrt{\frac{8g}{\bar{f}}} \tag{10}$$

$$\bar{n} = 1.486r^{1/6}\sqrt{\frac{\bar{f}}{8g}} \tag{11}$$

where r is the hydraulic radius, $\bar{U}$ the average velocity, g the gravitational acceleration and $\bar{S}$ the energy gradient.

Most relationships expressing the resistance to flow in open channels stem largely from studies based on boundary layer theory. The boundary layer is defined as the zone within which the velocity of the flow varies from zero at the boundary to the maximum value the velocity would have had in the absence of the boundary. Boundary layers are either laminar or turbulent. In turbulent layers three fairly distinct regions are easily recognized

(a) The laminar sublayer, in which the velocity distribution is a straight line and molecular diffusion predominates.

(b) A turbulent region which comprises the inner part of the layer where flow characteristics are governed by the wall shear, distance from the wall and fluid viscosity and the mean flow is virtually unaffected by pressure gradient.

(c) The outer region where eddies are limited in lateral extent and the mixing is free.

The inner region is very active in both production and dissipation of turbulent energy. The outer layer is an intermediate - it transfers kinetic energy from the mean flow and it leads it to the inner layer where turbulence production occurs.

There are two scales of turbulent eddy size. The smaller eddies have the major part of turbulent energy and they dissipate it into shear stress, and larger ones which transfer the turbulent motion across the flow. Large eddies gain energy from the main flow and this energy is lost to the smaller eddies by working against Reynolds stresses.

Prandtl proposed an expression for the unknown quantity $-\rho\overline{u\,v}$ in which he introduced the mixing length concept which is a function of

the distance from the wall, $\ell_1 = Ky$

$$-\rho\overline{uv} = \rho K^2 y^2 \left(\frac{dU}{dy}\right)^2 \tag{12}$$

by making few simplifications the semi-logarithmic equation of the velocity distribution may be written as

$$\frac{U}{U^*} = \frac{1}{K} \log_e \frac{y}{Y_1} \tag{13}$$

where U^* is the shear velocity and equals $\sqrt{\frac{\tau_o}{\rho}}$

and K is the Von Karman constant

if we substitute for $\bar{f}$ by

$$\bar{f} = 8 \frac{\tau_o/\rho}{\bar{U}^2} \tag{14}$$

we can write Eq. (10) in the usual form of the resistance coefficient

$$\frac{1}{\sqrt{\bar{f}}} = A \log \frac{y}{Y_1} + B \tag{15}$$

The factor Y_1 depends upon ν, U^* and Δ where Δ is a term which represents surface roughness and it is sometimes represented as

$$Y_1 = C \frac{\nu}{U^*} + D\Delta \tag{16}$$

In his comprehensive and systematic experiments in pipes, Nikuradse gave the constant K the value 0.4 for smooth boundaries, $Y_1 = \frac{0.111\nu}{U^*}$ and $Y_1 = \frac{\Delta}{30}$ for rough pipes. With these values Eq. (10) becomes

$$\frac{U}{U^*} = 5.75 \log_{10} \frac{(9.05\, y\, U^*)}{\nu} \tag{17}$$

for smooth boundaries and

$$\frac{U}{U^*} = 5.75 \log_{10} \frac{(30y)}{\Delta} \tag{18}$$

for rough boundaries.

Δ here is a representative length of the roughness elements and is called the equivalent sand roughness.

Keulegan's study of Nikuradse's data lead him to the expression of

average velocity

$$\frac{\bar{U}}{U^*} = 5.75 \log_{10} \left(3.67 \frac{r\, U^*}{\nu}\right) \tag{19}$$

for smooth channels, and

$$\frac{\bar{U}}{U^*} = 5.75 \log_{10} \left(12.27 \frac{r}{\Delta}\right) \tag{20}$$

for rough channels.

2.4 THE EFFECT OF FREE SURFACE

Some solutions to the problems of resistance to flow in open channels stem from a partial analogy with pipes. The turbulence structure near the wall in open channels is similar to that in pipes. There is a fundamental difference, however, further away from the wall. In the case of pipes the component v may be great at the centre due to the transfer of fluid mass across the plane whereas the existence of a free surface in open channels does not allow fluid mass to come out and v must be zero there. Some investigators reported that the effect of free surface on v is so great that v is suppressed at a distance as far as 0.4 times the depth below the free surface.

On the other hand, the similarity criterion that exists for both cases is that the Reynolds shear stresses $-\rho\overline{u\,v}$ are zero at the centre in the case of flow in pipes and at the free surface in the case of open channels.

Since the distribution of shear stress is linear in both cases, it may be said that similar velocity distribution laws hold in both cases. Experimental results confirm this theory.

In wide channels it is assumed that velocity distribution laws derived for pipes may hold but in narrow channels the flow is somewhat complicated by the non-uniform distribution of the shear stress and by the presence of secondary currents. The effect of these factors on the resistance coefficient is not known but it is generally believed that the resistance

coefficient is increased because of the non-uniformity in the distribution of shear stress and the presence of secondary currents.

2.5 REVIEW OF PREVIOUS WORK

Turbulence and resistance to flow in open channels are the most popular subjects in hydraulic engineering and there is a large amount of publications on these two subjects. The review here is directed at what is thought to be of direct relevance to the present work.

2.5.1 Resistance to flow in alluvial channels

The problem of the resistance to flow in alluvial channels has received extensive study. It is well known that the form of the bed varies with hydraulic quantities such as discharge and depth and with sediment size. When the bed consists of relatively fine sand and when the average velocity of the flow slightly exceeds a critical value, at which sand starts to move, certain bed configurations appear and start to influence the resistance to flow considerably. If the velocity is increased beyond the critical value the sediment discharge will increase and bed forms assume different pattern so as to increase the resistance to flow to a maximum value, which corresponds to a maximum stage of development of that particular form, and then it starts to decrease until a transition region is reached (Smith 1968).

In alluvial channels, the resistance to flow and the velocity distribution are complicated to a great extent due to the presence of bed configurations and sediment in the flow.

The difficulty of the problem is due to the fact that there are many variables, the individual effect of which must be separated, before their respective influences on the resistance to flow and the velocity distribution can be traced.

In his experiments, V.A. Vanoni showed the effect of the suspended load in reducing the resistance. He explained this phenomenon by the effect of the sediment in reducing turbulence level. The turbulence energy supplies the power to the flow to keep the sediment in suspension and thus the intensity of turbulence is damped and reduced.

In later work (1959), Vanoni dealt with the combined effect of the presence of bed configuration and suspended sediment. He assumed that while the appearance of bed configurations tends to increase the resistance to flow, the damping effect of the suspended sediment on the turbulence in the stream tends to reduce the resistance.

In natural streams, the two processes are always acting together and it is very difficult to separate their individual effects. Vanoni made an attempt to separate the two effects and hence to determine their relative order of magnitude. He concluded that the effect of the presence of the bed configuration is far more important than the effect of suspended sediment (for example, the dunes observed in one of his runs caused the friction coefficient $\bar{f}$ to attain a highe value $\bar{f} = 0.106$, as compared with $\bar{f} = 0.030$ for plane bed, whereas the damping effect on the velocity was of the order of 30 per cent only). Other investigators, Brooks for instance (1955) reported friction coefficients for dune-covered beds which were seven times larger than those for plane sand beds of the same material.

The general trend in the study of the resistance to flow in alluvial channels is to relate the boundary resistance of the channel with the flow characteristics and the bed material.

There is no formula that can express the resistance to flow in one relationship which includes all the variables encountered in the study of alluvial channels because such a relationship, even if it exists,

is greatly complicated by the interaction between the flow characteristics and the bed forms. Considerable scatter is almost invariably present in any non-dimensional or dimensional form of plotting. Added to this is the difficulty in correlating the results obtained from laboratory investigation with observations of natural streams and alluvial rivers.

What is needed, therefore, is extensive investigation into the fundamental question of the mechanism of formation of various bed configurations, their characteristics and the interaction between bed forms and flow conditions.

2.5.2 Resistance to flow of artificial elements

The aim of the experimental work in alluvial channels is to describe as closely as possible and to estimate quantitatively the resistance to flow as compared with natural streams, alluvial rivers and irrigation canals. Another branch in Hydraulics has emerged in this connection, which tends to use new geometrical forms of artificial roughness. Although this type of roughness is far from resembling any roughness elements that could ever be encountered in real life, it possesses nevertheless many advantages in clarifying specific problems, such as the inter-relation between turbulence structure and the mechanism of the resistance to flow. These problems are in the present stage of knowledge, far from being solved with certainty in the field of loose bed hydraulics because changes in flow conditions result in changes in bed forms, and even if the flow were steady it would be extremely difficult to carry out detail measurements because the bed form pattern will move and change when the probe of the measuring device is introduced.

In their experiments on artificial roughness, Robinson and Albertson (1961) used baffles fixed to the bottom of an 8 x 2 ft flume, each baffle being 6-inch wide against $1\frac{1}{2}$ inch height. They derived an

equivalent sand roughness Δ which was a function of the spacing of the roughening elements.

H.M.Morris (1959) studied the resistance to flow of artificial rugosity shapes and distinguished between five different types of flow. One of them, which is of relevance to the present investigation, he called the semi-smooth turbulent flow. Morris calculated the additional resistance caused by the existence of these elements. The additional resistance depends upon the roughness height, its spacing and the drag coefficient. He then adds this value to the original value calculated for the smooth turbulent flow to get the sum effect (Fig. 2) .

Recently Vanoni (1967) studied the resistance to flow of two stabilized bed forms. He came to the conclusion that the resistance caused by the form drag can be expressed as

$$\frac{1}{\sqrt{f''_b}} = 3.5 \log \frac{r_b}{\bar{e}_1 \bar{H}} - 2.1 \qquad (21)$$

where r_b is the bed hydraulic radius

$\bar{e}_1$ is the exposure parameter (it may be considered as the equivalent of the ratio of the height of the ripple or dune to its length)

and $\bar{H}$ is mean dune or ripple height.

Comparing this equation with the equation which expresses the resistance to flow with one parameter, namely the equivalent sand roughness Δ,

$$\frac{1}{\sqrt{f_b}} = 2 \log 2 \frac{r_b}{\Delta} + 1.74 \qquad (22)$$

Vanoni found that Δ is not constant for one type of roughness but varies with depth and average velocity and he concluded that the roughness parameter could not be expressed simply as a unique length Δ .

A comparison between the values of f''_b obtained from non-stabilized beds with those of stabilized beds for the same sets of experiments shows

little difference. No attempt was made to compare the other component of resistance f'_b.

Indeed, it may be said that there is no hydrodynamic similarity between the two cases because the natural surface roughness is very difficult to reproduce artificially. It is therefore very difficult to correlate the component of resistance to flow caused by surface roughness f'_b in artificial bed configuration with its counterpart in non-stabilized bed forms, let alone any correlation with real life.

It is common knowledge that when bed forms reach their maximum stage of development the resistance to flow is dominated by the influence of form resistance. Any tendency in the variation of form resistance with changing flow conditions must be reflected strongly on the total resistance. This is a natural result of the fact that surface roughness is not expected to affect the flow structure around the bed forms in the same way as the appearance of obstructions, which are the bed forms, affects the flow.

As the decomposition of the total resistance into two components f'_b, f''_b is sometimes a controversial issue it is always better if f''_b could be estimated directly. This is possible in the case of artificial projections when the pressure distribution is measured.

2.5.3 Turbulence measurements

Turbulence measurements were carried out by Sheen (1964). In his investigation, S.J. Sheen measured the turbulence quantities in the lee of an expansion caused by two kinds of models. One was a sand ripple formed spontaneously by the flow over a flat sand bed and the other was made by the strong back eddies behind a wall.

By a method similar to the standard X-wire technique in Aerodynamics, he was able to yaw the hot-film to make two different angles with the

main flow which yielded the R.M.S. velocity fluctuations in the longitudinal direction, the Reynolds stresses in this direction and the R.M.S. value of the transverse velocity fluctuations.

His method was based on the assumption that the nature of turbulence is ergodic (i.e. all time-averaged quantities do not differ when computed over different sample functions). This may be true for one direction but it is doubtful if it is correct to include, in a mathematical relationship intended to calculate , uv, v^2 at one point, readings taken at different instants of time. The reason for this is that a random physical phenomenon such as turbulence is unique. In other words, any given observation will represent only one of many turbulence time history records at a specific point. The method used could give a general picture of the flow pattern but no statistical analysis could be made on any measurement of $\overline{uv}$ or v^2 unless measured at one instant.

Two important conclusions may be drawn from his work. The first is that there is a strong resemblance in flow structure between the flow over a step which was observed by Walker (1961) and the flow in the lee of the expansion caused by the two models. The second conclusion is that due to the presence of turbulence which was concentrated locally the critical mean bed shear stress for the movement of the sand grains may be considerably lowered.

Recently Richardson and McQuivey (1968) have put forward a method to correct the readings of hot-films in extremely dirty waters. Their method was based on the hypothesis that the effect of dirt and air bubbles accumulating on the sensor is to reduce the mean voltage for a given velocity but frequency response is not affected. For a given sensor there exists a family of calibration curves for different overheat ratios. The effect of the film contamination in reducing voltage

output is similar to the case when the overheat ratio is reduced. The degree of the reduction in the mean voltage could be detected if the mean velocity was measured by a different method, i.e. pitot tube for example. This line of thought is promising for turbulence measurements in alluvial channels and indeed the authors suggested this. But the difficulty lies in the fact that it is not always possible, especially in alluvial channels, to keep the degree of contamination under controllable conditions for a long period if a record of the turbulence signal is required for subsequent statistical analysis.

CHAPTER THREE

ANALYSIS RELATING TO PRESENT INVESTIGATION

"When a thing is funny, search it
for a hidden truth"
(George Bernard Shaw)

3.1 RESISTANCE TO FLOW

3.1.1 Form drag and surface roughness.

The mechanism of resistance to flow, exerted by bed configurations in alluvial channels, can be simulated using triangular elements. This mechanism can be described as follows as the stream strikes the upstream face of the element, the velocity vector changes in magnitude and direction and thus increases the pressure in this region to above hydrostatic. The triangular element is shown in Fig. 3.

At the downstream face of the element, if the dimension of, and flow conditions around, the element are such as to allow separation to occur, the pressure is always less than hydrostatic. (In fact, the pressure is always less than hydrostatic due to the change in the velocity vector regardless of whether separation occurs or not). The drop in pressure on the downstream face is related to the formation of an eddy region. Thus the longitudinal effects produced by these elements are (a) an increase in pressure (to above hydrostatic) at the upstream face and (b) a decrease in pressure (to below hydrostatic) at the downstream face.

The form drag of the element is the product of the resultant sum of these pressures times the maximum area in the plane normal to the direction of flow (known as the main) and this

could be written as the integration of the pressure distribution over the area of the element

$$F_D = \int_s p \sin \bar{\alpha} \, ds \tag{23}$$

Surface shear is not constant along the element. Along the element the local depth drops from d to (d-h) at the crest. Consequently, the average velocity increases and the surface drag, which is approximately proportional to the square of the velocity, increases.

The change in the local height at a Section A of abssica x is

$$y = \frac{x}{\ell} h$$

The average velocity at this section is

$$U_x = \frac{Ud}{(d-y)} \tag{24}$$

The total loss caused by surface roughness is

$$F_s = \int_\ell \phi(U) \frac{ds}{\ell(1-\frac{hx}{\ell d})^2} \cos \bar{\alpha} \tag{25}$$

where $\phi(U) = \tau_s$

$$F_s = \frac{\ell \tau_s}{1 - h/d} \tag{26}$$

As separation occurs in the downstream face, the friction resistance caused in the wake zone is negligible and the reduction of this resistance is compensated for to a certain extent by the fact that shear stress is sometimes assumed constant.

3.1.2 The balance of resistance components.

The shear stress expression for uniform flow over flat bed is $\tau_0 = \gamma rs$ when the bed is not flat, i.e. the resistance is no longer confined to surface friction, but

form drag is present, the shear stress should be decomposed into two components: one caused by surface roughness and the other by form drag $\tau_s + \tau_F = \tau_o$ where τ_s is the shear caused by surface roughness and τ_F is the shear caused by the form drag. The value of τ_s corresponds to $u_b'^*$ and f_b' and the value of τ_F corresponds to $u_b''^*$ and f_b'' which are the familiar expressions for shear velocity and friction factor of the grain and form drag respectively.

If the distribution of shear stress is not uniform i.e. the walls have different roughness from that of the bed, τ must be corrected by using side wall correction and a new value τ_b' is obtained. There are several methods for side wall correction which take the low roughness of the side wall into account.

3.1.3 The momentum equation.

It is sometimes desirable to attempt to determine the relative order of magnitude of the terms which constitute the resistance to flow individually. To this end, the Reynolds equation is integrated over an arbitrary volume of fluid. By means of mathematical techniques associated with the names of Green and Gauss, and known as the divergence theorem it is possible to transfer the volume integral into surface integral and vice versa. The divergence theorem states that the surface integral of a vector over a closed surface is equal to the volume integral of the divergence of the vector throughout the enclosed volume. Thus, if $\vec{A}$ represents a vector the divergence theorem may be written as

$$\iiint_V \vec{\nabla}.\vec{A}\, dV = \iint_S \vec{A}.d\vec{S} \qquad (27)$$

The physical significance of the theorem may be better understood from the fluid mechanics point of view by the following example. If V_i (x,y,z), $\frac{\partial V_i}{\partial x_i}$ are continuous and single valued functions of a vector field $\vec{V}$ in a volume Ψ bound by a surface S then equation 27 may be written

$$\iiint_{\Psi} \left(\frac{\partial V_i}{\partial x_i}\right) d\Psi = \iint_S \left(V_i \frac{\partial x_i}{\partial n}\right) d\sigma \tag{28}$$

where $\frac{\partial x_i}{\partial n}$ is the direction cosines; n being the distance outward from the surface in the normal direction.

Since $d\vec{s}$ is taken normal to the surface it represents, the component of $\vec{A}$ that must be taken is the one perpendicular to the surface at a given point.

Integrating equation 4 over the volume Ψ we can write

$$\iiint_{\Psi} \rho\left[U_j \frac{\partial U_i}{\partial x_j} + \frac{\partial \overline{u_i u_j}}{\partial x_j}\right] d\Psi = \iiint_{\Psi}\left[\rho X_i - \frac{\partial P}{\partial x_i} + \mu \frac{\partial^2 U_i}{\partial x_j \partial x_j}\right] d\Psi \tag{29}$$

The first term $\rho U_j \frac{\partial U_i}{\partial x_j}$ of the left hand side in Equation 29 can be written as $\rho \frac{\partial U_j U_i}{\partial x_j}$ by virtue of the continuity equation i.e.

$$\rho U_i \frac{\partial U_j}{\partial x_j} = 0 \tag{30}$$

Applying the divergence theorem, the left hand side of equation 29 can be written as

$$\iiint_{\Psi}\left[\rho \frac{\partial U_i U_j}{\partial x_j} + \rho \frac{\partial \overline{u_i u_j}}{\partial x_j}\right] d\Psi = \iint_S \left[\rho U_j U_i \frac{\partial x_j}{\partial n} + u_i u_j \frac{\partial x_j}{\partial n}\right] dS \tag{31}$$

The right hand side of equation 31 represents the sum of the

flux of the mean and turbulent momentum across the surface S.

The right hand side of equation 29 can be written

$$\iiint_{\forall}\left[\rho X_i - \frac{\partial P}{\partial x_i} + \mu\frac{\partial^2 U_i}{\partial x_j \partial x_j}\right]d\forall = \iiint_{\forall}\rho X_i d\forall - \iint_S P\frac{\partial x_i dS}{\partial n} + \mu\iint_S \frac{\partial U_i}{\partial x_j}\frac{\partial x_j}{\partial n}\,dS \qquad (32)$$

where $\frac{\partial x_i}{\partial n}$ and $\frac{\partial x_j}{\partial n}$ are the ith and the jth components of the direction cosines.

If we equate the right hand sides of equations 31 and 32 we can write

$$\iint_S \rho\left[U_i U_j \frac{\partial x_j}{\partial n} + \overline{u_i u_j}\frac{\partial x_j}{\partial n}\right]dS = \iiint_{\forall}\rho X_i d\forall - \iint_S P\frac{\partial x_i}{\partial n}\,dS + \mu\iint_S \frac{\partial U_i}{\partial x_j}\frac{\partial x_j}{\partial n}\,dS \qquad (33)$$

In order, the right hand side of equation 33 represents the body force, the normal pressure on the region and the mean viscous tangential stresses on the surface of the volume.

In two dimensional flow $U_i = U$ and $U_2 = U_3 = 0$ equation 33 can be written in the x direction as

$$\rho\iint_S \frac{\partial x}{\partial n}U^2 dS + \rho\iint_S\left(\frac{\partial x}{\partial n}\overline{u}^2 + \frac{\partial y}{\partial n}\overline{uv} + \frac{\partial z}{\partial n}\overline{uw}\right)dS =$$

$$\iiint_{\forall}\rho X d\forall - \iint_S \frac{\partial x}{\partial n}p\,dS + \mu\iint_S\left(\frac{\partial x}{\partial n}\frac{\partial U}{\partial x} + \frac{\partial y}{\partial n}\frac{\partial U}{\partial y}\right)dS \qquad (34)$$

This integration can be performed over an element bound by two surfaces S1 and S2 as is shown in Fig. 4, where

dz is assumed to be unity.

Equation 34 can be written as

$$\rho\int_{y_3}^{y_4} U_{s2}^2\,dy - \rho\int_{y_1}^{y_2} U_{s1}^2\,dy + \rho\int_{y_3}^{y_4} \overline{u}_{s2}^2\,dy - \rho\int_{y_1}^{y_2} \overline{u}_{s1}^2\,dy =$$

$$\frac{\gamma}{2}\left[(y_1 - y_{ref})^2 - (y_3 - y_{ref})^2\right] - \int_{y_4}^{y_2} P\,dy + \mu\frac{dU}{dy}(x_1 - x_2) \quad (35)$$

for the volume shown in Fig. 4, by virtue of the following assumptions.

1. On the free surface and on the bed the turbulent shear $\rho\overline{uv}$ are zero, and $\tau_o = \mu\frac{dU}{dy}$ as can be seen in Fig. 1.

2. On the two surfaces S1 and S2 $\mu\frac{\partial U}{\partial x}$ is small and can be neglected.

3. The value of the boundary conditions for U and u' are zero.

Equation 35 can be written as

$$\left[\rho\int_{y_3}^{y_4} U_{s2}^2\,dy - \rho\int_{y_1}^{y_2} U_{s1}^2\,dy\right] + \left[\rho\int_{y_3}^{y_4} \overline{u}_{s1}^2\,dy - \rho\int_{y_1}^{y_2} \overline{u}_{s2}^2\,dy\right] =$$

$$\frac{\gamma}{2}\left[(y_1 - y_{ref})^2 - (y_3 - y_{ref})^2\right] - \int_{y_4}^{y_2} P\,dy + \tau_o(x_1 - x_2) \quad (36)$$

If we consider the mean and turbulent momentum at the surface S1 as a reference we can write equation 36 as

$$\text{constant} + \rho\int_{y_3}^{y_4} U_{s2}^2\,dy + \rho\int_{y_3}^{y_4} \overline{u}_{s2}^2\,dy = \text{body force} + \text{total loss flux} \quad (37)$$

Equation 37 can be interpreted as follows. The change in the total momentum flux of the mean and fluctuating

longitudinal velocity is balanced by the body force, normal pressure and viscous forces.

3.1.4. Energy balance

Turbulence is an important factor in energy dissipation. The energy is dissipated by turbulence into heat through the action of viscosity. The rise in the internal shear stresses caused by the turbulent eddies causes the large energy dissipation.

Part of the potential energy producing the flow is transformed gradually into turbulent energy and is then changed into heat by the action of viscosity. The rate at which potential energy is transformed into turbulent energy is different from the rate of energy dissipation into heat at one point. The turbulent energy can be diffused to other points by the action of eddies and then dissipated into heat.

To estimate the order of magnitude of turbulent energy, turbulent dissipation and diffusion, consideration of the equation of energy is necessary. To obtain the energy equation, equations 3 are multiplied by the density and the corresponding component of velocity and then the three equations are added together. The energy equation can be written as

$$\tfrac{1}{2}\,\rho V_j \frac{\partial V_i V_i}{\partial x_j} = \rho V_i X_i - V_i \frac{\partial P}{\partial x_i} + \mu V_i \frac{\partial^2 V_i}{\partial x_j \partial x_j} \qquad (38)$$

In two dimensional flow and where external forces are negligible equation 38 becomes

$$\tau_0 \frac{dU}{dy} = \frac{d}{dy}\left(\rho v \frac{u^2 + v^2 + w^2}{2} + v^2 p\right) + \mu \overline{\left(\frac{\partial u_i}{\partial x_j}\right)\left(\frac{\partial u_i}{\partial x_j}\right)} \qquad (39)$$

Equation 39 which was developed by Laufer (1954), states that the energy produced by the turbulent shear forces at a certain point is partly diffused and partly dissipated.

Equation 39 cannot be considered here for comparison. With the present state of knowledge and development of hot-film anemometer reached in this investigation, no component other than the longitudinal component u of the fluctuating velocity was considered.

3.2 TURBULENCE MEASUREMENTS

Constant resistance anemometry was used in the present investigation to measure the fluctuating component of the longitudinal velocity. Hot-wire probes were used in air and hot-film sensors in water. The anemometers were developed and made at the Institute of Sound and Vibration of the University of Southampton. Fundamentally, the detecting element in anemometry consists of a heated metalic wire or film. This element forms one arm of a Wheatstone bridge. When a fluid flows over it, the metallic element is cooled by forced convection. The cooling of the element is a function of the flow velocity, fluid characteristics and film dimensions and temperature. If all but one of the fluid flow and film variables are kept constant, the heated element can measure the remaining variable.

The most important application of this device is turbulence measurements. The output voltage of the anemometer is either detected directly or recorded on a magnetic tape for subsequent processing. The measurement made using the anemometer are the following.

3.2.1. Root mean square values

In non-linear anemometry, the root-mean-square value of the fluctuating component is not directly proportional to the R.M.S. meter readings. The relationship between the two values is derived in chapter six. In linear anemometry the root mean square of the fluctuating velocity $\sqrt{\overline{u}^2}$ is directly related to the R.M.S. meter reading and the relationship between the two discussed in chapter six.

3.2.2. Probability density function

It is known that due to its random character, turbulence has a probability density function that approaches a Gaussian distribution. The probability density function f(x) of a variable x represents a function such that f(x)dx indicates the probability that the value of x lies between x_i and $x_i + dx$

$$f(x) = \text{Prob.}\ (x_i < x\ (t) < x_i + dx) \tag{40}$$

3.2.3. Correlation and frequency spectrum functions.

- The general space-time correlation function is

$$R_{oij}\ (X',s,\tau) = \frac{1}{T}\int_o^T u_i\ (X',\ t)\ u_j\ (X' + s,\ t + \tau)dt \tag{41}$$

and it is used in two special forms, the spatial correlation function with τ=o where τ is time lag and the autocorrelation function with s=o where s is separation distance.

The autocorrelation function in the longitudinal direction is

$$R_{O11}\ (X',O,\tau) = \frac{1}{T}\int_o^T u\ (X',t)\ u\ (X',t + \tau)\ dt \tag{42}$$

and the normalized autocorrelation function is

$$R_{11}\ (X',O,\ \tau) = \frac{1}{\overline{u}^2 T}\int_o^T u\ (X',t)\ u\ (X',\ t + \tau)\ dt \tag{43}$$

- The frequency spectrum of the velocity fluctuations was found by G.I. Taylor to be the Fourier transform of the autocorrelation function.

In Fig. 5 a random function is shown with the notations used in the present analysis. The normalized frequency spectrum is given by the equation

$$F_{11}(f) = 4 \int_0^\infty R_{11}(\tau) \cos 2\pi f \tau d\tau \qquad (44)$$

where $F_{11}(f)$ is the quantity such that the fractional contribution to the total energy of turbulence $\overline{u}^2$ of the band of frequencies f, f + df is $F_{11}(f)\,df$.

3.2.4. Scales of Turbulent Motion.

- In isotropic turbulence there is a number of spatial correlation functions which may be expressed in the form

$$R_{ij}(X',s,O) = \frac{1}{\overline{u}^2 T} \int_0^T u_i(X',t)\, u_j(X' + s,\, t)dt \qquad (45)$$

These functions are related by virtue of the basic definition of isotropy.

In the longitudinal direction, this correlation function may be written as

$$R_{11}(X',s,O) = \frac{1}{\overline{u}^2 T} \int_0^T u(X',t)\, u(X' + s,\, t)\, dt \qquad (46)$$

In the neighbourhood of s=o, it can be shown by expanding expression 46 in Taylors series that the larger terms approach zero very rapidly, so that a good approximation may be obtained from the first two.

$$R_{11}(s) \simeq 1 + \frac{s^2}{2} \frac{\partial R_{11}(s)}{\partial s^2} \qquad (47)$$

As a result, $R_{11}(s)$ can be expressed in terms of a length parameter λ called the microscale of turbulence

$$\frac{1}{\lambda^2} = \frac{\partial^2 R_{11}(s)}{\partial s^2} \Big| \; s \to o \tag{48}$$

Thus we obtain near the origin

$$R_{11}(s) \cong 1 - \frac{s^2}{2\lambda^2} \tag{49}$$

which means that the parameter λ^2 is the radius of curvature of the curve $R_{11}(s) \mathcal{V}\ s$ at s=o. Since $\frac{\partial R_{11}(s)}{\partial s}$ $\to o$ as $s \to o$ λ is the intercept of the parabola $1 - \frac{s^2}{\lambda^2}$ fitted to the R_{11} (f) curve, See Fig. (6).

- Another scale of turbulence known as the macroscale or integral scale of turbulence is

$$L_x = \int_o^\infty R_{11}(s)\, ds \tag{50}$$

- Taylor suggested a space-time transformation where he assumed

$$\frac{s}{U} = \tau$$

$$\frac{\partial}{\partial t} = U \frac{\partial}{\partial x} \tag{51}$$

From this assumption equation 44 can be written as

$$F_{11}(f) = \frac{4}{UT} \int_o^\infty R_{11}(s) \cos 2\pi \frac{s}{U}\, ds \tag{52}$$

From which equation 50 can be written as

$$L_x = \frac{U\, F_{11}(0)}{4} = U \int_o^\infty R_{11}(\tau)\, dt \tag{53}$$

and the microscale can be written as

$$\frac{1}{\lambda 2} = \frac{4\pi^2}{U^2} \int_o^\infty f^2 F(f)\, df \tag{54}$$

The validity of Taylor's hypothesis is not easy to determine, since most turbulent flows that are encountered in Hydraulics are far from isotropic. Nevertheless,Taylor's method can be used as a qualitative indication to learn more about the eddy structure.

3.3 PHYSICAL SIGNIFICANCE OF TURBULENT FLOW STRUCTURE

In order to attach physical significance to the idea of turbulence, it is helpful to consider that turbulence consists of eddies of different sizes being transported past a point by the mean flow. The large eddies contain most of the turbulent energy and they contribute little to the viscous dissipation of energy; the small eddies contain very little of the turbulent energy and they dissipate the energy by viscous work. The kinetic energy of turbulent motion in larger eddies goes down to eddies of smaller scale. Thus the general picture of energy dissipation is as follows: large eddies form an energy reservoir which supplies its content to the smaller eddies where the viscous forces become most effective and the predominent part of the energy dissipation occurs.

The important principle of flow similarity states that the large scale properties of turbulent flow (mean velocity distribution, turbulent intensities, Reynolds stresses, correlation functions, probability density function and transport properties) are independent of the viscosity and dissipation process, provided the Reynolds number of the turbulent motion is sufficiently high. A consequence of this principle is that the loss of turbulent energy from large eddies to small eddies depends on the structure of

large eddies and is independent of the magnitude of viscosity.

The behaviour of the largest eddies must be regarded with some reserve since it depends on the experimental apparatus i.e. the size of the measuring probe as compared with the eddy size. If the general scale of turbulence is much smaller than the dimension of the probe, a proper interpretation of the results is necessary in order to avoid this complication. One method of solving it is by extending the integral for macroscale over a distance much larger than the scale but still much smaller than the size of the probe.

The existence of Reynolds shear stresses depends on the correlation between the longitudinal and transverse components of velocity fluctuations, and the coefficient of this correlation is necessarily less than 1. In free turbulent flows, this coefficient $\frac{\overline{uv}}{\overline{u^2}}$ is found to be nearly constant and between 0.4 and 0.5.

The above considerations lead to the central theme of the momentum-transfer theory in which the mixing length - defined earlier - relates Reynolds stress to mean velocity gradient.

$$\overline{uv} = \ell_1^2 \left(\frac{dU}{dy}\right)^2 \qquad (55)$$

This relation can be applied consistently only to wall turbulence where production and dissipation of turbulent energy are very rapid, in which case the transfer of turbulent energy from one part of the flow to another has little effect on the turbulent motion and ℓ_1, as

another scale of turbulence must be estimated from other considerations.

3.4 METHODS OF CALCULATIONS

3.4.1. Root mean square values

The R.M.S. values of the fluctuations were measured by a true R.M.S. meter. Few readings were compared with the mean square values as obtained from the digital computer at the Data Analysis Centre as follows: If the root-mean-square level is σ, we have

$$\sigma^2 = \int_0^\infty F_{oll}\ (f)\ df \tag{56}$$

where $F_{oll}(f)$ is the non-normalized frequency spectrum function.

The digital computer prints the mean and the mean square values. From these values we have

$$\sigma^2 = \text{Mean square value} - (\text{mean value})^2$$

This discrepancy arises because conventional analogue equipments are a.c. coupled and hence do not include the d.c. level in the calculations. In the digital process the mean square value is determined before reducing the data to zero mean value.

3.4.2. Probability density function

Suppose the two end points of a signal are u_1 and u_n the interval between the two values is divided into a number of ranges. Each value in the sample is tested to determine in which range its value is. The sum of the number of values in each range divided by the total number of the individual values gives the function f(u)

The mean deviation is

$$\eta = \Sigma \, |u \, f \, (u)| \tag{56a}$$

The standard deviation $\bar{\sigma}$ is

$$\bar{\sigma} = \sqrt{\Sigma \, \bar{u}^2 f(u)} \tag{56b}$$

The flatness FL

$$FL = \frac{\Sigma u^4 f(u)}{\bar{\sigma}^4} \tag{56c}$$

The skewness SK is

$$SK = \frac{\Sigma u^3 f(u)}{\bar{\sigma}^3} \tag{56d}$$

3.4.3. Correlation and frequency spectrum

The length of the record and the time lag are to be decided on after the highest frequency and the degree of accuracy are known.

To obtain an auto-correlation function which represents the signal characteristics, the true lag τ must be less than half the minimum period expected i.e.

$$\tau \leqslant \frac{1}{2f_m} \tag{57}$$

where f_m is the maximum frequency expected which is called sometimes "cut-off frequency".

The maximum number of correlation lag values M is

$$M = \frac{1}{B_e \tau} \tag{58}$$

where B_e is the desired equivalent resolution band width for frequency spectrum calculation.

The numerical value of an integration according to Simpson's rule is

$$I = \frac{G}{3} (y_o + 4y_1 + 2y_2 + 4y_3 \cdots + 2y_{n-2} + 4y_{n-1} + y_n) \tag{59}$$

where G is the interval taken between the initial and final points of integration y_o and y_n respectively.

Here $G=\tau$ and $y_o=R_{(o)}$ and $y_n=R(M\tau)$. If m is a dummy variable, equation (24) may be written in a numerical form as

$$F(f) = 4 \sum_{o}^{M} R(m) \cos 2\pi f m \tau \qquad (60)$$

Applying Simpson's rule we can write

$$F(f) = \frac{4\tau}{3}\left[R(O) + SUM2 + SUM4 + R(M) \cos (2\pi fm) \right] \qquad (60a)$$

in this expression M must be even

where $SUM2 = \Sigma R(m) \cos 2\pi fm\tau \quad m = 2,4,6.... M-2$ (60b)

and

$$SUM4 = \Sigma R(m) \cos 2\pi fm\tau \quad m = 1,3,5,7...M-1 \qquad (60c)$$

The limitation on the frequency f is contained in the expression $\cos 2\pi fm\tau$ terms because m takes integral values and f represents the "centre frequency".

The expression $2\pi fm\tau$ can be written as $2\pi \frac{mf}{2f_m}$ assuming $\tau=\frac{1}{2f_m}$. If mf is assumed to represent certain frequency f_1 we can write

$$\cos 2\pi \frac{f_1}{2f_m} = \cos 2\pi (2m f_m \pm f_1) \frac{1}{f_m} \qquad (61)$$

Thus all data at frequencies $2mf_m \pm f_1$ have the same cosine function as data at frequency f_1 when data are sampled at points $\frac{1}{2f_m}$ apart.

For example, if f_m is 50 c/sec, then data at 30 c/sec would be aliased with data at frequencies 70, 130, 170 230 c/sec..etc.,

The method used in the present investigation to handle this aliasing problem was to choose τ sufficiently small so that it was physically unreasonable for data to exist above the maximum frequency chosen which was 50 c/sec.

CHAPTER FOUR

APPARATUS AND EXPERIMENTAL PROCEDURES

4.1 PRELIMINARY INVESTIGATION

4.1.1 Wind tunnel

The wind tunnel used for the preliminary investigation was located at the low speed laboratory of the Department of Aeronautics and Astronautics of the University of Southampton.

The original working section was about 4 feet long and this distance did not allow sufficient growth of the boundary layer. The working section was replaced by a 16 feet long piece. The cross section of the working section was 1 ft square. The sides were provided with four panels of perspex to make flow visualization possible (Plate One). The inside of the tunnel was varnished with phenoglaze and was very smooth.

The upstream part (the effuser) in which air accelerated from rest to the required velocity was about 7' long and 4' wide decreasing to 1' at the working section. The diffuser was about 10' long ending by a side of 2'3". Originally the wind tunnel was designed for a maximum velocity of 120 ft/sec.

Air speed used in this investigation was 65 feet per second which was considered high enough for the background turbulence not to influence the results. The driving motor and the fan were capable of providing such a velocity after the extension of the working section.

4.1.2 Experimental procedures

(a) Reference velocity

The reference velocity was measured at the entrance of the working section at mid depth with a cylindrical Pitot tube. The differential

pressure was measured by an air-water manometer with an accuracy of the order of 0.001".

(b) Velocity and turbulence

Velocity and turbulence variations were measured by hot-wire probe at the middle of the cross section. The holder of the probe was attached to a micro manipulator which enabled the probe to be moved in the vertical direction to an accuracy of 0.001".

The mean velocity or the D.C. output of the anemometer was measured by an AVO meter No. 8 and the value $\sqrt{\bar{u}^2}$ of turbulence was measured by an R.M.S. true voltmeter make DAWE. Since the voltage output of the anemometer is not a linear function of the velocity, the relationship between turbulence $\sqrt{\bar{u}^2}$ and $\sqrt{\bar{e}^2}$ the reading of the meter is not a linear one. The details of hot-wire anemometer will be discussed in the following chapter.

(c) Auto-correlation and frequency spectrum

Auto-correlation and frequency spectrum functions were evaluated by a combination of analogue and digital methods.

The signals which were to be analysed were recorded on a magnetic tape at speed $1\frac{7}{8}$"/s. The tape recorder used in this investigation was made at the Institute of Sound and Vibration and its frequency response is flat from D.C. to 50 K.C. The auto-correlation function was calculated by an analogue method using the correlator . The correlator is a machine which performs the following operations :

Delaying the signal by a time displacement equal to τ seconds. The time delay can be adjusted according to the cut-off frequency and the frequency resolution required for the frequency spectrum (as was explained earlier). The value was chosen to be 0.5 millisecond which corresponds to a cutoff frequency of 1000 Hz.

Multiplying the signal at any instant by the value that had occurred τ seconds before.

Averaging the instantaneous product value over the sampling time.

The time delay was accomplished by the function of a magnetic drum recorder. This drum displaces the signal in time where the location of the play-back head is variable relative to the location of the record head.

Then the signals to be correlated are applied to the input of an R.M.S. meter. The two output channels of the R.M.S. meter are applied to the input of a function generator, which consists of a quarter square multiplier and its associated summing amplifiers; the purpose of this is to multiply the two signals together. The voltage output of the function generator is proportional to the input signals. This output is then integrated and the integration is fed to the analogue to digital converter which converts the integrated products into pulses, the number of which is proportional to the magnitude of the integrated signal.

The integration time T was 10 seconds. The teleprinter gives three figures as output; the first is the value of the integration

$$R_{II}(\tau) = \frac{1}{T}\int_{o}^{T} u(t)\, u(t+\tau)\, dt$$

the second and the third are $\overline{u(t)}^2$ and $\overline{u(t+\tau)}^2$ respectively.

The normalized auto-correlative function is

$$R(\tau) = \frac{R_{II}(\tau)}{\sqrt{\overline{u(t)}^2 \times \overline{u(t+\tau)}^2}}$$

The correlator gives the three figures typed and on a punched tape as well.

The punched tape was fed into the digital computer with the auto-correlation values on it and the frequency spectrum function was obtained using Fourier transform (discussed earlier).

4.2 INSTRUMENTATION

4.2.1 Hot-Film Anemometer

A separate investigation was carried out to examine the feasibility of using hot-film anemometer to measure turbulence in water. As a result of the preliminary investigation in the wind tunnel, experience in using and operating hot-wire anemometer was gained. This experience helped in the development of the hot-film anemometer and its subsequent use in water. The results of this investigation are described in details in the following chapters.

4.2.2. Pressure transducer

Measuring pressure fluctuations as independent quantity may help in understanding turbulent flow more clearly. To this end, a pressure transducer was needed to measure pressure fluctuations in water.

The details of the development work are to be found in Chapter 5.

4.3 FLUME

The experiments in water were conducted in a 15" x 18" x 21' recirculating flume. The flume is shown schematically in Fig. 7. It was equipped with a centrifugal pump with a constant speed drive of 1450 revs/minute, flow meter, a butterfly type valve, two end tanks and a 6 inch return pipe. Along the top of the channel are mounted brass rails and a movable instrument carriage which can measure vertical elevations relative to the flume to a 0.01" accuracy. The entire flume is mounted on a truss. With a fixed pivot support at one end and adjustable at the other end, the slope of the truss and hence the slope of the flume can be adjusted easily. The required level in the flume can be obtained by raising or lowering the end gate.

Several methods were tried to improve the entrance conditions. A simple and successful method was found. The water enters the end

tank through a T piece and impinges on the walls of the end tank loosing some of its kinetic energy. Then the water is forced to go through a layer of 1" stones which has a thickness of about 6". From this layer the water emerges very tranquil and the flow was maintained by the required slope. The instrument carriage runs longitudinally along the flume and can be run either up or down and crosswise with the carriage in any position. Thus with a point gauge, Pitot tube, hot-film probe it is possible to reach any position in the flume.

The bottom of the flume was a steel channel and the sides were made of Perspex (Plate 2).

The triangular elements were located at about 6' from the entrance and the measurements were made over the fifth element.

4.4 EXPERIMENTAL PROCEDURES

4.4.1 Discharge

The discharge was measured with a venturi meter connected to a water-mercury differential manometer. The coefficient for the venturi meters and the differential manometer calibration were given by the makers (Kent Industrial Instrument Ltd.). The calibration was checked by measuring the discharge over the sharp crested weir at the end of the flume using the formula given by B.S. 3680 (Part 4A 1965 page 23). Several discharges were calculated and the results agreed fairly well with the discharges given by the differential manometer.

4.4.2 Depth

The mean depth of flow was defined as the average difference between the water surface and bed of the flume in that part of the flume where uniform flow was established. The water surface elevations were measured at four points with a point gauge mounted on a movable carriage. The accuracy of the measurements was in the range of 0.001 ft. Because

of the small disturbances on the water surface, every reading was repeated several times and the average was taken.

4.4.3 Slope

At the beginning of a run, the discharge is set to the required values and by adjusting the flume slope and the height of the weir the required depth of the uniform flow is obtained. The water surface slope is always a very difficult quantity to measure. Two different approaches were adopted to measure the slope. Four pressure tappings along the wall of the flume gave a reasonable representation of the water surface and the water surface slope was calculated from their readings. Another method was used to check the water surface slope and the uniformity of the flow. A mark was fixed on the wall of the flume to indicate the horizontal position of the flume bed which was determined by levelling. This mark was fixed at a known distance from the constant pivot of the truss. When the flume is tilted the deflection is measured to a hundredth of a millimetre accuracy and the slope of the bed is calculated. The slope calculated by this method was compared with the water surface slope. This was another check on the uniformity of the flow. The maximum difference between the two methods was about 5 per cent which was considered a reasonable difference due to the difficulty in measuring the slope.

4.4.4 Velocity

For a few runs, vertical velocity profiles were measured. A $\frac{3}{8}$ inch Prandtl-pitot tube connected to a paraffin-water manometer was used. The manometer is shown in Plate 3. It was made of two rigid perspex straight tubes. All the bends were made of soft polythene tubing and the connections were sealed off with Tensol Cement. The closing and opening of air purging outlets was achieved by Hoffman clips fitted to

rubber tubes. The top of the manometer was filled with red paraffin, the specific gravity of which is 0.787 which gives a magnification of about five. The meniscus was sighted using a cathetometer with accuracy of $\frac{1}{100}$ mm as is shown in Plate 3.

Velocity was also measured by monitoring the D.C. component of the anemometer voltage output.

4.4.5 Pressure

Fifteen normal static pressure tappings were taken over the length of one ripple and were connected to the bank of manometers as can be seen in Plates 3 and 4. In every run pressure readings were repeated four times and the arithmetic mean was calculated. The use of the cathetometer enabled the pressure to be read to a $\frac{1}{100}$ mm accuracy.

Dynamic pressure was measured with resistive type transducers. The details of pressure transducers are in Chapter 5.

4.4.6 Surface Shear

Surface shear was measured at some positions along the ripple with a Preston tube. The Preston tube was made of stainless steel hypodermic tubing of 0.152 inch outside diameter. The tip of the tube was machined so as to remove all burrs and to insure smooth flow. The differential pressure was measured using the manometer described earlier. The details of the Preston tube theory and calibration are in Appendix One.

CHAPTER FIVE

PRESSURE TRANSDUCER

5.1 INTRODUCTION

The study of pressure fluctuations in unsteady flow throws some light on the very complex phenomenon of turbulence. In order to measure these pressures accurately, a transducer was required which would be capable of working in water and was of sufficiently small size to be buried in the element. For the intended application the transducer required, in addition, the following characteristics: high sensitivity to measure total head pressures in the region of 0.2 lb/in^2 and fluctuating pressures to $\pm$ 0.05 lb/in^2; high system resonances, to permit frequencies up to 100 Hz to be linearly recorded; low electrical impedance, to permit the use of long signal wires and to simplify electronic amplification. The choice of transducer design was made after careful consideration of all types of transducers, such as piezo-electric, variable inductance, capacitance, etc. The construction was based on the model requirements and on previous experience in transducer design. Two forms of calibration were carried out on the transducer. One was a static calibration to prove its linearity. The second was a pulse test, to determine the frequency at which resonance occurred.

5.2 TRANSDUCER DESIGN

5.2.1 Pressure sensor

The design, based on the requirements set out in the introduction, is for a pressure sensing element which creates a

strain, in a sensor, which in turn produces a voltage that is proportional to pressure. In selecting a suitable strain sensor, consideration must be given to the relationship between strain and resistance change, for any given type of strain gauge. This relationship can be expressed in the following equation

$$\varepsilon' = \frac{\Delta L}{L} = \frac{\Delta R'}{R'} \times \frac{1}{K'} \qquad (62)$$

where ε' is the unit strain, $\Delta R'/R$ is relative change in resistance and K' is the gauge factor.

It can be seen from equation 62 that the resistance change and hence the output voltage change is directly proportional to the gauge factor K'.

For piezo-resistive elements this gauge factor can be as high as 200 whilst for wire and foil type gauges it is between 1.9 and 2.2.

5.2.2 Pressure actuated element

The simplest arrangement for producing a strain from a given pressure is to allow the pressure to influence a thin diaphragm, in a sealed cavity, so as to create a strain in the diaphragm.

By bonding a strain-gauge to this diaphragm the pressure can then be detected.

Consider a clamped circular diaphragm Fig. 8 of radius a', thickness t' at a pressure difference p' between its two sides. The maximum normal stress will occur near the clamped edges. For small loads this stress is given by

$$\sigma' = \frac{3}{4} p' \left(\frac{a'}{t'}\right)^2 \qquad (63)$$

For high loads the relationship becomes non-linear, and this relationship can be expressed generally as

$$\sigma' = \beta' \, p' \, \left(\frac{a'}{t'}\right)^2 \qquad (64)$$

where β' is a function of the dimensionless load factor $\frac{p'}{E'} \times \left(\frac{a'}{t'}\right)^4$.

Thus for practical applications, i.e. within the linear range of equation 65, the strain is given by

$$\varepsilon' = \frac{3}{4} \, p'/E' \, \left(a'/t'\right)^2 \qquad (65)$$

In the light of equations 63 and 65, the stresses and strains in diaphragms made of brass were studied, and the values at which linearity exists between pressures and strains are given in Table 5. It can be seen from this table that a diaphragm having an a'/t' ratio in the region of 100 is the most suitable for this particular application, since its response is linear up to 0.55 lb/in^2 with a strain of about 0.026% for a stress of 4400 lb/in^2. It was because of the very low strains expected that a semi-conductor strain gauge with K' = 200 was selected.

5.2.3 Diaphragm cavity and inlet pipe

For a transducer to have a high frequency response, careful consideration must be given to the dimensions of the diaphragm and of the inlet pipe. Two resonant systems must therefore be considered:

(i) The mechanical resonance of the diaphragm and (ii) the acoustic resonance of the inlet pipe and cavity.

Timoshenko (1961) gives the natural frequency of a vibrating circular plate, clamped at the boundaries as

$$f' = \frac{1}{2\pi} \frac{10.21}{a'^2} \sqrt{\frac{8D'}{\gamma' t'}} \qquad (66)$$

In the case of thin plates the mass of the fluid in which the plate vibrates may considerably affect the frequency. To take this effect into account, Timoshenko uses the following equation

$$f' = \frac{1}{2\pi} \frac{10.21}{a'^2 \sqrt{1 + B_2}} \sqrt{\frac{gD'}{\gamma' t'}} \qquad (67)$$

in which $B_2 = 0.6689 \frac{\gamma}{\gamma'} \frac{a'}{t'}$ where $\frac{\gamma}{\gamma'}$ is the ratio of the specific weight of the fluid to the specific weight of the plate. Therefore in order that f' shall be as high as possible, the plate must have a small radius, whilst maintaining a high a'/t' ratio. Practical dimensions were in fact chosen for the thickness and radius giving an a'/t' ratio of 187. The most practical way of communicating the pressure to be measured to the sensing diaphragm is through a pipe and into a cavity enclosing the surface area of the diaphragm.

In his tests, Burton (1966), treated the inlet pipe and the diaphragm as a simple spring mass system without damping and developed the following equation

$$f' = \frac{1}{2\pi} \sqrt{\frac{gA_1}{\gamma L_1}} \sqrt{\frac{192}{\pi a'^6} \left(1 + \frac{\tau_2 a'^2}{8D'}\right)} \qquad (68)$$

where A_1 is the cross-sectional area of the inlet pipe, L_1 its length, γ', is the specific weight of the diaphragm

material, τ_2 is the tension applied to the edges of the diaphragm and D' is the flexural rigidity, $D' = (Et'^3)/|12(1 - \nu'^2)|$. Burton plotted L_1/A_1 against $1/f'^2$, and obtained a straight line (Fig. 9). An accurate comparison between the gradient computed from equation 68 and that of the experimental line was not possible because the tension τ_2 applied to the diaphragm was not known accurately. However, one may consider that the nature of the relationship between L_1, A_1 and f' is of the type given in equation 68.

5.3 CONSTRUCTION

5.3.1 Transducer

A practical transducer designed to measure the mean and fluctuating components of pressures in a turbulent flow of water is shown in Fig. 10.

The transducer was made of brass, which is non-corrosive in water. The brass diaphragm was clamped at its edges and tensioned in a special jig. The "rings" of the transducer case were then treated with liquid solder and held in contact with either side of the tensioned diaphragm. The whole assembly was then placed in an oven and the temperature was raised to the melting point of the solder. After cooling, the transducer assembly was removed from the jig and excess diaphragm material was trimmed off. The strain gauge was then bonded to one side of the diaphragm. Signal wires were fed out through pre-drilled holes in the case wall and cemented in "Araldite". The back plate, inlet pipe and flange were next cemented into position and a small bleed screw fitted into the side of the cavity, to permit air purging.

5.3.2. Electronic Circuit

Resistance strain-gauges are usually connected to form one or more arms of a Wheatstone bridge configuration. Any resistance changes in adjacent legs of the bridge are algebraically subtractive and those in opposite legs are algebraically additive. Thus equal resistance changes of the same sign in adjacent legs will cause no change in the output voltage. This principle was employed for temperature compensation in this work.

With the abovepoints in mind, a strain gauge was chosen having a double element, the characteristics of which are shown in Fig. 11. As the maximum operating current allowed was 30 mA, the voltage output was consequently low and the use of a high gain amplifier was necessary in order to obtain an output large enough for a tape recorder.

Connected to the simple circuit shown in Fig. 12 the transducer was tested in air to check its linearity and to examine the voltage output before amplification of the signal.

After testing in air, the transducer was connected in the final circuit arrangement shown in Fig. 13 and tested again in water.

5.4 CALIBRATION

5.4.1. Static calibration

The preliminary test of the transducer was carried out in air. The inlet pipe of the transducer was connected to one limb of a methylated spirit manometer. Negative and positive pressures were created by changing the level of

the supply tank. The calibration curve is shown in Fig. 14.

The calibration in water was carried out using a variable head tank, with the inlet pipe of the transducer connected to one orifice in the tank. This tank was provided with an electromagnetic vibrator, a signal generator and amplifier to produce a near-sinusoidal fluctuation of pressure. The static calibration curve in water is shown in Fig. 15.

It is seen from both calibration curves that linearity is well established within the design range.

5.4.2. Frequency response tests.

With the head of water over the inlet pipe kept constant at 5 in. in the variable head tank, the diaphragm response was examined over a band of frequencies.

This test was repeated for four different conditions of inlet pipe. It can be seen from Fig. 16 that the resonant frequency of the diaphragm was 510 Hz. The final arrangement adopted was a lid over the diaphragm with $L_1 = 0$ and a hole of $\frac{1}{8}$ in diameter. From Fig. 17 the resonant frequency of the diaphragm with the final arrangement is seen to be 210 Hz.

5.4.3 Dynamic Calibrations.

In order to test the dynamic performance, and to check the resonant frequency measured in the variable head tank, the transducer was subjected to a step impulse created by an under-water explosion. The explosion, generated as described in detail by Burton (1966) was initiated by charging a condensor with a

high voltage and then discharging it through a fine copper wire as in Fig. 18. The response of the transducer to this explosion was fed via the bridge and amplifier to an oscilloscope where the trace was photographed, as shown in Fig. 19. From the photographs it was possible to approximate closely to the resonant frequency of the diaphragm. The experiment was repeated several times, in various containers, under different heads and for two different inlet pipe arrangements. This was to make sure that the resonant frequency was that of the diaphragm and not of the cavity or the container.

5.5 MOUNTING OF PRESSURE TRANSDUCER

The ¾" diameter transducer was mounted onto the pressure tapping with special arrangements. A strap was bolted to its backplate. This strap can be inserted inside two right angles soldered onto the backside of the triangular element. Turning the transducer anti-clockwise the strap was inserted into the right angles. With a rubber O ring placed on top of the transducer, the pressure was transmitted to the diaphragm through the ⅛" diameter hole. The difficulty in mounting the transducer at different pressure tappings did not allow measurements of dynamic pressure at several locations.

CHAPTER SIX

TURBULENCE MEASUREMENT TECHNIQUES

6.1 INTRODUCTION

It has been established for some time that hot-wire anemometer gives precise results and is easy to use for measuring turbulence in air. Unlike Aerodynamics, Hydraulics is still lacking information concerning turbulence due to difficulties encountered in using hot-films in water.

In this chapter the hot-wire anemometer, as used to measure turbulence in the preliminary investigation, is discussed briefly. Also in this chapter are details of the experiments conducted in the development study for the use of hot-film sensors in water.

6.2 HOT-WIRE ANEMOMETER

Mark I constant temperature anemometer with a standard 5 microns hot-wire probe were used in the wind tunnel investigation. The anemometer and the probes were developed and made in the Institute of Sound and Vibration of the University of Southampton.

The wire, being a resistance material, forms one arm of a symmetrical wheatstone bridge. The wire is heated above the ambient temperature of the surrounding fluid by passing an electric current through it. When the probe is placed in air at rest, a considerable amount of heat will be lost by free convection. The bridge is kept in balance by the servo-amplifier which supplies enough heating current to maintain the wire resistance at a constant value. When the probe is placed in a moving fluid,

the wire will be cooled by forced convection and the servo-amplifier will be required to offset the heat losses by increasing the heating current. The rate of heat loss can be related to the flow velocity and the power supplied can be monitored to give the required information about mean and fluctuating velocity components if the wire and fluid characteristics were kept constant.

6.3 THEORY OF HOT-WIRE ANEMOMETER

From the potential flow theory, heat loss from a cylinder can be expressed as

$$\frac{I'^2 R}{R-Ra} = A'_1 + B'_1 \sqrt{V} \qquad (69)$$

in which I' is the heating current; R wire resistance at operating temperature R_a wire resistance at ambient temperature A'_I and B_1 coefficients and V the flow velocity

Equation (69) may be written as

$$E^2 = R^2_a \, (OR)\,(OR-1)\,(A'_1 + B'_1 \sqrt{V}) \qquad (70)$$

$$= A' + B' \sqrt{V} \qquad (71)$$

where OR is the overheat ratio and equals $\frac{R}{R_a}$ and $E = I'R$

Equation (71) can be written as

$$E = E_o + C' V^{\frac{1}{4}} \qquad (72)$$

where E_o is the voltage output of the anemometer for zero velocity and is a function of the characteristics of the system. The basic problem in non-linear hot-wire anemometry is how to relate the voltage fluctuations resulting from the heat transfer to velocity fluctuation.

In two dimensional flow, when the wire is held perpendicular to the mean flow direction, fluctuation in the wire cooling are essentially caused by the longitudinal velocity component (U). If the wire is placed at an angle to the mean flow direction both the longitudinal and transverse fluctuation components (u,v) will affect its cooling.

From Fig. 21 the numerical value of the velocity vector $\vec{V}$ can be written as

$$V = \{(U + u)^2 + v^2 + w^2\}^{\frac{1}{2}}$$

$$V = U\{1 + \frac{2u}{U} + (\frac{u}{U})^2 + (\frac{v}{U})^2 + (\frac{w}{U})^2\}^{\frac{1}{2}}$$

$$V = U\{1 + \frac{u}{U}\} \qquad (74)$$

by neglecting the higher order terms for low turbulence intensity flow.

The change in slope $\frac{dE}{dU}$ of the calibration curve is assumed to be small over the range of the velocity fluctuations encountered during a measurement (Fig. 20). Thus the tangent to the voltage velocity curve at certain mean velocity may be used to convert voltage fluctuations into velocity fluctuations.

Equation (72) can be written as

$$Eb = C'V^{\frac{1}{4}}$$

where

$$Eb = E - E_o \qquad (75)$$

$$V^{\frac{1}{4}} = U^{\frac{1}{4}}\{1 + \frac{u}{U}\}^{\frac{1}{4}}$$

$$= U^{\frac{1}{4}}\{1 + \frac{u}{4U}\}$$

$$Eb = C'U^{\frac{1}{4}}\{1 + \frac{u}{4U}\}$$

Averaging

$$\overline{Eb} = C'U^{\frac{1}{4}} \qquad (76)$$

$$\sqrt{\overline{u}^2} = \frac{4U^{\frac{3}{4}}\sqrt{\overline{e}^2}}{C'} \qquad (76a)$$

where $\sqrt{\overline{e}^2} = \sqrt{(\overline{Eb-\bar{E}b})^2}$ = R.M.S. (77)

the value $\sqrt{\overline{e}^2}$ is read by an R.M.S. voltmeter. It is necessary to obtain the value of $\frac{dEb}{dU}$ to be able to calculate the root mean square of velocity fluctuation (Fig. 20)

The value of $\frac{dEb}{dU}$ which is $\frac{CU^{\frac{1}{4}}}{4U}$ can be obtained either by plotting it against U graphically or from the above expression. The expression for $\frac{dEb}{dU}$ was calculated and plotted against U.

6.4 HOT-WIRE MANUFACTURE AND CALIBRATION

The wire material used in the investigation was tungsten. The diameter of the wire was 5μ and was provided by Mullard Raw Materials Division. The part of the wire which is cooled by the flow is 2mm long. The attachment to the probe support must be made carefully so as to avoid any interference with the flow past the wire. An arrangement to make the soldering of the wire possible is made by plating tungsten with other material. The material used to plate tungsten is copper and the method followed is described here briefly (Fig. 22). A special plating bath with a bridge of 2mm width running across it, is used to plate the wire leaving the active part of it exposed.

The plating bath is filled to the top with copper sulphate solution with 10% excess sulphuric acid.

A low tension D.C. supply is connected to the bath so as to connect + to the bath and the negative to the wires and

the frame. The plating current should not exceed 0.1 mA for the first two minutes and afterwards this could be doubled. The plating will result in increasing the wire diameter to around 25μ. The probe was made from ⅛" stainless steel cable with nickel conductors. The wire is soldered to the probe tips by mounting the probe to a micromanipulator and the frame, with wires wound to it, is clamped to a bench vice so that the wire can be accurately positioned relative to the probe. Calibration curve of the standard probe with the different wire used in the investigation are shown in Fig. 23 . The calibration of the hot wire was made against a pitot tube connected to an air-water manometer.

6.5 HOT-FILM CHARACTERISTICS

6.5.1. Introduction

The hot-wire sensor is not readily adaptable for use in water. Dirt generally, but particularly fine fibres, collect around the wire after a relatively short period. At the same time, the high local heat transfer rate may result in the formation of bubbles on the surface of the wire. The consequent change in the heat transfer characteristics between the wire and the fluid causes a large amount of "drift" or variation in the electrical signal for a constant fluid velocity.

Results reported by a number of investigators indicate that the most successful form of sensor for use in water is the hot film. The sensing element of this device consists of a thin platinum film, fused to a glass surface and with the connecting wires embedded in the glass. The

film can be formed on the tip of a wedge or parabolic sensor, or slightly back from the tip of a conical probe, as shown in Fig. 24.

6.5.2. Basic principles

Because of the effect of temperature change on the electrical resistance of most materials, there is an approximately linear relationship between the temperature of the sensor and its resistance.

Experience has shown that constant temperature operation is in general most satisfactory for heated sensors. An outline arrangement is shown in Fig. 25 in which the sensor forms one arm of a wheatstone bridge. A change in the fluid flow conditions over the sensor will cause the sensor temperature, and hence its resistance, to change by very small amounts. This produces an error voltage (e') across the bridge, which when amplified by A, causes the current through the sensor to change restoring, its resistance to a value close to the original. Hence the sensor resistance is virtually constant, regardless of flow conditions. The bridge voltage will vary, however, and this can be related to the flow velocity of the fluid.

With the sensor held in the fluid at rest, a considerable amount of heat will be lost by thermal convection. This means that the amplifier A must supply a finite current through the sensor for zero fluid velocity.

If the output voltage of the amplifier for zero fluid velocity is E_o, the output voltage of the amplifier for a given steady fluid velocity will be

$$E = E_o + G'e' \tag{78}$$

where G' is the amplifier gain and (e') is the amplifier input signal, i.e. the error voltage.

From the electrical properties of the bridge circuit

$$e' = \left(\frac{R_1}{2R_1} - \frac{R}{R + R_r}\right)E \tag{79}$$

combining equations (78) and (79)

$$E = E_o + G'E\,\frac{R_r - R}{2R_r + R} \tag{80}$$

or

$$\frac{R}{R_r} = \frac{G' - 2\,(1 - E_o/E)}{G' + 2\,(1 - E_o/E)} \tag{81}$$

If the amplifier gain G' is made ufficiently high, the value of R/R_r can be made very close to unity, so that the sensor resistance R will remain substantially equal to the value of the reference resistance R_r, despite variations, in the heat lost to the fluid. The value of the reference resistance is selected to correspond to the desired sensor operating temperature. The relationship between fluid velocity and heat transfer from the sensor was systematically investigated by Ling (1960). The electrical power consumed can be related to the difference between the hot film temperature T' and the ambient fluid temperature T_a by a heat transfer coefficient which is a function of the fluid velocity U and the fluid properties. The value of the heat transfer coefficient is almost independent of the value of T_a, although dependent on the hot-film temperature. The general relationship between the anemometer output and the flow velocity is

$$E^2 = A'' + B'' V^n \tag{82}$$

where n depends strongly on flow velocity. Richardson (1968) reported that n for a cylindrical film of 0.002 in diameter was 0.31 for velocities between 0.2 and 0.6 ft/sec, 0.35 for velocities from 0.6 to 1.5 ft/sec and 0.45 for velocities from 1.5 to 3 ft/sec.

In the present investigation, the precise value of n was not required. The anemometer Type ISVR 201 was provided with two outputs; linear and non linear. The films were calibrated by various methods to obtain non-linear calibration curves accurately. Then, with the non-linear calibration curve in hand, the linearizer circuit was set to follow the inverse of the voltage-velocity characteristics of the type of probe used.

6.5.3. Temperature compensation

For a given steady fluid velocity U, the heat transfer relationship can be written

$$\frac{E^2}{R} = H(T_1 - T_a) \tag{83}$$

where H is heat transfer coefficient. For an increase ΔT in the ambient temperature of the fluid, the velocity U remaining constant, the voltage will change to E_1, the new conditions being expressed by

$$\frac{E_1^2}{R} = H(T_1 - T_a - \Delta T)$$

If ε is the relative voltage drop due to the fluid temperature change ΔT, that is

$$\varepsilon = \frac{E - E_1}{E}$$

then

$$\varepsilon = 1 - \left(1 - \frac{\Delta T}{T_1 - T_a}\right)^{\frac{1}{2}} \tag{85}$$

For a typical case of a hot wire in air, with a value of (T_1-Ta) of, say, 300°C and a value of T around 10°C, the relative voltage change is 0.02.

For a model test in water, in which the water temperature was completely uncontrolled, ΔT could be of the order of 10°C, due to heating from pumps etc. If T_1-Ta has an initial value of about 35°C then the relative voltage drop is 0.15. Hence some method of temperature compensation or, alternatively, close control of fluid temperature is essential.

Two different methods were used to compensate for change in ambient temperature.

a) From equation (79) it is clear that any resistance change in adjacent legs are algebraically substractive. If the rate of resistance change, in the leg adjacent to the probe, can be maintained equal to that of the probe; ambient temperature fluctuations will have no effect on the probe output.

In Fig. 25 this principle is outlined. A box containing two potentiometer RL, Rp is connected to the compensating resistance and the box respectively. The basic requirement for the compensating circuit which has an equivalent resistance Rc is

$$\Delta Rc = \beta' \Delta Ra_1 \qquad (86)$$

where β' is compensation coefficient which varies according to temperature coefficient of the compensating resistance. In the present work $\beta' = 5$.

b) For zero velocity of flow, equation (83) becomes

$$\frac{E_o^2}{R} = H_o (T_1 - T_a) \qquad (87)$$

If the fluid temperature T_a varies, the output voltage E_o for zero fluid velocity will also vary. If the amplifier output is adjusted to bring E_o back to its original value, then the output voltages for all other points on the calibration curve will similarly coincide. This adjustment was checked at the beginning of every run.

Under fairly precise laboratory conditions, such as might be encountered during experiments mainly concerned with hot film measurements, the fluid temperature can be thermostatically controlled to fairly fine limits. When hot-film measurements only represent part of the investigation, somewhat coarser control is satisfactory. In the present investigation, the town water supply is generally colder than water in the laboratory and it was found that a small, controlled input of town water can maintain the water in circulation at a temperature constant to about $\pm \frac{1}{2}C^{o}$ and this degree of control was acceptable for most measurements.

6.5.4. Frequency response

When turbulent velocity fluctuations, which cause the instantaneous velocity to be greater or less than the mean velocity U, occur in the fluid the question of frequency response arises. It is important to know, whether the effect of heat storage in the hot-film and its support, combined with the bridge and amplifier loop etc, will cause distortion, so that the output signal from the bridge will not represent the true velocity fluctuations.

One way of assessing the dynamic performance of the hot-film anemometer is to produce a shock wave and to record

the time trace of the resulting output signal. Alternatively, if a small square wave Δe is injected into the bridge, as shown in Fig. 26, an instantaneous change in (e') will be reflected by a change ΔE in the bridge voltage. The change in bridge voltage will initiate a change in temperature, and hence resistance, of the sensor. A new equilibrium position can be set up, and the speed with which this is accomplished is a measure of the dynamic performance of the system. The time trace follows a typical exponential curve, from the properties of which the time constant τ' can be read off at a value corresponding to 0.37 δ (Appendix 2 and Fig. 66).

Fig. 27 shows a line drawing of the oscilloscope trace from this type of dynamic test on a parabolic hot-film sensor. The time constant may be read off as approximately 0.42 milliseconds. From this, allowing for a reasonable safety margin, it appears that the frequency response is satisfactory for measuring turbulent velocity fluctuations with frequencies up to about 400 Hz.

6.5.5. Stability

- In Fig. 28 the results of some stability tests carried out in the present investigation are plotted, and for purposes of comparison, some tests by Delleur (1966) are also shown. For these tests the hot-films or wires were either placed in a stream of water flowing at constant velocity, or, alternatively, rotated at a constant speed in a circular testing channel containing water. The temperature of the water was kept

approximately constant throughout the tests.

In Fig. 28 E_t is the output voltage after time t has elapsed and E is the output voltage at the commencement of the test. The variation of the ratio E_t/E is shown for continuous tests lasting up to 6 hours.

A Thermo-Systems quartz-coated parabolic hot-film sensor in de-ionized water gave an output voltage which showed effectively no variation over a period of 6 hours. In this test precautions were taken to eliminate dirt and air bubbles as far as possible.

Tests with the same sensor in tapwater, with no special precautions other than temperature control, gave results which could equally be regarded as very satisfactory, the drop in output voltage after 6 hours being only 1.55%. A thermo-systems quartz - coated conical hot-film in tap water gave comparable results, about 1% drop in output voltage after 6hours. Variations of output voltage of this order do not suggest contamination from dirt.

In addition, some tests on uncoated hot-wires by Delleur (1966) have been re-interpreted, and plotted in Fig. 28. They show a reduction of output voltage of up to 4% in tap water after 5 hours. Tests were under carefully controlled conditions Fig. 28 also shows one of the results of a number of stability tests carried out in the present investigations on uncoated hot-wires in tap water, when no special precautions were taken. Conditions were perhaps typical of a normal hydraulic model test except that some fine screens were fitted at

the inlet to the flume. The ratio E_t/E fell sharply, there being a 16% fall in output voltage after about 3 hours. Most of this reduction could be attributed to the collection of fine fibres around the wire. It seems evident that, unless the most stringent precautions are taken, hot wires cannot give stable results in water.

During routine tests with hot-films in water, it was found an acceptable procedure to set E_o to its correct value at the beginning of operations, and to check three points on the calibration curve. Three points on the calibration curve are again checked at the end of the run.

6.5.6. Calibration

The function of the linearizer is to produce a linear relationship between the output signal and fluid velocity. This greatly facilitates the direct introduction of the electrical output into analysing equipment. In contrast with non linearized signal, fluctuations of the linearized output signal about the mean represent the turbulent velocity fluctuations directly. The anemometer type ISVR 201 is outlined in Fig. 29 and shown in plate 6. The stability control adjusts the gain of the loop formed by the bridge and amplifier A_1. Amplifier A_2 is simply a calibration device, in which the off-set control serves to remove the standing voltage E_o at zero flow, and the gain control, marked calibrate can be adjusted to compensate for variation in sensor characteristics. A_3 is the linearizer amplifier.

A major problem in the low speed calibration of hot-films is to provide a uniform flow with a known speed. At relatively high speeds, pitot tube may be used for calibration purposes. The conical probe was calibrated in a circular tank which was rotated by a D.C. motor with a variable speed control. The box of the tank was fitted with small paddles to maintain the water speed at that of the tank. On the outer part of the tank a 6 inches channel was used for calibration.

Prior to filling the tank with de-ionized water, it was rinsed thoroughly with tap water and then with de-ionized water. Subsequently the tank was filled with water and allowed to stand still for 24 hours to liberate all air bubbles. To check the precision of the calibration procedure, the operation was checked against pitot tube. To this end, a normal pitot tube was placed at a selected point and the velocity was determined for different speeds of the motor. The pitot tube was then removed and the probe placed in the same position and the speed of the motor was altered as before.

Because the rotating tank was not available permanently, a calibration device proved very simple to use for the calibration of the parabolic hot-film and it is shown in Fig. 30. The sensor is positioned on the centre-line of a one inch diameter perspex pipe, through which the discharge can be varied. The velocity at the centre line is known from generalized velocity data.

Fig. 31 shows the results of calibration tests, carried out in the rotating tank, for a conical quartz coated hot-film sensor in de-ionized water. The initial calibration was carried out at a fluid temperature of 15°C, and the calibration curve is shown in the full line
The dotted lines were derived from this curve for other values of fluid temperature, using equation (79). Corresponding tests points are shown, and these compare quite well with the derived curves.

In Fig. 32 results are shown for calibration tests on a quartz coated parabolic hot-film sensors in tap water. The test facility was the perspex pipe shown in Fig. 30. The non linearized and linearized calibration curves are shown, and these are consistent.

6.6 OPERATIONAL DIFFICULTIES

6.6.1. Ageing of hot film.

The use of hot-wires in air and hot-films in water is by no means perfect. The most serious problem encountered with turbulence measurements is drift. When the parabolic film was new, the drift was within acceptable limits as was shown earlier. Every run did not take longer than 20-30 minutes. With the frequent use of the film, the quartz coating started to become worn out and drift started to become high (about 10% within 30 minutes). Fortunately, this occurred near the end of the experimental programme.

A microscopic examination of the film tip revealed that the coating had almost been worn out and the film itself had become thinner in the middle which caused its resistance to go up to about 8.25Ω (the

original was 8.11Ω). This rise in the resistance caused a slight change in the calibration curve and subsequent adjustment to the anemometer was found necessary. It is estimated that the film had been used for about 40 hours in a very turbulent flow but in relatively clean water. The time during which the film could be used was given by the manufacturers to be around 500 hours. This figure is too high. It might be valid for less turbulent flows and lower velocities. But what resulted from these experiments was that the film may behave in a peculiar fashion after 30 hours of being in use.

The anemometer itself was reliable. Its versatility made it possible to operate different types of probes with different characteristics by changing the linearizer card with some minor adjustment to the different amplifiers.

6.6.2. Operational difficulty in measurements.

The flume in which experiments were conducted had not been designed for refined measurements of fluctuating quantities. The most serious effect of the extraneous noise was the vibration in the body of the flume resulting in the vibration of the mass of water. This vibration was caused by the pump, the return pipe and the valve mounted to it. The speed of the pump drive was 1450 revs/min. The vibration was reflected on the frequency spectra where a semi-peak appears in the region of 20-25 Hz. The effect of this vibration on the root mean square values is believed to be around 5 per cent.

6.7 PROCESSING OF TURBULENCE DATA.

The data collected on turbulence were stored on a magnetic tape. The tape recorder used was a Thermionic 2000. The gain control on the tape recorder was set for all the signals at a value of about 10.

Subsequently data were processed at the Data Analysis Centre of the Institute of Sound and Vibration. The Centre is equipped with a digital computer which has two parallel channels of analogue to digital converters. The computer was already programmed to carry out most of the analyses needed in random data processing. The system is controlled by pressing few buttons to answer specific questions asked by the machine in plain English. Data output from the machine may be punched on paper tape or in graphical form directly onto a graph plotter. All the results were obtained in graphical form with a suitable scale.

The details of operating the machine are to be found in Memorandum ISAV No. 209.

An example is given here for analysis carried out to obtain frequency spectrum.

The questions to be answered to the machine are the following

Q What is the analysis required?

A Spectral analysis. The programme is fed

Q How many samples are required?

A Any number up to the capacity of the machine

Q What is the sampling rate?

A A multiple of 312.5/sec not exceeding the capacity of the machine

Q Is wave form required?

A Yes or no

Q Is power spectrum required or cross spectrum?

A Zero for the first, one for the second

Q What is the lowest frequency of interest

A Any thing down to nearly zero

Q What is the highest frequency of interest?

A Any thing up to the capacity of the machine

Q What is the desired output medium?

A One if graph only, two if paper tape only and three for both

Q What are the scales of the graph?

A Any thing up to 12" x 12"

Start now

The answers are punched in order on a tape and fed into the machine. The machine can analyse signals with a frequency content from 0 to 20,000 Hz. The maximum sampling rate is 40,000 samples/sec and the minimum is 312.5 samples/sec. The choice of conversion or sample rate is obviously not arbitrary but must be greater than twice the highest frequency present in the signal if aliasing is to be avoided (as was explained earlier).

The maximum number of samples is 16000 samples but with the disc two million words can be stored.

CHAPTER SEVEN

PRESENTATION OF RESULTS

7.1 COMPONENTS OF RESISTANCE TO FLOW

7.1.1. Selection of triangular element.

The element which was used to simulate ripple formation in alluvial rivers has a triangular shape with a mild slope upstream and a 30 degrees angle downstream. The dimensions are given in details in Fig. 3. Its general pattern, although may not exist in nature, is very similar to typical bed formations in alluvial rivers. The dimensions chosen associated with the flow conditions selected may represent dunes for relatively fine sand or ripples for relatively coarser sand.

7.1.2. Resistance to flow.

The form drag for the element was measured for three depths 6", 9" and 12" in flume experiments. For every depth the form drag was measured for seven different average velocities. For the same flow conditions direct surface shear measurements were made. The sum of the two components was compared with the total shear calculated from depth and water surface slope measurements.

7.2 COMPARISON BETWEEN FLOWS OVER RIGID BEDS AND IN ALLUVIAL RIVERS

Velocity measurements were made for different flow conditions. Three typical depths which have the same shear velocity were selected. Characteristics of the

flow in the present investigation and those of the flow in some alluvial rivers were compared. This comparison included the variation of resistance to flow, the effect of relative roughness and the variation of the Von Karman constant.

7.3 MOMENTUM BALANCE

For a 12" depth and a velocity of 1.89 ft/sec which represents a Reynolds number 1.56×10^5 the momentum balance was studied.

7.4 TURBULENCE AND PRESSURE FLUCTUATIONS.

Turbulence measurements were made for 12" depth and two Reynolds numbers namely 1.08×10^5 and 1.56×10^5. For the two cases mean velocity was measured for different locations and the variation of turbulence intensity with relative position was studied. Also some turbulence measurements made by Sheen (1964) were plotted for comparison. Auto-correlation and frequency spectrum functions were evaluated for selected positions for the two cases. Spatial correlation function and macroscale of turbulence were evaluated for one velocity at different relative positions. Probability density functions were evaluated for one velocity and three different relative positions.

7.5 COMPARISON OF FLOW IN WATER AND IN AIR

The characteristics of flow over an adverse slope and a triangular element at different locations was made for a Reynolds number of 1.75×10^5. The Reynolds

number is based on the reference velocity and the reference half depth. Autocorrelation and Frequency spectrum functions were also evaluated for one Reynolds number and different relative positions.

CHAPTER EIGHT

COMPONENTS OF RESISTANCE TO FLOW

8.1 NORMAL PRESSURE DISTRIBUTION

In Fig. 33 the normal pressure distribution in excess of hydrostatic is shown for one foot depth and several velocities. From Fig. 33, it can be seen that the pressure distribution diagram may be divided into three distinct regions :

a) The region of negative pressure which represents the continuation of the third region of the preceding element. This region is characterized by diffusion downstream of turbulence from where it was generated.

b) The region of positive pressure which contains the reattachment of the main flow to the boundary. In this region the stagnation point, which represents the re-attachment point, is marked by a local rise in pressure, and it may be said that the point of maximum pressure is the re-attachment point (this is supported by the streamline pattern as will be seen later).

c) The lee region where pressure decreases rapidly and attains its maximum negative value and then starts to increase. As the re-attachment point is represented by the point of maximum pressure, it may be expected that the point of maximum negative pressure represents the first appearance of separation (although this is not very clear from the streamline pattern).

It can be seen from Fig. 33 that there is a definite trend in the pressure distribution indicating that for a constant flow depth the curve of pressure distribution over the bed tends to be similar for all velocities.

Pressure distributions for two other depths (0.75 ft and 0.5 ft) are given in Tables 11 and 12. By inspecting their values, it appears that the qualitative nature of the distribution of mean pressure is independent of flow depth and velocity. It seems possible that the distribution of mean pressure is, rather, a function of the geometrical characteristics of the element (even though the form drag varies with depth and velocity).

8.2 SURFACE SHEAR DISTRIBUTION

In Fig. 34 the surface shear is plotted for one depth (12") and several velocities. From tappings 4 to 10 measurements showed steadily increasing shear stress and this is evident for all the curves. From tapping 1 to 4 the shear stress was negative and of small values. Since there was only one tube of outside diameter $d_o = 0.152$ inches to be used the small values of $(P_t - P_o)$ would result in

$$\log \frac{(P_t - P_o)\, d_o^2}{4 \rho \nu} < 4.5$$

in which case the formula given by Preston is no longer valid (Appendix 1).

Any transfer of quantitative nature of the results obtained over artificial roughness to natural loose beds is misleading. The grains in motion in alluvial channels would affect the order of magnitude of the stress measured on the fixed bed model, and it may even change the shape of the curve altogether.

Therefore, Fig. 34 may be looked upon as an indication of how the shear stress varies over the inclined surface without any reference to the nature of surface texture. Also, the combined action of surface shear and turbulence in connection with the development of the boundary layer may be better understood in the light of surface shear distribution.

Surface shear distributions for the other two depths is given in Tables 11 and 12. From Tables 11 and 12, it appears that the distribution

of surface shear has the same shape for different depths and velocities. This suggests that the shape of surface shear distribution depends on surface roughness and the geometrical characteristics of the body (even though the magnitude of surface shear depends on flow conditions).

8.3 MEAN VELOCITY AND STREAMLINE PATTERN

In Fig. 35 the distribution of mean velocity and streamline pattern are shown for 12" depth and a Reynolds number of 1.08×10^5.

A study of the velocity profiles reveals that there are three distinct regions of different characteristics and they may be described separately -

(a) The lee of the element

(b) The back flow region

(c) The region of upstream face

The first region is no doubt the main source of turbulence. The velocity gradient is very high just past the crest of the element, reducing its value quickly throughout the region of back flow. At this region most of the turbulence is generated and the reduction in the velocity gradient is a result of the mixing effect of this turbulence.

At the back flow region, separation occurs resulting in further reduction of velocity gradient and a flow in opposite direction to the main stream.

At the region where the flow re-attaches itself to the boundary, the flow assumes a different pattern and the velocity gradient decreases along the upstream face.

From the velocity profiles the mean streamline pattern was developed. It is not assumed that the positioning of the streamlines is accurate, but it is expected that the flow pattern over the triangular elements will display that general shape. It is not possible to construct an accurate diagram of the streamline pattern due to two reasons :-

(a) Velocity profiles, on which the prediction of the streamlines is based, are not plotted with certainty especially very close to the boundary, where a uniform distribution is always assumed.

(b) The assumption, on which the theoretical aspect is based, was made that the flow is irrotational. This assumption is not valid because the flow over the triangular elements is of a developing boundary layer type especially after the re-attachment point. Nevertheless, the streamline pattern may be looked at as an indicative diagram. The values of the stream functions are relative ones.

The general pattern of the streamlines in the main flow is sinusoidal. It falls over the crests of the elements and starts rising just past them. The top of the streamline zero and the crest of the following element act as an imaginary boundary to the main flow. The latter is in phase with the former and is out of phase with the actual boundary. The streamline pattern highlights the pressure distribution curves discussed earlier. The pressure is negative where there is a back flow and it starts to increase where the interface starts to direct itself towards the boundary and at the re-attachment point, which is at a distance downstream of about 4 times the height of the crest, the pressure attains its maximum positive value.

After the re-attachment point, the streamlines converge due to the increasing velocity, and the pressure starts to drop and it attains the value of zero where the streamlines fall to their lower point just before the crest. With decreasing pressure, separation occurs past the crest and the whole pattern is repeated periodically.

Comparison of mean velocity distribution in Fig. 35 with that shown in Fig. 36 for Re = 1.56×10^5 shows that they are similar and almost identical. It is not expected that the Reynolds number would be an important factor in the interaction between the elements at the bed and the main flow.

A noteworthy point is that the maximum velocity close to the water surface changes slightly with positions along the element, whereas, the velocity near the boundary depends largely upon the location. This point is compatible with the assumption made earlier that the elements act as roughness elements of large scale.

It is commonly taken for granted in most boundary layer equations, although the assumption appears not to have a proper theory, that the point of separation coincides with the point of zero wall frictions. What can be said from observations of separated flows is that the two points are usually close; experiments are hampered by the instability of the flow on the downstream side of the separation point and by the lack of adequate measuring devices to detect any change in the wall friction. The important conclusion that could be drawn from the boundary layer theory is that, provided the distribution of the mean velocity remains unchanged, the position of the point of zero wall friction is independent of the Reynolds number. By the same reasoning, the re-attachment point is independent of the Reynolds number and this is what was found in the present investigation.

8.4 BALANCE OF RESISTANCE COMPONENTS

In Table 1, 2 and 3, the two components of the resistance to flow are shown for the 12", 9" and 6" depth of flow respectively. The mean shear τ_0 in column 2 was computed from depth and slope measurements.

In column 3 is the contribution of form drag to the total shear and in column 4 is the contribution of surface shear to the total shear. Both column 3 and 4 were deduced from the direct measurements of normal

pressure and surface shear. In column 5 is the relative error of the balance.

In Table 1, 2 and 3 the sum of the form drag and skin friction falls short from the total resistance, before performing side wall correction, by a relative error which ranges from 7.55% to 12.3% in Table 1, from 0.365% to 12.2% in Table 2, and from 5.34% to 11.07% in Table 3.

The relative errors here are reasonable and are caused by experimental imperfections. Side-wall correction was performed using Einstein-Johnson method and the results are presented in column 6 for the bed shear . The balance of resistance components was studied again using the "adjusted" shear. Inspection of column 9 in Tables 1, 2 and 3 reveals that the relative error increased considerably in the case of the two depths 12" and 9". The re-calculation of the balance has little effect in the case of the shallower depth. It appears that the side-wall correction in the case of deep flows is not accurate when Einstein-Johnson method is used. Since the direct measurements of form drag and surface shear are more reliable than the indirect calculation of the bed shear, Einstein-Johnson method is not the real answer to the non-uniformity in shear distribution. The discrepancies found between the total resistance as calculated from measurements of slope and depth and the sum of surface shear and form drag may be attributed to the following reasons :

(a) When Einstein's method for side wall correction was performed, the resulting total resistance of the bed was greatly exaggerated in the case of deep flows, whereas, it was not when the flow was shallow.

(b) In deep flow the boundary layer was not fully developed, and its development throughout the flow field necessitated energy consumption. This energy was provided by the mass of flow which would result in further drop in pressure.

(c) There are two other possible sources of error, the accuracy of slope measurements and the effect caused by pressure fluctuations. The former was checked always by direct measurements of the bed slope and compared with that of the water surface, whereas the effect of pressure fluctuations was very difficult to determine because mean values were read off visually. Obviously, some erroneous readings were inevitable in this case.

(d) It was thought that the Preston tube used in the present investigation might have been another source of error because it was not calibrated. On second thought, the balance reveals that the effect of the Preston tube, if any, would be negligible because the contribution to the total resistance of the surface resistance is very small and any error in lack of Preston tube calibration would not be expected to affect the balance of resistance considerably.

8.5 MOMENTUM BALANCE

As an alternative to the energy equation, the integration of the momentum equation over an element of the bed can be presented graphically. This equation is plotted in Fig. 37. From the equation the momentum flux of the mean and turbulent component of the flow is balanced by the body force, normal forces, and tangential forces. The value of the term $\rho\int U^2 dy$ is read off on the right hand side and the values of all the other terms are read off on the left hand side.

Inspection of Fig. 37 reveals that the difference between the two sides is at its peak in the back eddy region, it becomes zero at the middle, and it goes back to a peak value at the lee region.

Velocity and turbulence profiles were not extended sufficiently close to the boundary where the gradients are very high; assumption had to be made to complete profiles down to the boundary.

In addition, the measurements at the two regions, where discrepancies were at their peaks, were not of reliable accuracy as to make a sum of very small quantities give the right answer.

If accurate measurements of mean and fluctuating components of velocity are possible, another check on the resistance to flow can be made.

CHAPTER NINE

FLOW CHARACTERISTICS IN LABORATORY FLUME AND ALLUVIAL RIVERS

9.1 EFFECT OF DEPTH ON RESISTANCE TO FLOW

9.1.1 Flume experiments

The phenomenon of resistance to flow of bed formation cannot be separated from the depth of flow. In the case of deep flows, bed formations diffuse their influence on the flow within a limited region and they act as though they were roughness elements of large scale. When the depth of flow decreases, the relative area of influence increases and bed formations begin to act differently upon the flow. When a certain critical depth is reached, the whole basic nature of resistance to flow assumes a different pattern and bed formations begin to play an important role as cross-sectional non informity elements.

Therefore, when analysing the resistance to flow of bed formation particular attention must be focused on the inter-relation between bed formations and the depth of flow.

In Table 4 some results of the variation of resistance to flow with change in flow condition obtained by Vanoni (1967) in a 46 ft. flume are given.

From Tables 1, 2 and 3 if the fluctuations of the ratio $\frac{\tau_F}{\tau_o}$ for one depth are overlooked (these are caused by experimental imperfections), it can be seen that the contribution of form drag to total resistance increases when the depth of flow decreases or, in other words, when the ratio h/d increases.

For the 12" depth the contribution of the form drag is about 80%, whereas it is about 90% for the 6" depth.

The bed form resistance f'_b given by Vanoni was reduced to bed shear and the contribution to the total resistance was calculated.

It appears from Vanoni's results that the effect of depth on the form drag is similar to the effect found in the present investigations. In the first set it can be seen that the ratio $\frac{\tau_F}{\tau_o}$ varies from 91% to 83.5% for h/d of 1/3.3 and 1/9.1 respectively, h being the average height of the bed forms and d the depth of flow. In the second set the ratio $\frac{\tau_F}{\tau_o}$ varies from 84% to 75.5% for h/d of 1/4 and 1/10.5 respectively.

9.1.2 Observations in alluvial rivers

The effect of the variation of the relative roughness $\frac{h}{d}$ is not the same in model and prototype. In Fig. 38 the form drag friction factor f''_b is plotted against the particle Froude number for a variety of rivers. Details of flow conditions are known for two rivers, the New Bedford River and the Nene.

The New Bedford River is an artificial trapezoidal channel in the Great Ouse Basin (Plate 7). It is a tidal river. The depth of flow varies from 3.5 ft to about 11.5 ft and the average velocity varies from 1.2 to about 3.5 feet/sec. Observations showed that its bed is covered with ripples only.

It appears from Fig. 38 that the form drag friction factor f''_b is strongly dependent on the particle Froude number and less dependent on the relative roughness.

In the Nene Estuary, the bed material is coarser and the flow is deeper. Observations showed that the bed is covered with dunes (about one foot high and twenty feet long). These dunes are not affected by the influence of the tidal cycle. Here again, Fig. 38 shows that the form drag friction factor f''_b is a function of the particle Froude Number $\frac{U}{\sqrt{gD50}}$.

It may be concluded that for a small relative roughness the form drag friction factor depends strongly on the particle Froud number.

There is no sufficient observations to make any accurate comparison possible between the form drag friction factor in model and prototype.

9.2 EFFECT OF DEPTH ON VELOCITY DISTRIBUTION

9.2.1 Flume experiments

From Equation 18 the effect of change in flow depth on velocity distribution can be studied. For the same shear velocity U* and the same roughness Δ, Equation 18 is expected to give the same velocity U at the same height y above the bed irrespective of the depth of flow. This conclusion is to be expected if two conditions are satisfied. Firstly, the roughness Δ must act upon the flow in the same manner irrespective of the depth of flow. Secondly, the Von Karman "constant" K must be constant for all flow conditions.

These two conditions do not seem to be satisfied in the flume experiments. In Fig. 39 three velocity profiles are shown. The shear velocity U* is nearly the same although the depth of flow varies from 6" to 12". Here the value of Δ is the same even though its influence varies with a change in depth of flow. Fig. 39 shows that for the same height above the bed y the velocity distributions do not overlap, i.e. do not give the same velocity U. Fig. 39 suggests that for shallow flow Δ must be greater than its value for deep flow. This is reflected upon the form resistance. For the 6" depth the form resistance F_D = 0.152 lb/element, for the 9" depth the form resistance is F_D = 0.146 lb/element and for the 12" depth is 0.128.5 lb/element.

9.2.2 Observations in alluvial rivers

In Fig. 40 three velocity profiles are shown for three different depths. The shear velocity is nearly the same for the three depths. From Fig. 40 it appears that away from the influence of bed formations, the velocity profiles overlap. The deviation from overlapping is caused by two

Factors. There is a discrepancy between the shear velocity as calculated from slope and depth measurements and that deduced from velocity distribution assuming the Von Karman K to be 0.4. This discrepancy appears to be present in several cases in the New Bedford River observations. The same discrepancy between the two shear velocities was observed in flume experiments.

This kind of discrepancy suggests that a deviation of the Von Karman K from 0.4 might be possible or a modified depth should be used to calculate the shear velocity.

In Fig. 41 three velocity profiles in flume experiments are plotted on a logarithmic scale. The shear velocity as calculated from slope and depth measurements is nearly the same for the three cases, being 0.206, 0.198 and 0.198 ft/sec for the three depths 6", 9" and 12" respectively. It appears that from the velocity profiles shown in Fig. 41 the shear velocity cannot be deduced assuming the Von Karman K to be 0.4 and using the shear velocity as calculated from the water surface slope and the total depth.

In Fig. 42 three velocity profiles from the New Bedford River observations are plotted on a logarithmic scale. The three profiles are for different depths but for nearly the same shear velocity; the latter being calculated from water surface slope and depth measurements assuming a Von Karman K to be 0.4. Fig. 42 shows that the three velocity profiles are not parallel although the shear velocity for the three curves is the same. Since water surface slope and depth measurements are fairly reliable in the New Bedford River it seems possible that the Von Karman K deviates from 0.4.

Indeed, the shear velocity calculated from depth and water surface slope measurements was substituted in Equation (13) to calculate the Von Karman K. This calculation was repeated for several cases in the New Bedford River and the results are plotted in Fig. 43. Fig. 43 shows that the Von Karman K is different from 0.4 for most of the cases. This difference can be attributed,

among other factors, to the presence of sediment in the stream which would change the eddy structure in the flow.

CHAPTER TEN

TURBULENCE AND PRESSURE FLUCTUATIONS IN FLUME EXPERIMENTS

10.1 TURBULENCE INTENSITY DISTRIBUTION

The distribution of root-mean-square values of the fluctuating longitudinal component (u) is shown in Figs. 36 and 44 for the Reynolds numbers 1.08×10^5 and 1.56×10^5 respectively.

In Fig. 36 the root-mean-square values are shown for $\bar{U} = 1.32$ ft/sec and 12" inches depth. It can be seen that turbulence attains its maximum generative force in the region of the back eddy and it starts to decrease after the re-attachment point but it does not reach its background level. The energy of turbulence is no doubt generated where turbulence level is at its maximum. When turbulence energy starts to decrease dissipation and diffusion absorb a fair amount of the turbulence. From Fig. 36 and 44 it is clear that turbulence is very high before the re-attachment point is reached. This is obvious because much of the turbulent energy is needed to maintain a vortex layer of turbulence-producing nature which contributes, to a great extent, to the occurrence of the mixing phenomenon where separate layers of fluid at different velocity exist.

At the back eddy region the peak value of $\sqrt{\bar{u}^2}$ is five times its minimum value and it decreases to two times just before the crest. This definite trend is not evident for the lower velocity where the ratio of the peak value of $\sqrt{\bar{u}^2}$, at the back eddy region, to the minimum value is two and it is reduced to one and a half just before the crest. It is not certain whether this represents any real difference that warrants explanation of any hydrodynamic nature. It is probable, however, that the additional turbulence generated by the bed elements in the case of the lower velocity has its relative influence curtailed due to the high level of background turbulence.

An inspection of the integration $\int \bar{u}^2 \, dy$ for the higher velocity which represents the rate of turbulence generation helps to understand the process of turbulent actions.

In Fig. 37, the back eddy region represents the high content of turbulent energy. After reaching the re-attachment point, the integration decreases because the rate of turbulence generation is not equal to the rate at which turbulent diffusion and dissipation occur. The difference between the two actions attains its maximum just before the crest and it starts to decrease just past the crest.

10.2 VARIATION OF TURBULENCE WITH RELATIVE POSITION

In Figs. 45 and 46 the variation of turbulence intensity $\sqrt{\frac{\bar{u}^2}{U}}$ with relative position is shown for two Reynolds numbers Re = 1.08×10^5 and Re = 1.56×10^5 respectively. U here is the mean velocity where $\sqrt{\bar{u}^2}$ is measured. Both curves display the general tendency found in most similar curves. Turbulence intensity is equal to the background intensity near the surface and it increases gradually when the boundary is approached. The background turbulence intensity is about 0.10 in the case of the Reynolds number 1.08×10^5 whereas it is about 0.08 in the case of the Reynolds number 1.56×10^5; the maximum values near the boundary being about 0.40 and 0.50 respectively. A similar curve was obtained, Fig. 47, by plotting the results reported by Sheen(1964) after they have been brought to the same method of plotting used in the present investigation and the same tendency was noticed.

These curves reveal two facts :

a) There is no inherent change in the shape of this type of curve due to the existence of boundary obstructing elements. This means that the influence of these elements on the flow is limited to a certain height as far as the fluctuating component of the velocity is concerned.

b) The only difference is quantitative. The maximum turbulence intensity reported here is higher than that reported by other investigators. The maximum value was about 0.40 to 0.50.

10.3 VARIATION OF REYNOLDS SHEAR STRESSES

The Reynolds shear stresses obtained by Sheen (1964) are normalized with respect to τ_o and plotted in Fig. 48 against the relative depth $\frac{y_1}{d_1}$. Equation 5 is plotted in Fig. 1. Comparison of Fig. 1 and Fig. 48 shows the discrepancy. If the method used by Sheen is reliable, which is not certain, the comparison between Fig. 38 and Fig. 1 reveals some interesting remarks.

It is clear from the lower part of the curve that the values of $\rho\overline{uv}$ which are the values of the turbulent shear stress are much higher than the wall shear and the deviation from the linear distribution is quite noticeable. This emphasizes the role played by turbulence agitation in the movement of particles. The difficulty in using these observations for practical application is how to express them quantitatively.

10.4 AUTO-CORRELATION AND SPECTRUM FUNCTIONS

10.4.1 Auto-correlation functions

In Fig. 49 and 50 the variation of the auto-correlation function $R(\tau)$ with the time delay (τ) for the Reynolds number 1.08×10^5 and two different locations. The auto-correlation function $R_o(\tau)$ has been normalized with respect to its value at zero delay time (the mean square of the turbulent velocity fluctuations). All the curves in Fig. 49 show a rapid decrease from unity to small value in a delay time of the order of 0.5 sec and then a periodic oscillation about the line of zero correlation. In Fig. 49 the time of zero crossing at different vertical locations does not vary considerably indicating similarity in the macroscale distribution in the vertical direction.

In Fig. 50, where the auto-correlation function reflects the process of the back eddy region, it is clear that the auto-correlation values decrease more slowly when the boundary is approached. For the correlation curve which represents $y/d = 0.166$ it can be seen that the zero crossing time is 0.25 sec whereas it becomes 0.4 at $y/d = 0.25$ and it decreases for $y/d = 0.8$ to about 0.08 sec.

The auto-correlation curves reflect any periodicity or any harmonic components in the signal. If the velocity fluctuations contain a harmonic component of the type $X_1(t) = \bar{X} \sin 2\pi f\tau$, for a large τ it could be proved that only the deterministic term will keep contributing to $R(\tau)$ yielding $R_1(\tau) = \frac{1}{2} \bar{X}^2 \cos 2\pi f\tau$.

In Fig. 49 there are some spikes in the auto-correlation functions. These spikes are caused by noise from the recording machine.

10.4.2 Frequency spectrum functions

In Figs. 51 and 52 the frequency spectral function E(f) is plotted against the frequency f in Hz for two different locations and one mean velocity $\bar{U} = 1.32$ ft/sec. In Fig. 51 is shown the frequency spectrum at one vertical location (Station 6) upstream of the element. In Fig. 52 the frequency spectrum at a vertical location (Station 14) in the lee region is shown.

In order to bring together the spectral functions of the different vertical positions, the scale F(f) had to be made a relative one. The values of y/d are shown on every curve representing different vertical positions.

From Figs. 51 and 52 it can be seen that the frequency spectra display the same characteristics. There is high content of energy in the low frequency range (up to about 25 Hz). The contribution to the total energy of frequencies higher than 25 Hz is very small and becomes almost negligible in the range of about 50 Hz.

In Figs. 53 and 54 frequency spectra are shown for two different horizontal locations and one mean velocity of $\bar{U}$ = 1.89 ft/sec.

In Fig. 55 are shown the flow conditions in which the frequency spectra of Fig. 51, 52, 53 and 54 were obtained. In Figs. 51, 52, 53 and 54 the absolute values of the ordinates are relative to 100.

The physical significance of the frequency spectrum can be clarified if the wavenumber concept is introduced. If, for a velocity of U = 1.2 ft/sec, for instance, the significant values of the frequency spectrum are around 2.5 Hz, then an observer moving with the water, i.e. at 1.2 ft/sec, will encounter eddies having a wavelength $1.2 \times \frac{1}{2} = 0.48$ ft which corresponds to a wavenumber, of about 2.1.

Some of the frequency spectra shown in Figs. 51, 52, 53 and 54 are plotted on a non-dimensional base in Figs. 51A, 52A, 53A and 56 respectively. The abscissae are $\frac{f\,h}{U}$ and the ordinates are $\frac{F(f)U}{h}$ where h is the height of the element and U the local velocity. These figures show generally that the wavenumber becomes larger for a relatively more significant values of $\frac{F(f)U}{h}$ when the boundary is approached.

The wavenumber marks the range of the energy containing eddies. In order to relate the average size of the energy-containing eddies to the wavenumber, the wavenumber is made non-dimensional by multiplying it by a characteristic length that represents the turbulent eddies. This length is usually chosen as the macroscale

of turbulence L_x which was defined by Equation 50. In the present investigation the length L_x depends on the height of the triangular elements and hence the choice of h to make the wavenumber non-dimensional. The value of $\frac{f\,h}{U}$ that corresponds to an average eddy size, of the order of the turbulent macroscale, is in the range of one.

10.5 SCALES OF EDDY SIZE

In order to evaluate the turbulent macroscale, the spatial correlation function R(s) was deduced from the auto-correlation function $R(\tau)$ using Taylor's hypothesis as was stated in Equation 51. By averaging the spatial correlation function the turbulent macroscale can be obtained. In Fig. 57 the absolute values of the macroscale of turbulence for the Reynolds number of Re = 1.56×10^5 in water and 1.75×10^5 in air. For comparison, some results obtained by Laufer (1954) in air for a Reynolds number of 0.616×10^5 and by Raichlen (1967) in water for a Reynolds number of 0.662×10^5 are plotted.

In Laufer and Raichlen experiments the boundary was relatively smooth and the macroscale can be related to a characteristic length of the flow; to the depth in Raichlen's experiments and to the duct half width in Laufer experiments.

In the present investigation the roughness elements are expected to have some influence on the size of eddies.

In Figs. 57A and 58A the variation of the non-dimensional macroscale of turbulence with relative depth is shown for the present experiments and for Laufer and Raichlen investigations respectively. In Fig. 57A the macroscale L_x is plotted relative to h on which the macroscale is expected to depend. In Fig. 58A the macroscale is plotted relative to the depth in Raichlen's experiments, and to the duct half width in Laufer experiments. Fig. 57A shows that the size of the eddies can be related to elements height and the average value of L_x is of the same order of magnitude as h. Fig. 58A shows that in Laufer and Raichlen experiments the macroscale depends on the depth of flow; the former being of the same order of magnitude as the latter.

10.6 PROBABILITY DENSITY FUNCTION

In Fig. 59 the probability density function is shown for three different vertical positions at Station 10 for the Reynolds of 1.56×10^5. The values of mean deviation η and standard deviation σ are shown on the figure. The maximum deviation from the Gaussian distribution being αt.

the value $\frac{y}{d} = 0.2$ and the minimum is at $\frac{y}{d} = 0.66$. This confirms the conclusion reached earlier that the main flow is turbulent shear flow. Isotropic turbulence, which has a near Gaussian distribution, is only reached at high values of $\frac{y}{d}$ i.e. close to the water surface.

10.7 PRESSURE FLUCTUATIONS

In Tables 6 the characteristics of pressure fluctuations are presented. In Table 6 the characteristics of pressure fluctuations at Stations 6 and 10 are presented for one depth and several velocities. From Table 6 it appears that the values of α are higher and those of β are lower than the values reported for turbulent boundary layers. At Station 10 the values of both coefficients are in fairly good agreement with those for turbulent boundary layers.

In Table 6 some characteristics of turbulent boundary layer are also presented from Aki's (1967) results. It appears from Table 6 that the values of α are in fairly good agreement with the values reported in Aerodynamics. The values of τ_o in Aki's work are deduced from velocity profile.

In Fig. 60 frequency spectrum functions are shown for turbulent boundary layer flow and re-attaching flow.

There is no inherent difference between re-attaching flow and boundary layer flow as far as frequency structure is concerned.

The results reported by Aki (1967) are for totally different flow conditions. Average velocity is much higher and a turbulent boundary layer exists. Station 4 is the closest point to re-attachment position. The four curves in Fig. 60 all seem to follow the same general tendency, although the contribution of various frequencies to spectral density varies slightly from one curve to another.

CHAPTER ELEVEN

COMPARATIVE STUDY OF FLOW IN AIR AND IN WATER

11.1 MEAN VELOCITY AND TURBULENCE INTENSITY

In Fig. 61 mean velocity distribution and root-mean-square $\sqrt{\overline{u^2}}$ values are presented. The adverse slope was placed at the entrance of the wind tunnel and the flow over and after it was studied. The Reynolds number for this investigation was 1.75×10^5 using half the depth and the reference velocity. It appears from Fig. 61 that the boundary layer, being thin at the entrance, grows suddenly at the back eddy region. Immediately after the crest, the velocity gradient becomes very high and high level turbulence is generated. High turbulence level exists well away downstream. At a position as far as $x = 26$ h the original shape of turbulence distribution is not fully restored. The mean velocity distribution recovers its shape with a fully developed boundary layer at a position of about $x = 26$ h. This suggests that the adverse slope affects the fluctuating component more than it affects the mean component. While the distance at which mean velocity recovers its shape is about 26 h, it may require a longer distance for turbulence generated by the adverse slope to restore its shape. Similar results were obtained by placing a triangular element. No inherent difference in the flow structure was observed.

In Fig. 62 a series of triangular elements are placed in a similar position to that of the elements used in flume experiments. In Fig. 62 mean velocity distribution and turbulence are presented. Measurements were not extended higher than 0.7 the depth to avoid interference from the top of the tunnel.

It appears from Fig. 62 that velocity distribution has a similar shape to that of the velocity distribution in flume experiment. The comparison

can be made if the influence of the free surface is neglected. The re-attachment point is expected to be reached in this case faster than in the case of the element placed at the entrance. Visual observation of smoke injection showed that the re-attachment point in the first case, for low velocities, is reached at a distance downstream of about 10 - 15 h. One cause for the shorter distance of re-attachment in the second case is the presence of another inclined surface in the immediate vicinity of the separation zone. This forces the separating flow to accelerate and to re-attach itself faster.

11.1.2 Auto-correlation and frequency spectrum

In Fig. 63 the auto-correlation function R (τ) is plotted against the time delay (τ) for different relative positions and one Reynolds number. Fig. 63 shows that the auto-correlation function has the same general pattern for different relative positions. It displays a value near unity at zero time lag and a rapid decrease to zero afterwards. The value of zero crossing here varies from two to four milliseconds. The negative part here is well established and it continues up to values ranging from eight to fourteen milliseconds. The values of the auto-correlation function becomes negligible after 15 milliseconds. The variation of the auto-correlation function with time lag is different from that encountered in flume experiments. The difference is in the order of magnitude of time lags. The frequency structure of the flow in the wind tunnel is different from the free surface flow. The contribution of high frequency, as will be seen later, is greater in the case of air than it is in the case of water. This explains the small values of time lags at which zero crossing occurs.

In Fig. 64 the frequency spectrum F(f) is plotted against the frequency f for the Reynolds number 1.75×10^5 and different relative positions.

In Fig. 65 are plotted the non-dimensional frequency spectra versus the non-dimensional wavenumber for the experiments in water and in air. The Reynolds number for the experiments conducted in air was 1.75×10^5 and that for water experiments was 1.56×10^5. The values h and U, where h is the height of the element and U the local velocity, were chosen to convert the frequency and the spectrum into two nondimensional quantities because this wouldcorrelate the average size of the energy-containing eddies with the height of the triangular elements.

It appears from Fig. 65 that the frequency spectra for both experiments can be correlated using such parameters. The scatter here can be attributed to the fact that both experiments were not conducted under exactly similar flow conditions and that two different analysing equipments were used to calculate the frequency spectra.

Using the average velocity $\bar{U}$ instead of U to obtain non-dimensional parameters did not give better results. It appears, therefore, that for similar flow conditions and using the same analysing equipments the frequency spectra of velocity flutuations for air and water can be brought together using a characteristic length and the local velocity to obtain non dimensional parameters.

CHAPTER TWELVE

CONCLUSIONS

1. Observations have shown that hot-films, when new, can be used satisfactorily to measure velocity and turbulence in water under the normal conditions of hydraulic laboratories. However, purity of water and reasonable control of its temperature are essential for good performance.

2. Conical and parabolic sensors give good results generally from the view-point of avoiding dirt collection.

3. The constant temperature anemometer type ISVR 201 proved to be reliable and versatile. Provided the non-linear calibration curve for any probe used is known a reasonably linear output from the anemometer can be obtained.

4. A pressure transducer of resistive type can be made using some theoretical considerations. The sensitivity of such a transducer is a function of the ratio of its diameter to the thickness of its diaphragm.

5. The frequency response of the transducer is a function of the dimensions of the diaphragm, its material and the ratio of the length of inlet pipe to its cross-sectional area. A resonant frequency of 4000 Hz with reasonable sensitivity and inlet pipe size, can be obtained for a size of 0.17" diameter and a thickness of 0.0025" for the diaphragm.

6. The computer at the Data Analysis Centre of the Institute of sound and vibration can provide any statistical analysis of random data. It is reliable versatile, precise, much faster than any other machine and its output can be chosen to suit any requirement. It can produce print out,

punched tape, and plotted results.

7. The form drag of the triangular elements depends strongly on the ratio of the height of the element to the depth of flow. The form drag for one depth appears to be unaffected by velocity changes for the range covered in the present experiments which agrees with results reported by Vanoni and Hwang (1967).

8. In some alluvial rivers the form drag friction factor was found to be partly dependent on the particle Froude number. This agrees with results reported by Alam, Cheyer and Kennedy (M.I.T. Report No.78, June 1966).

9. A modified expression is needed to describe the roughness of substantially large scale compared with the depth of flow; the same conclusion was reached by Vanoni and Hwang (1967) and they suggested the roughness concentration as parameter.

10. In alluvial rivers, where relative roughness is very small, it is possible to use a constant equivalent roughness if bed forms are known to have a fairly consistent shape.

11. There is a discrepancy, in some flow donditions in alluvial rivers, betwen shear velocity as calculated from depth and slope and that deduced from velocity profile assuming K to be 0.4. This suggests either a modified expression for the shear velocity is needed or a deviation of K from 0.4.

12. The same discrepancy between the two shear velocities was observed in flume experiments which suggests the same conclusion as 11 for flume experiments.

FLOW GEOMETRY

13. The streamline pattern of the flow over triangular elements is sinusoidal. Separation occurs at the lee of the element and the flow reattaches itself on the following element.

14. The position of the re-attachment point is almost constant. It appears that it is not affected by change in the depth of flow; nor is it affected by velocity variation. It may be concluded that the separation pattern and re-attachment region are, rather, dependent on the geometry of the body that produces separation.

15. Velocities near the bed are very much dependent on the location along the element. The velocity near to the water surface does not appear to be affected by the influence of the bed elements. It may be concluded that for the range covered in the present investigation the influence of bed formations is limited.

TURBULENCE AND PRESSURE FLUCTUATIONS

16. There is a zone in the lee of the element, where separation occurs, that generates turbulence. The turbulence generated at this region is diffused into the flow and most of it is decayed before the following crest is reached.

17. The variation of turbulence intensity with relative position has the same shape as reported by other investigators. Turbulence intensity has the value of about 40 to 50 per cent near the bed and drops to about 6 to 8 per cent near the water surface.

18. The general shape of the auto-correlation function is not affected by a change in flow velocity. The relative position has a little effect on the shape of the auto-correlation function.

19. The frequency spectrum preserves its general shape for different locations in the direction of flow. This confirms that the flow in the present investigation is a shear flow.

20. The low frequency content in the turbulent energy is considerable. Most of the energy is confined generally to the band from zero to about 25 Hz.

21. The probability density function of the fluctuating velocity is nearly Gaussian near to the water surface. Its deviation from the Gaussian distribution increases when the bed is approached.

22. The R.M.S. of pressure fluctuations can be related to surface shear and to the velocity fluctuations by coefficients which depend, in the present investigation, on the position along the triangular elements.

23. In the reattached part of the flow over the triangular elements, the frequency structure of pressure fluctuations was found to be similar to that of the turbulent boundarylayer reported by Aki (1967).

24. The macroscale of turbulence can be related to the height of the triangular elements in the present investigation. It was found that the macroscale near the crest level was of the order of 1.2 times the height of the element.

25. Up to half the depth of flow in a wind tunnel there does not seem to be a basic difference in flow pattern between the flow under the free surface influence and the flow in wind tunnel. This indicates that flow in wind tunnels can simulate flow in open channels.

26. The non-dimensional frequency spectrum $\frac{F(f)U}{h}$ for velocity fluctuations versus the non-dimensional wave number $\frac{f.h}{U}$ can be used to correlate results obtained in water and in air if flow conditions are similar.

CHAPTER THIRTEEN

EVALUATION OF RESULTS

The experiments conducted for the design of pressure transducer of a strain gauge type proved to be useful. With a fair degree of skill such a transducer can be built and operated. The cost is very low compared with the cost of commercial transducers.

The transducer is designed basically for dynamic measurements but some modifications can be introduced to adapt it for static measurements.

The hot-film anemometer can be used for mean and fluctuating velocity but it needs patience. If a research programme does not include measurements of fluctuating quantities it is better not to use hot-film anemometer. The time, the costs, and the efforts required in the use of hot-films make it a very expensive piece of equipment indeed. Besides, using hot-film anemometer for measurements of mean velocity has no real advantage. Conventional techniques such as pitot tube, miniature current meters are much simpler to use and less time consuming.

When a research programme includes measurements of fluctuating quantities careful consideration must be given to the selection of the type of equipment to be used. Hot-film anemometer has the advantage of producing an output that can be stored on a magnetic tape for subsequent analysis. Or, if on line computer facilities are available the output of the anemometer can be analysed while experiments are conducted.

This advantage is very important if statistical quantities such as autocorrelation, frequency spectrum are required as was found in the present investigation.

If the research programme does not cover such a sophisticated analysis and is confined to absolute values of the fluctuating velocity hot-film anemometer may be less attractive to the research worker. Photographic techniques, difficult as they may be, can appeal to him, though tediousness starts when he comes to the analysis. Yet, perhaps, the total effort will be less than that needed in the case of hot-film anemometer.

Since measurements of turbulence and the statistical analysis of the fluctuating velocity have become recently very popular subjects of research, the use of hot-film anemometry is mandatory. The present investigation can contribute some information to users of such a technique.

The flume experiments may not be related directly to the flow in alluvial rivers. The elements used to simulate bed formations do not correspond to any ripples or dunes under the flow conditions adopted in the flume experiments. This also can be said about artificial roughness elements which are used to prove models.

Bed formations are not expected to keep their geometrical characteristics under changing conditions of depth and average velocity of the flow. Therefore the conclusion that the form drag is dependent on the depth of flow may not be valid for moveable beds. However, this conclusion may be very useful when a model of an alluvial river is to be built. Models of alluvial rivers are

proved in the first stage with fixed roughening elements. When the model is distorted i.e. the vertical length scale is not equal to horizontal length scale; inevitably the friction factor in the model ought to be higher than its counterpart in the prototype. The higher the degree of distortion the higher is the friction factor in the model. Therefore some information on the variation of the friction factor in a model studies such as the flume experiments conducted in the present investigation is very helpful in this respect. The values 0.3 or 0.4 for a friction factor, very high as they may be, can be encountered quite normally in model studies of alluvial rivers.

As to turbulence measurements, the results obtained in the present investigation can contribute to both, model studies of rigid and loose beds. The mechanism of turbulence generation, dissipation and diffusion in the present investigation can help research workers in alluvial rivers. For instance where maximum turnulence intensity occurs one would expect a high degree of erosion. Spatial correlation functions can tell what the distance travelled by a moved grain may be before it is picked up by another disturbance.

Measurements of pressure fluctuations showed that surface shear and turbulent fluctuations can be measured by indirect methods which may be useful for the future.

The comparison between the flow in water and in air may offer some information to the people who adopt air as the medium for their models.

The present work on the whole can be very useful to research workers as well as to people who build models of erodible channels. The present work is by no means perfect. The imperfections in the present study are no more than those which are common among research workers who have the same facilities and are dealing with the same problems, within the same period of time.

CHAPTER FOURTEEN

RECOMMENDATIONS FOR THE FUTURE

"what one man imagines, another can fulfil" Jules Verne

Ever since Osborne Reynolds had observed the diffusion of dye in his experiment, numerous efforts have been made to understand the problem of turbulence and its association with resistance to flow. In scale - model experiments, where viscosity plays an important role, the study of the combined effect of viscous and turbulent shear is of primary interest to hydraulic engineers.

In alluvial channels the problem is further complicated but the viscous influences are quite negligible.

To reconcile the two phenomena the answers to the following questions deserve some thought.

1. How can dynamic similarity be achieved?

2. What are the best parameters to be chosen in the prototype to represent the same two phase flow conditions in the model i.e. to produce bed formations, resistance to flow, sediment discharge that have a certain relationship to the prototype?

3. Is the influence of turbulence in the model and the prototype the same?

Investigations on the variation of the friction factor with change in flow conditions of depth and average velocity is a very challenging study and it is a long way ahead before this problem is satisfactorily solved.

Further investigation to study the flow characteristics over rigid models is needed. More information is needed on the variation of the resistance to flow with varying bed formation and flow conditions.

Man may reach the moon, and other planets, graft hearts and brains, use atom as his servant but flowing waters will remain a great mystery on the earth which nobody will claim to have completely solved.

APPENDIX ONE

SURFACE SHEAR MEASUREMENTS

PRESTON TUBE METHOD

J.H. Preston expressed the shear stress τ_o at the wall as a dependent variable, assuming that the velocity distribution in the turbulent boundary layer over a smooth bed can be expressed as

$$\frac{U}{U^*} = f\left(\frac{U^* y}{\nu}\right)$$

Preston demonstrated that the shear stress τ_o can be calculated from the dynamic pressure measured by a round Pitot tube of sufficiently large diameter to make the viscous effect of the laminar sublayer negligible. He demonstrated that the stagnation pressure at the face of the tube is a function of the velocity distribution in the turbulent boundary layer which was found to be expressible as the seventh power law

$$\frac{U}{U^*} = 8.61 \left(\frac{U^* y}{\nu}\right)^{1/7}$$

and obtained the equation

$$\log \frac{\tau_o d_o^2}{4\nu^2} = -1.396 + 0.875 \log \frac{(P_t - P_o) d_o^2}{4\rho\nu^2}$$

This equation was valid only for

$$4.5 < \log \frac{(P_t - P_o) d^2}{4\rho\nu^2} < 6.5$$

A preliminary design for the Preston tube was similar to that described by Ippen (1962), where the static pressure is measured by a static tube positioned above the total head tube.

Due to difficulties in mounting arrangements it was found easier to obtain the static pressure from the normal pressure tappings drilled at the surface of the element.

Because the number of readings in each test was high it was necessary to find a direct expression for τ_o against $(P_t - P_o)$ and plot it graphically

with d_o = 0.152 inch

ρ = 1.94 slug/ft^3 and

ν = 1.1 x 10^{-5} ft^2/sec

The original equation was re-arranged in the form

$$\log \tau_o = -1.777 + 0.875 \log \bar{h}$$

where $\bar{h}$ = $(P_t - P_o)$ expressed in cm of water

and τ_o lb/ft^2

The limitation on this equation is that h should not be less than 0.1 cm in order that

$$\log \frac{(P_t - P_o) d_o^2}{4\rho\nu^2} > 4.5$$

and this value corresponds to a shear stress

$$\tau_o = 0.0022 \text{ lb/ft}^2$$

Although some values lower than this were observed they were not considered accurate.

APPENDIX TWO

TEMPERATURE-TIME CURVES

When heat is generated in a resistor the temperature attained depends on heat generation and heat transfer characteristics. The thermal balance is attained when the rate at which heat is lost will be exactly equal to the rate at which it is generated, and the resistor will then attain its maximum temperature T_1.

The rate of heat generation can be expressed as $\frac{E^2}{R}$ where E the voltage drop across the resistor and R its resistance. The rate at which heat is lost is $H(T_1-Ta)$ where Ta is the ambient temperature and H a heat transfer coefficient. Thus the thermal equilibrium can be expressed as

$$H(T_1-Ta) = \frac{E^2}{R}$$

At a temperature T' less than T_1 the rate at which heat is stored is equal to the thermal capacity of the body C'' multiplied by the rate $\frac{dT'}{dt}$ at which temperature increases.

$$P' = C'' \left(\frac{dT'}{dt}\right) + HT'$$

where P' is the heat generation in watts.

(C'' is the energy in Joules required to raise the temperature by $1^{o}C$).

$$T' = \frac{P'-C''\left(\frac{dT'}{dt}\right)}{H}$$

To solve this equation we assume

$$y = \frac{a-b\ dy/dt}{c}$$

$$y - \frac{a}{c} = -\frac{b}{c}\frac{dy}{dt}$$

$$\frac{dy}{y - \frac{a}{c}} = -\frac{c}{b}\,dt$$

Integrating

$$\log_e (y - \frac{a}{c}) = -\frac{c}{b}\,t + \log_e d'$$

where $\log_e d'$ is constant of integration

thus

$$y - \frac{a}{c} = d'e^{-\frac{ct}{b}}$$

$$y = \frac{a}{c} + d'\,e^{-\frac{ct}{b}}$$

substituting P' for a; H for c; C'' for b and y for T'

we have

$$T' = \frac{P'}{H}(1 - e^{-Ht/C''})$$

$$\frac{dT'}{dt} = \frac{P'}{C''}\,e^{-Ht/C''}$$

hence the initial rate of rise of temperature is

$$(\frac{dT'}{dt})_{t=o} = \frac{P'}{C''} \text{ and}$$

$$T' = \frac{P'}{H}$$

The constant $\tau' = \frac{C''}{H}$ is called the temperature time constant which is in fact the time in seconds required for the temperature rise to reach the definite fraction 0.63 T'.

If we apply the same treatment for the cooling effect we obtain similar equations and the time constant τ' will be the time required to reach the fraction 0.37 T'.

Fig. 66 shows the relationship between the different values.

BIBLIOGRAPHY

1) AKI SHUICHI "Dynamic Characteristics of the Forces Acting on the Spillway Chute". Proc. 12th Congress of I.A.H.R. Fort Collins, Colorado 1967, Vol II pp. 163

2) BENDAT B., PIERSOL G. "Measurements and Analysis of Random Data". John Wiley & Sons, Inc, New York 1966.

3) BURTON J. "A Theoretical and Experimental Analysis of the Flow in Regenerative Pump" Southampton Univ. Ph.D. thesis 1966.

4) DAVIES, P.O.A.L. and DAVIS, M.R. "The Hot-wire Anemometer" Southampton Univ., Institute of Sound and Vibration Research, Report No. 155, Oct. 1966.

5) DELLEUR, J.W., TOEBES, G.M. and LIU, C.L. Purdue Univ. School of Civil Engineering, Technical Report No. 13, 1966.

6) LAUFER, J. "Investigation of Turbulent Flow in a two-dimensional channel", N.A.C.A. Report 1053.

7) LING, S.C. "Heat Transfer Characteristics of Hot-film Sensing elements used in Flow Measurements" ASME Journal of Basic Engineering, Transactions 1960, pp. 629-634.

8) MEMON H.M., "Resistance to Flow in Open Channels" Ph.D. Thesis, December 1967 Imperial College of Science and Technology, University of London.

9) MORRIS H.M. "Design Methods for Flow in Rough Conduits" Journ. Hydru. Div. Proc. ASCE July 1969.

10) PACIFICO R.E. "The Development of a miniature pressure transducer and associated circuitry" Southampton Univ., Institute of Sound and Vibration Research Memorandum No. 106 1964.

11) RAICHLEN F. "Some Turbulence Measurements in Water" Journ. Engineering Mechanics Div. Proc. ASCE April 1967.

12) RICHARDSON E.V. & MCUIVEY R.S. "Measurement of Turbulence in Water" Journ. Hyd. Div. Proc. ASCE March 1968.

13) RIFAI M.F. & RACCIFICO R.E. "The Development of a Miniature Pressure Transducer for Use in Water" Journ. Sound and Vibration, March 1968.

14) ROUSE H. "Advanced Mechanics of Fluid" New York John Wiley & Sons Inc. 1959.

15) ROUSE H. "Critical Analysis of Open-Channel Resistance" Journ. Hyd. Div. Proc. ASCE July 1965.

16) SHEEN S.J. "Turbulence Over a Sand Ripple" M.Sc. Thesis University of Auckland 1964.

17) SMITH K.V.H. "Alluvial Channel Resistance Related to Bed Form" Journ. Hyd. Div. Proc. ASCE, January 1968

18) SMITH K.V.H., & RIFAI M.F. "Turbulence Measurements in Water Using Hot-Film Sensors" Civil Engineering and Public Works Review, September 1968.

19) TIMOSHENKO S. 1961 "Vibration Problems in Engineering" Princeton, N.J. Princeton University Press.

20) VANONI, V.A. and Hwang I.S. "Relation between Bed Forms and Friction in Streams" Journ. Hyd. Div. Proc. ASCE, May 1967.

21) WALKER G.R. "Study of the Two-dimensional Flow of a Turbulent Fluid Past a Step" M.Sc. Thesis University of Auckland 1961

22) WOLD I and MASON, J. "Simplified Operating Instructions for the I.S.V.R. Constant Temperature Hot-wire Anemometer" Southampton Univ. Institute of Sound and Vibration Research, Memorandum No. 187.

References

1. **BROOKS, N.H., "Mechanics of Streams with movable Beds of Fine Sands" Proc. A.S.C.E., Vol. 81, Separate No. 668, April 1955**

2. **IPPEN, A.T. & DRINKER, P.A., "Boundary Shear Stresses in Curved Trapezoidal Channels" Proc. A.S.C.E., Jour. Hyd. Div. Sept. 1962.**

3. **ROBINSON, ALBERTSON & SAYRE, "Roughness Spacing for Open Channels" Proc. A.S.C.E., Journ, Hyd. Div. May 1961.**

4. **VANOUI, V. & NOMICOS, G.N. "Resistance Properties of Sediment-Laden Streams" Proc. A.S.C.E., Journ. Hyd. Div. May 1961.**

TABLE 1

BALANCE OF RESISTANCE COMPONENTS d = 12 inches

Flow Velocity	Mean Shear	Contribution of Form drag	Contribution of Surface drag	Relative error	Bed Shear	Contribution of Form drag	Contribution of Surface drag	Relative % error
$\bar{U}$ ft/sec	$10^3 \times \tau_o$ lb/ft^2	$\frac{\tau_F}{\tau_o}$ %	$\frac{\tau_s}{\tau_o}$ %	$1-\frac{\tau_F+\tau_S}{\tau_o^2}$	$10^3 \times \tau_b$	$\frac{\tau_F}{\tau_b}$ %	$\frac{\tau_s}{\tau_b}$ %	$1-\frac{\tau_F+\tau_S}{\tau_b^2}$
0.88	17.2	78.8	8.9	12.3	33	40.6	0.45	59.95
1.23	32	83	8.55	8.45	62.4	42.5	0.44	57.05
1.32	37	80	7.7	12.30	72.7	40.6	0.4	59
1.41	42.5	815	10.63	7.87	83	42	0.55	57.45
1.58	53.5	82.5	9.95	7.55	104	42.5	0.50	57
1.76	65.2	80	9.20	10.80	128	40.6	0.45	58.95
1.89	75.5	80	8.60	11.40	147	41.2	0.43	58.37

TABLE 2

BALANCE OF RESISTANCE COMPONENTS d = 9 inches

Flow Velocity	Mean Shear	Contribution of Form drag	Contribution of Surface drag	Relative error	Bed shear	Contribution of Form drag	Contribution of Surface drag	Relative error %
$\bar{U}$ ft/sec	$10^3 \times \tau_o$ lb/ft^2	$\frac{\tau_F}{\tau_o}$ %	$\frac{\tau_F}{\tau_o}$ %	$1-\frac{\tau_F+\tau_s}{\tau_o^2}$	$10^3 \times \tau_b$	$\frac{\tau_F}{\tau_b}$ %	$\frac{\tau_s}{\tau_b}$ %	$1-\frac{\tau_F+\tau_s}{\tau_b^2}$
0.88	25.7	79.5	8.9	11.6	43.5	47	3.2	49.8
1.04	35.7	82.2	5.6	12.2	59.2	49.5	3.46	47.04
1.14	42.0	85.6	5.35	9.05	70.5	51	4.52	44.48
1.42	63	92.5	7.65	0.15	104	56	4.18	39.82
1.54	78	90	5.35	4.55	124	56.5	3.70	39.80
1.60	82	94	5.635	0.365	136	56.7	3.38	39.92
1.78	96	94.1	5.48	0.415	159	48.5	3.2	49.3
1.91	106	88.5	5.70	5.80	178	59.5	3.28	62.78

TABLE 3

BALANCE OF RESISTANCE COMPONENTS d=6 inches

Flow Velocity	Mean Shear	Contribution of Form drag	Contribution of Surface drag	Relative error	Bed shear	Contribution of Form drag	Contribution of Surface drag	Relative error %
$\bar{U}$ ft/sec	$10^3 \times \tau_o$ lb/ft^2	$\frac{\tau_F}{\tau_o}$ %	$\frac{\tau_s}{\tau_o}$ %	$1-\frac{\tau_F+\tau_s}{\tau_o}$ %	$10^3 \times \tau_b$ lb/ft^2	$\frac{\tau_F}{\tau_b}$ %	$\frac{\tau_s}{\tau_b}$ %	$1-\frac{\tau_F+\tau_s}{\tau_b}$ %
0.985	61.5	87.5	1.43	11.07	62.4	86.6	1.40	12
1.08	79	91	1.24	7.76	80.5	89.9	1.22	8.88
1.18	92	91	1.53	7.47	93	90.5	1.51	8.49
1.28	105	93	1.64	5.46	106	92.5	1.63	5.87
1.38	118	92.5	2.16	5.34	120	91.2	2.12	6.68
1.48	141	87	2.06	9.94	143	85.5	2.04	12.46
1.58	153	89	2.13	8.87	155	88.5	2.10	9.40

TABLE 4

BALANCE OF RESISTANCE COMPONENTS VANONI (1967)

Run No.	d ft	$\bar{H}/d$	$\bar{U}$ ft/sec	$10^3 x \tau_o$ lb/ft^2	τ_F/τ_o*	Remarks
A-5	0.171	1/3.3	1.23	64	0.91	
B-5	0.230	1/4.4	0.98	46	0.872	Run 9-14 is the original run $\bar{r}$ = 0.151, $\bar{s}$ = 1.59 x 10^{-3} $\bar{U}$ = 0.749 ft/sec, $\bar{H}$ = 0.052 ft
C-5	0.348	1/6.7	1.40	33.6	0.85	
D-5	0.472	1/9.1	1.03	27	0.835	

Run No.	d ft	$\bar{H}/d$	$\bar{U}$ ft/sec	$10^3 x \tau_o$ lb/ft^2	τ_F/τ_o*	Remarks
A-5	0.182	1/4	0.74	13.2	0.84	Run 9-15 is the original run $\bar{r}$ = 0.156 ft, $\bar{s}$ = 2.86 x 10^{-3} $\bar{U}$ = 1.250 ft/sec, $\bar{H}$ = 0.046 ft
B-5	0.241	1/5.25	1.25	36	0.825	
C-5	0.361	1/7.8	1.62	46	0.78	
D-5	0.482	1/10.5	1.50	25.1	0.755	

* $\tau_o = \dfrac{\rho \bar{U}^2 f_b}{8}$

TABLE 5

STRESS AND STRAIN ON BRASS DIAPHRAGM

Ratio a'/t'	10	100	200	1000
Pressure $\lvert p(lb/in^2)\rvert$	5.5×10^{3}	0.55	0.25	5.5×10^{-5}
Strain $\lvert\varepsilon'\rvert$	2.6×10^{2}	2.6×10^{-4}	5×10^{-5}	2.6×10^{-6}
Stress $\lvert\sigma'(lb/in^2)\rvert$	44×10^{4}	44×10^{2}	7.2×10^{2}	44

TABLE 6

PRESSURE FLUCTUATION CHARACTERISTICS

Station 6

Run No.	$\bar{U}$ ft/sec	Cf	τ_o lb/ft^2	$\sqrt{\bar{p}^2}$ lb/ft^2	$\sqrt{\bar{u}^2}$ ft/sec	α	β
H3	0.88	0.0041	0.0031	-	-	-	-
H2	1.32	0.0034	0.0068	0.041	0.3	7.05	0.23
H2a	1.41	0.0031	0.0061	0.040	-	6.70	-
H2b	1.58	0.00295	0.0071	0.051	-	7.10	-
H1	1.89	0.0027	0.0091	0.071	0.4	7.55	0.23

Station 10

Run No.	$\bar{U}$ ft/sec	Cf	τ_o lb/ft^2	$\sqrt{\bar{p}^2}$ lb/ft^2	$\sqrt{\bar{u}^2}$ ft/sec	α	β
H2	1.32	0.0065	0.011	0.030	0.18	2.72	0.48
H1	1.89	0.0059	0.0208	0.042	0.28	2.02	0.27

TABLE 6

PRESSURE FLUCTUATION CHARACTERISTICS

AKI(1967) (Comparison)

$\bar{U}$ ft/sec	Cf	δ ft	δ^* ft	τ_o lb/ft^2	$\sqrt{\overline{p^2}}$ lb/ft^2	β
17.5	0.0036	0.02	0.0046	1.08	3.22	3.02
24.5	0.0034	0.0193	0.0046	2.00	4.24	2.12
33.1	0.0032	0.0196	0.0046	3.32	10.20	3.10

δ is the displacement thickness

δ^* is the momentum thickness

c_f boundary layer friction factor

TABLE 7

OBSERVATIONS FOR DEPTH d = 1 ft

1	2	3	4	5	6	7	8	9	10	11
Run No	Discharge	Slope	Mean Velocity	Shear Velocity	Shear Stress	Reynolds Number	Bed Shear	Bed Shear Velocity	Form drag	Surface drag
	Q cusecs	$\bar{S}$	$\bar{U}$ ft/sec	U^* ft/sec	$10^3 x \tau_0$ lb/ft^2	$\frac{\bar{U}d_1}{\nu}$	$10^3 x \tau_b$ lb/ft^2	u_b^* ft/sec	$10^3 x F_D$ lb/element	$10^3 x F_s$ lb/ lement
H3	1	0.00075	0.88	0.092	17.2	71900	.33	0.132	28.4	3.25
H3a	1.1	0.00087	0.97	0.103	20.2	79420	39.2	0.142	——	——
H3b	1.2	0.00103	1.05	0.11	23.4	90420	46.2	0.153	——	——
H3c	1.3	0.00117	1.14	0.118	27.0	93320	52.8	0.165	——	——
H3d	1.4	0.00139	1.23	0.129	32	103220	62.4	0.180	55.4	5.91
H2	1.5	0.00161	1.32	0.138	37	108000	72.7	0.194	62.8	6.15
H2a	1.6	0.00184	1.41	0.148	42.5	112200	83	0.208	73.5	9.65
H2b	1.8	0.00232	1.58	0.166	53.5	122600	104	0.232	94	11.12
H2c	2	0.00284	1.76	0.184	65.2	137200	128	0.258	112	12.25
H1	2.15	0.00328	1.89	0.198	75.5	156000	147	0.276	128.5	13.5

TABLE 8

OBSERVATION FOR DEPTH d = 0.75 ft

1	2	3	4	5	6	7	8	9	10	11
Run No	Discharge	Slope	Mean Velocity	Shear Velocity	Shear Stress	Reynolds Number	Bed Shear	Bed shear Velocity	Form drag	Surface drag
	Q cusecs	$\bar{S}$	$\bar{U}$ ft/sec	U^* ft/sec	$10^3 x \tau_0$ lb/ft^2	$\frac{\bar{U}d_1}{\nu}$	$10^3 x \tau_b$ lb/ft	U^*_b ft/sec	$10^3 x F_D$ lb/element	$10^3 x F_S$ lb/element
M1	0.715	0.00125	0.88	0.115	25.7	62120	43.5	.151	44.2	2.94
M1-1	Q.85	0.0017	1.04	0.136	35.7	74220	59.2	.175	61.5	4.35
M2	0.93	0.0020	1.14	0.149	42	81520	70.5	.19	76.5	6.77
M3	1.15	0.00298	1.42	0.184	63	102300	104	.224	117	8.17
M2-1	1.25	0.00353	1.54	0.198	78	110000	124	.252	148	9.22
M4	1.30	0.00387	1.60	0.212	82	114250	136	.265	156	9.75
M5	1.45	0.00452	1.78	0.227	96	127230	159	.287	195	10.80
M6	1.55	0.00507	1.91	0.24	106	136210	178	.312	199	12.40

TABLE 9

OBSERVATION FOR DEPTH d = 0.5 ft

1	2	3	4	5	6	7	8	9	10	11
Run No	Discharge	Slope	Mean Velocity	Shear Velocity	Shear Stress	Reynolds Number	Bed Shear	Bed shear velocity	Form drag	Surface drag
	Q cusecs	$\bar{S}$	$\bar{U}$ ft/sec	U^* ft/sec	$10^3 \times \tau_o$ lb/ft^2	$\frac{\bar{U}d_1}{\nu}$	τ_b lb/ft^2	U_b^* ft/sec	$10^3 \times F_D$ lb/element	F_S lb/element
L1	0.5	0.0039	0.985	0.179	61.5	46 900	62.4	0.18	114	1.88
L1-1	0.55	0.00505	1.080	0.206	79	51 450	80.5	0.206	152	2.09
L1-2	0.60	0.0058	1.18	0.218	92	56 240	93	0.219	177	2.98
L2	0.65	0.0066	1.28	0.236	105	60 950	106	0.236	208	3.67
L3	0.70	0.0075	1.38	0.248	118	65 760	120	0.249	231	5.33
L4	0.75	0.0087	1.48	0.270	141	70 500	143	0.270	262	6.18
L5	0.80	0.0093	1.58	0.282	153	75 270	155	0.282	290	6.92

TABLE 10

PRESSURE AND SHEAR MEASUREMENTS d = 1 ft

Mean Pressure in excess of hydrostatic in cm of water.

Station	Mean Velocity						
	0.88	1.23	1.32	1.41	1.58	1.76	1.89
1	-0.015	-0.057	-0.047	-0.027	-0.075	-0.150	-0.127
2	0.015	0.013	0.113	0.062	0.060	0.015	0.058
3	0.065	0.145	0.238	0.254	0.285	0.288	0.400
4	0.140	0.249	0.293	0.381	0.368	0.406	0.523
5	0.105	0.219	0.268	0.325	0.382	0.466	0.478
6	0.098	0.196	0.238	0.312	0.280	0.400	0.446
7	0.105	0.172	0.218	0.253	0.263	0.346	0.384
8	0.090	0.132	0.143	0.231	0.182	0.216	0.248
9	0.085	0.107	0.138	0.135	0.082	0.129	0.155
10	0.035	0.003	0.068	0.055	0.005	0.035	0.038
11	0.005	-0.056	-0.055	-0.060	-0.119	-0.186	-0.200
12	0.000	-0.065	-0.075	-0.075	-0.126	-0.208	-0.222
13	0.015	-0.060	-0.067	-0.060	-0.158	-0.199	-0.253
14	-0.005	-0.088	-0.082	-0.070	-0.162	-0.228	-0.289
15	0.010	-0.103	-0.107	-0.080	-0.160	-0.209	-0.272

Shear Stress Measurements $lb/ft^2 \times 10^3$

Station	Mean Velocity						
	0.88	1.23	1.32	1.41	1.58	1.76	1.89
1	—	-1.2	-2	-2.12	-2.02	-3.21	-4
2	—	—	-1.1	-1.4	-1.67	-1.87	-2.1
3	—	—	—	—	—	—	-1.1
4	1.1	2.0	2.8	2.3	2.18	+2.1	2.1
5	2.6	4.12	4.6	5.0	5.82	7.11	8.4
6	3.2	4.77	5.8	6.11	7.11	8.3	9.4
7	4.2	6.52	8.8	8.22	9.25	9.82	11.1
8	5.3	7.22	8.1	8.8	10	11.71	13.6
9	5.0	8.14	9.9	11.2	14.62	17.3	19.1
10	6.0	8.32	11.1	13.7	17.21	18.72	20.8

TABLE 11

PRESSURE AND SHEAR MEASUREMENTS d = 0.75 ft

Normal Pressure in excess of hydrostatic in cm of water

Station	Mean Velocity ft/sec							
	0.88	1.14	1.42	1.60	1.78	1.91	1.04	1.54
1	0.043	0.108	-0.001	-0.183	-0.021	-0.063	0.020	-0.084
2	0.058	0.173	0.204	0.055	0.228	0.359	0.029	0.127
3	0.163	0.293	0.304	0.280	0.500	0.645	0.125	0.321
4	0.154	0.358	0.394	0.340	0.637	0.740	0.205	0.425
5	0.128	0.333	0.339	0.327	0.564	0.690	0.141	0.348
6	0.078	0.223	0.269	0.235	0.461	0.600	0.148	0.324
7	0.108	0.243	0.234	0.180	0.404	0.515	0.105	0.230
8	0.088	0.208	0.164	0.120	0.300	0.417	0.118	0.172
9	0.078	0.148	0.109	-0.025	0.192	0.186	0.075	0.113
10	0.020	0.123	0.009	-0.125	0.021	0.105	0.051	-0.013
11	-0.022	0.033	-0.121	-0.325	-0.236	-0.101	-0.050	-0.208
12	-0.032	0.013	-0.131	-0.330	-0.287	-0.215	-0.065	-0.255
13	-0.022	0.043	-0.131	-0.345	-0.275	-0.212	-0.083	-0.216
14	-0.022	-0.012	-0.141	-0.380	-0.319	-0.250	-0.096	-0.271
15	-0.042	+0.043	-0.161	-0.340	-0.311	-0.242	-0.096	-0.243

Surface Shear Stress Measurements $lb/ft^2 \times 10^3$

Station	Mean Velocity ft/sec							
	0.88	1.04	1.14	1.42	1.54	1.60	1.78	1.91
1	—	—	—	-1.00	—	-1.12	-2.1	-3
2	—	—	—	—	—	—	—	-2.19
3	—	—	1.8	2.0	2.11	2.06	2.4	-1.80
4	1.8	2.1	2.17	2.12	2.27	2.82	3.8	—
5	2.88	3.27	3.98	4.88	5.11	4.37	6.2	6.82
6	3.12	3.22	5.12	6.45	7.24	5.19	10.6	9.33
7	4.21	5.30	6.24	7.22	6.12	8.69	10.8	9.40
8	5.28	6.11	7.30	8.12	8.24	9.87	13.0	12.30
9	5.84	7.33	9.21	10.2	11.20	12.37	15.9	14.57
10	6.32	8.07	10.81	13.7	15.11	16.22	19.1	19.30

TABLE 12

PRESSURE AND SHEAR MEASUREMENTS d=0.5 ft

Mean Pressure in excess of hydrostatic cm of water

Station	Mean Velocity ft/sec						
	0.985	1.080	1.18	1.28	1.38	1.48	1.58
1	0.007	-0.059	-0.066	-0.060	-0.175	-0.113	-0.115
2	0.037	0.026	0.013	0.076	0.013	0.085	0.137
3	0.132	0.142	0.175	0.278	0.206	0.358	0.407
4	0.187	0.193	0.258	0.374	0.288	0.482	0.550
5	0.147	0.159	0.220	0.364	0.276	0.525	0.505
6	0.137	0.157	0.182	0.303	0.236	0.452	0.482
7	0.107	0.116	0.147	0.264	0.163	0.400	0.355
8	0.082	0.053	0.095	0.181	0.133	0.286	0.288
9	-0.007	0.023	0.057	0.148	-0.005	0.185	0.185
10	-0.043	-0.059	-0.051	-0.013	-0.130	0.015	-0.003
11	-0.048	-0.170	-0.156	-0.172	-0.355	-0.303	-0.500
12	-0.053	-0.192	-0.220	-0.212	-0.379	-0.360	-0.501
13	-0.088	-0.194	-0.216	-0.199	-0.379	-0.355	-0.506
14	-0.063	-0.200	-0.253	-0.255	-0.391	-0.400	-0.534
15	-0.063	-0.194	-0.210	-0.232	-0.400	-0.389	-0.556

Surface shear stress $lb/ft^2 \times 10^3$

Station	Mean Velocity ft/sec						
	0.985	1.080	1.18	1.28	1.38	1.48	1.58
1	-1.0	-1.1	-1.3	-	-	-1.1	-
2	-	-1.1	-1.3	-1.0	-1.1	-	-
3	-	-	-	-	-	2.2	1.12
4	-	1.12	-	-	1.13	2.9	3.19
5	1.88	2.03	2.03	1.12	2.20	3.3	5.1
6	1.24	3.21	2.11	1.68	4.12	3.19	4.88
7	2.87	3.88	3.38	2.87	6.26	5.4	5.12
8	3.56	4.13	4.12	4.88	6.94	8.30	7.63
9	3.18	4.98	5.18	6.13	8.88	10.28	9.28
10	5.24	5.88	6.23	7.4	9.18	10.11	12.4

1. General view of wind tunnel

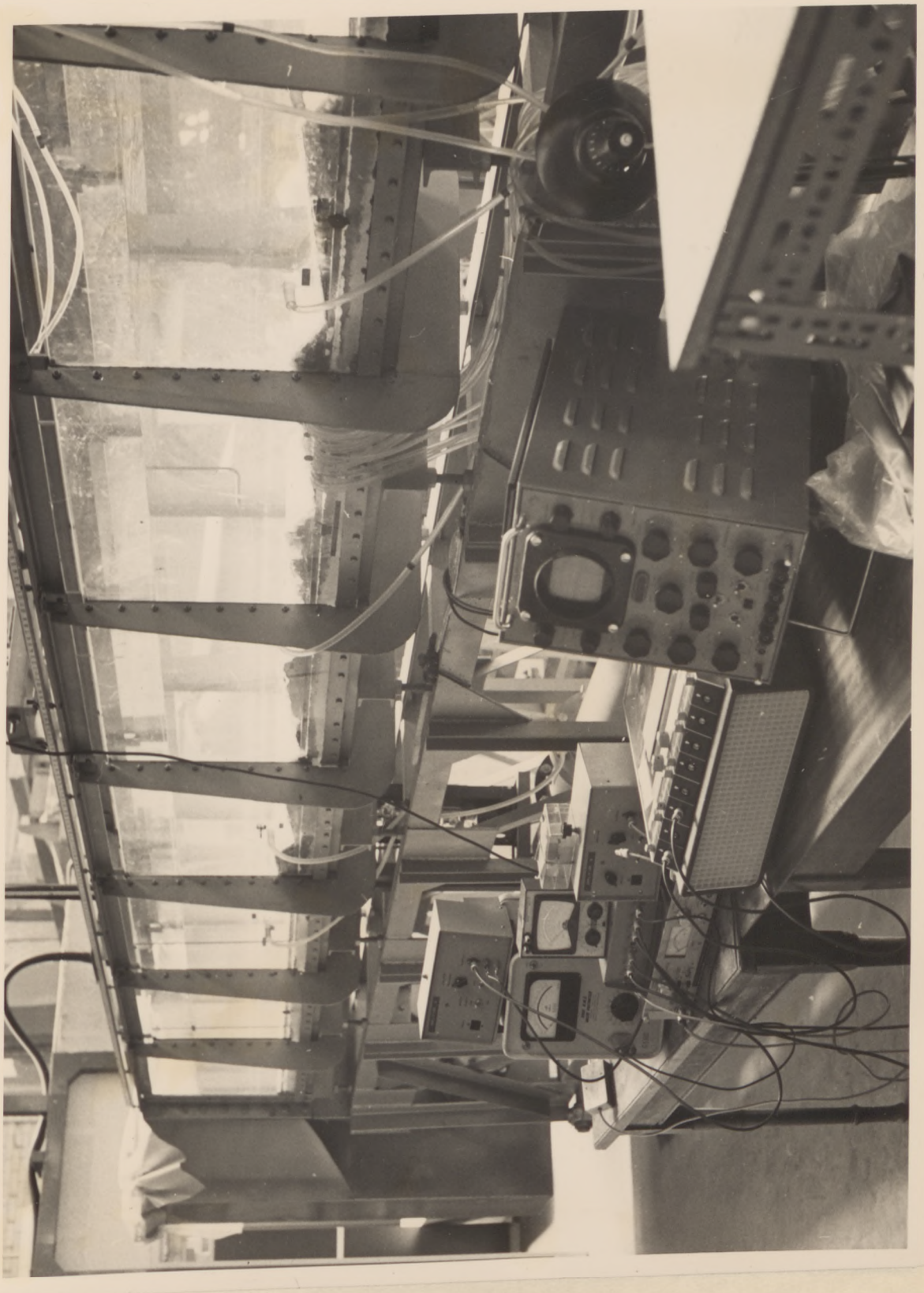

2. General view of apparatus

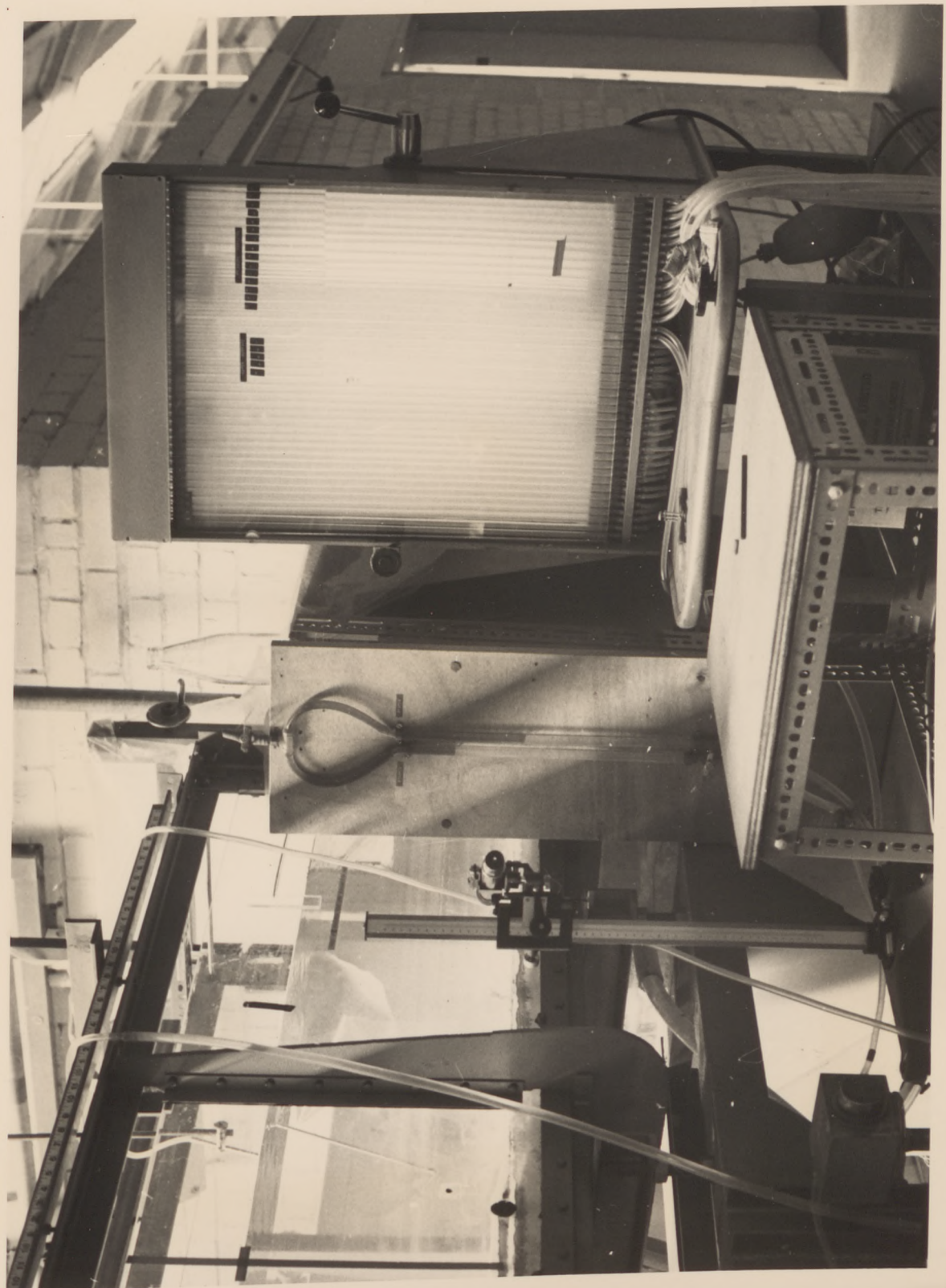

3. View of Differential manometer

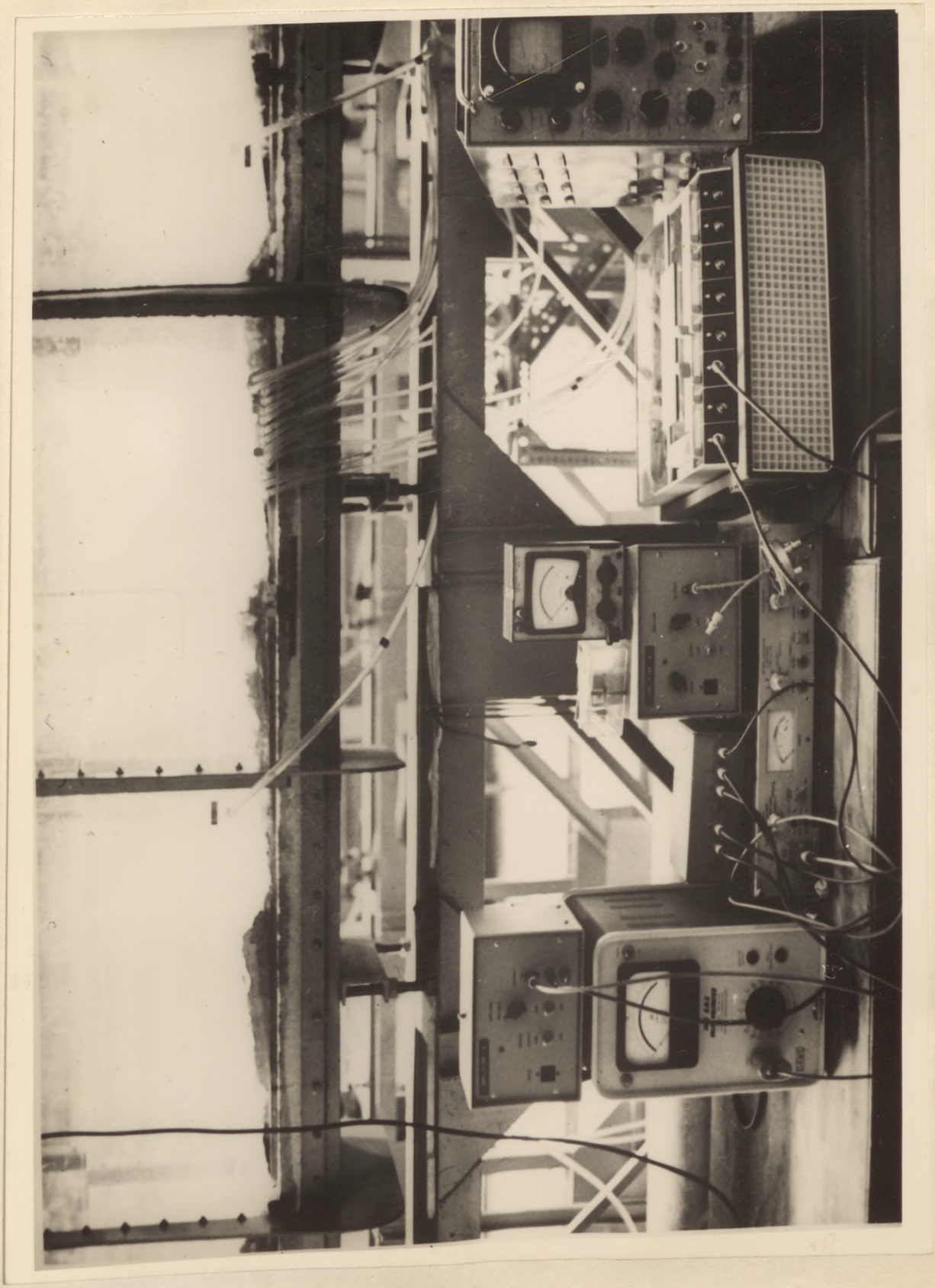

4. View of electronic equipments

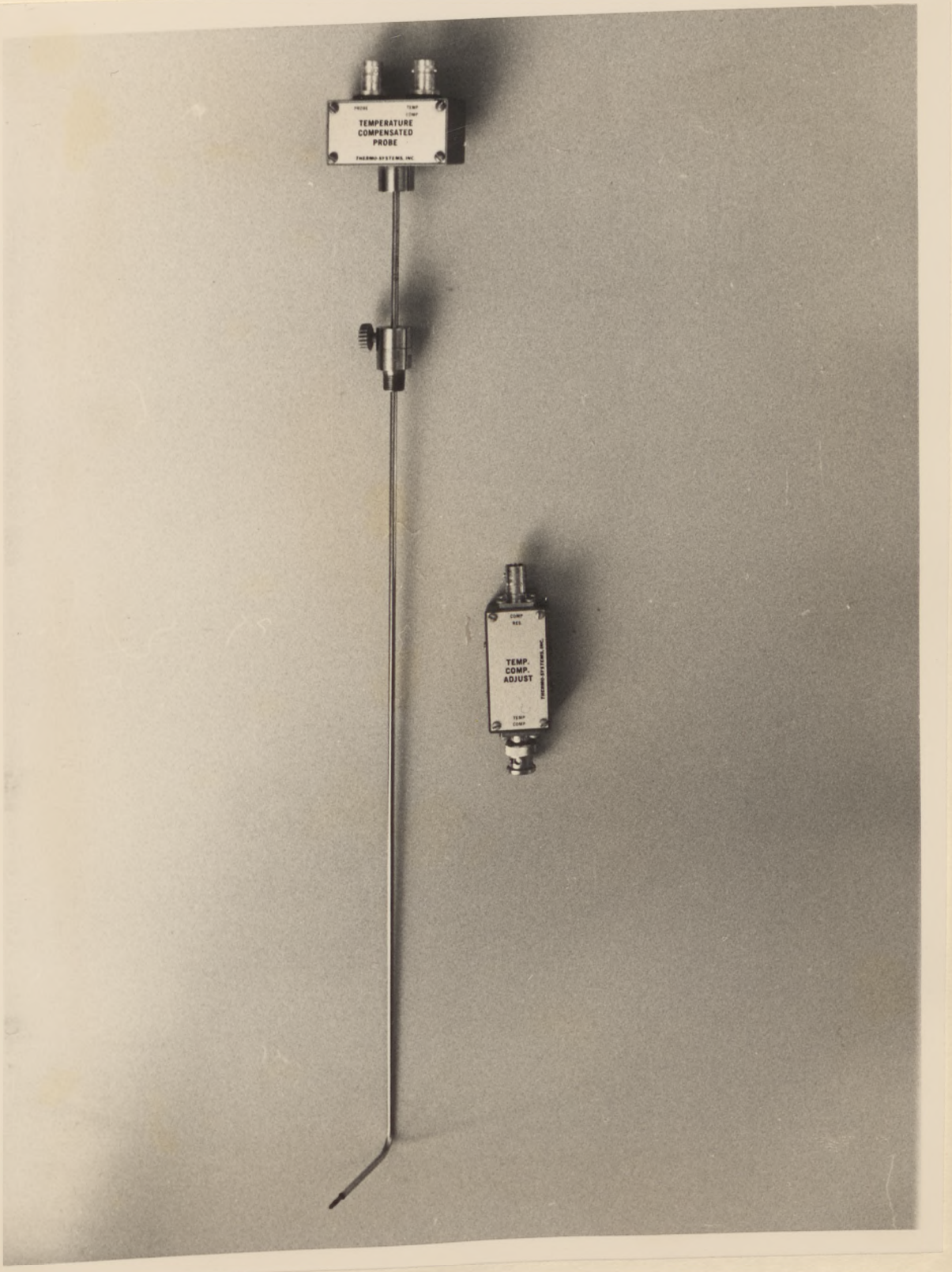

5. Temperature compensated probe

6. Anemometer type ISVR 201

7. View of the New Bedford River

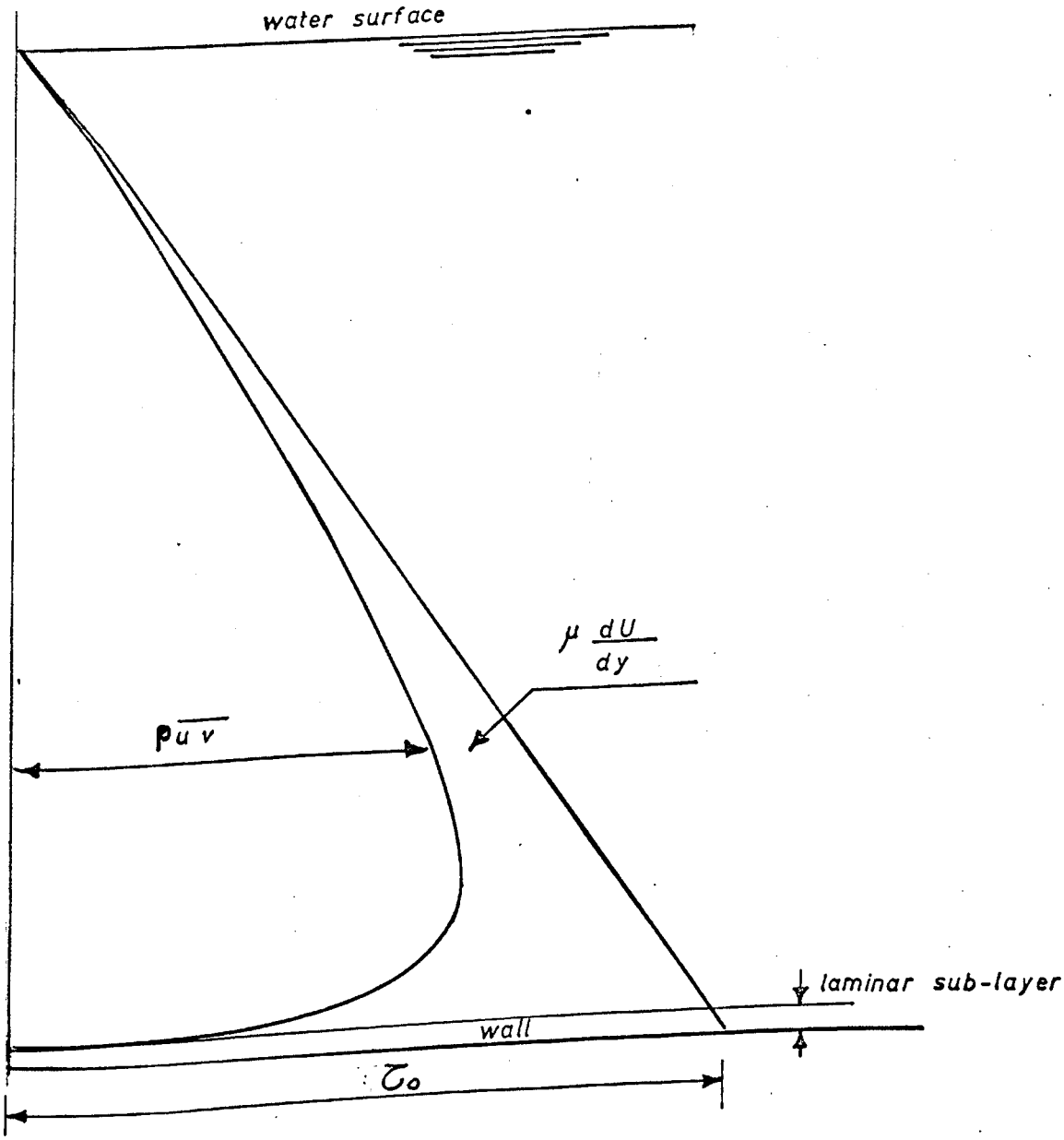

VARIATION OF SHEAR STRESS WITH DEPTH

FIG 1

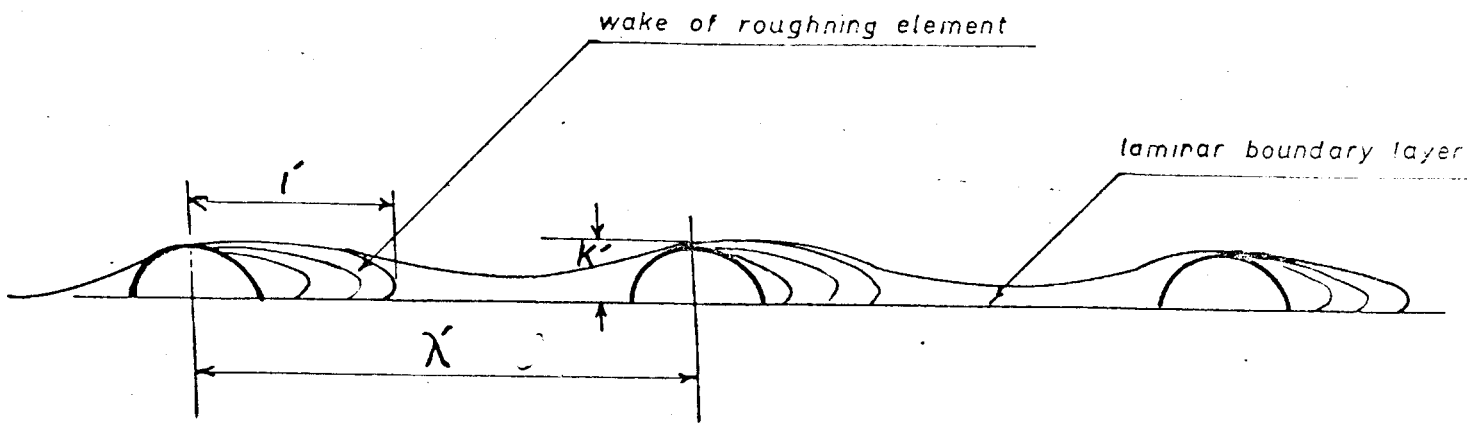

SEMI - SMOOTH TURBULENT FLOW

FIG 2

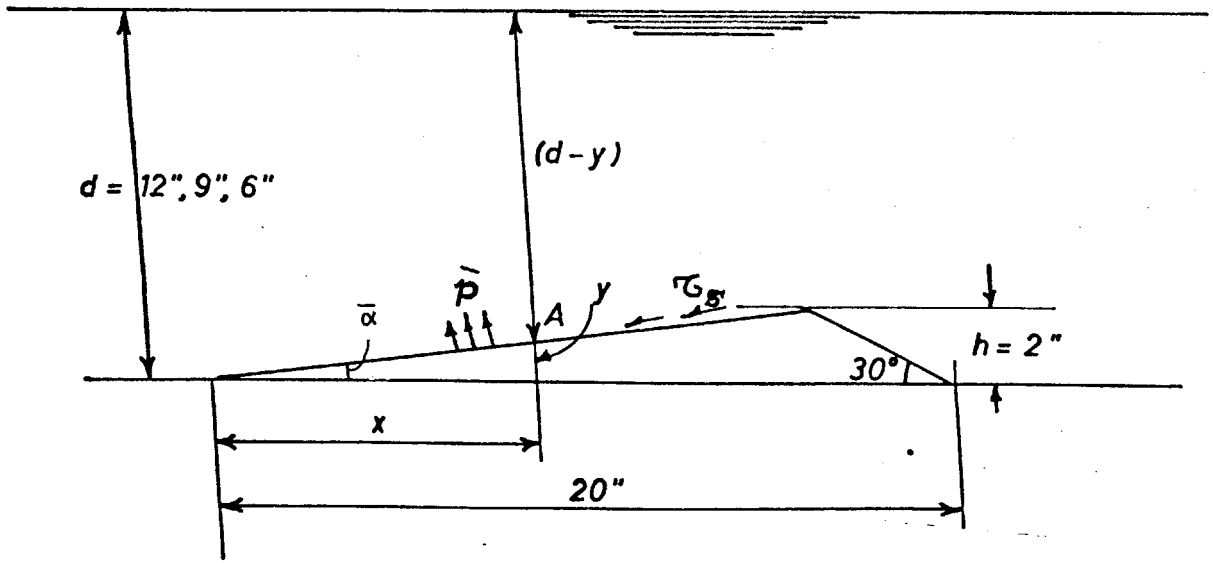

TRIANGULAR ELEMENT

FIG 3

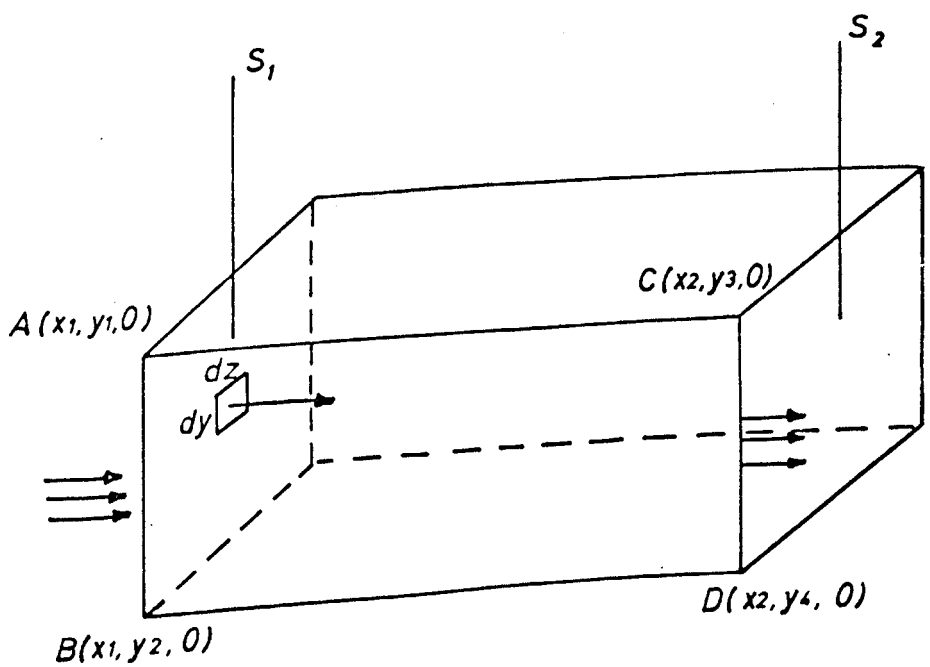

MOMENTUM BALANCE

FIG 4

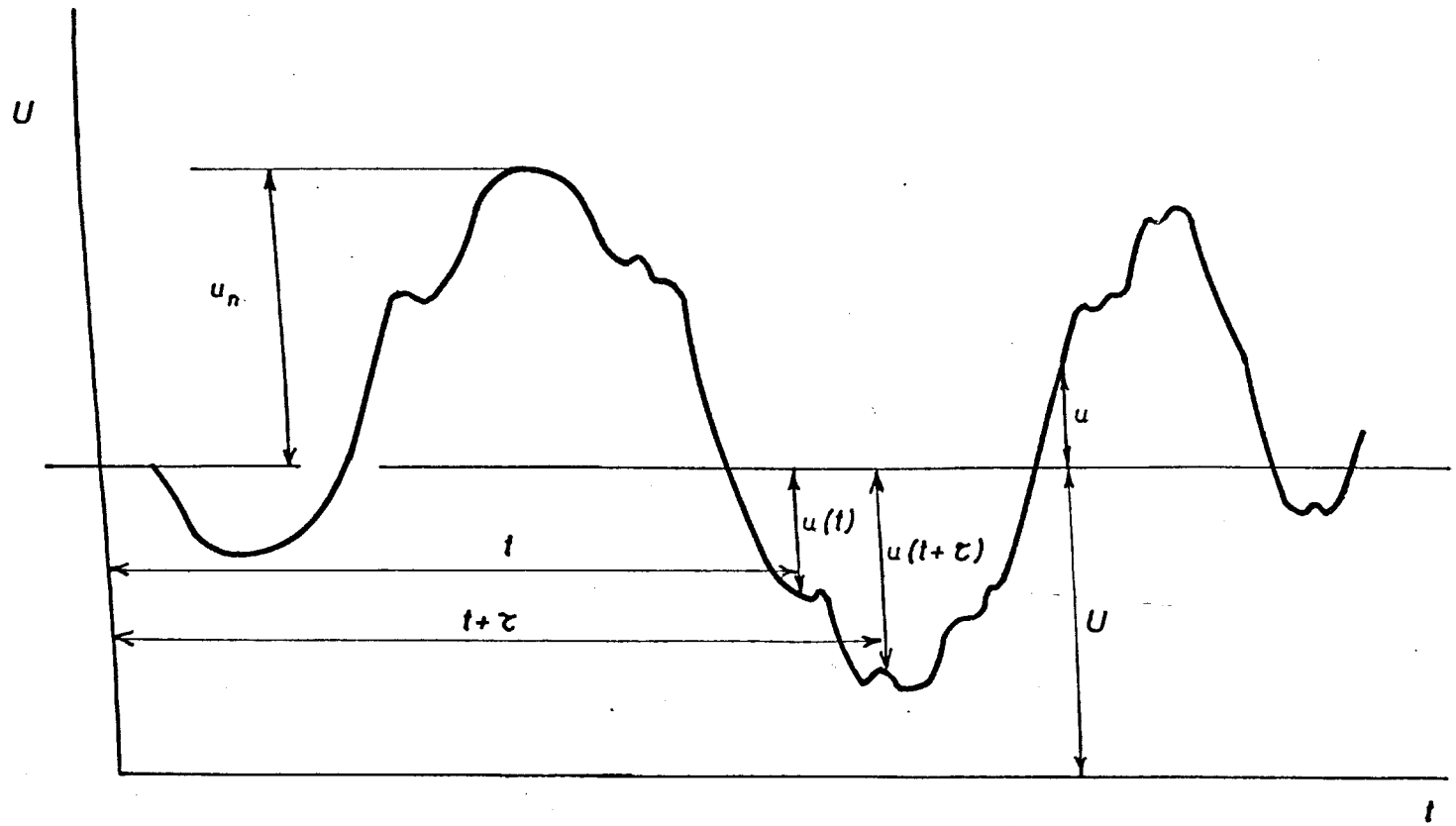

VELOCITY FLUCTUATIONS

FIG 5

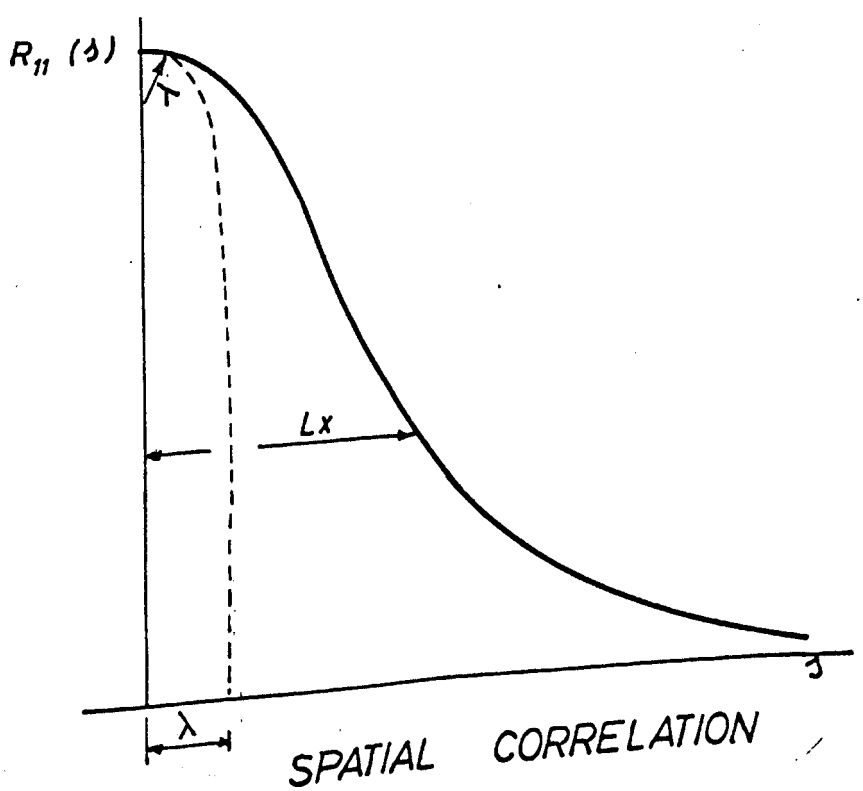

FIG 6

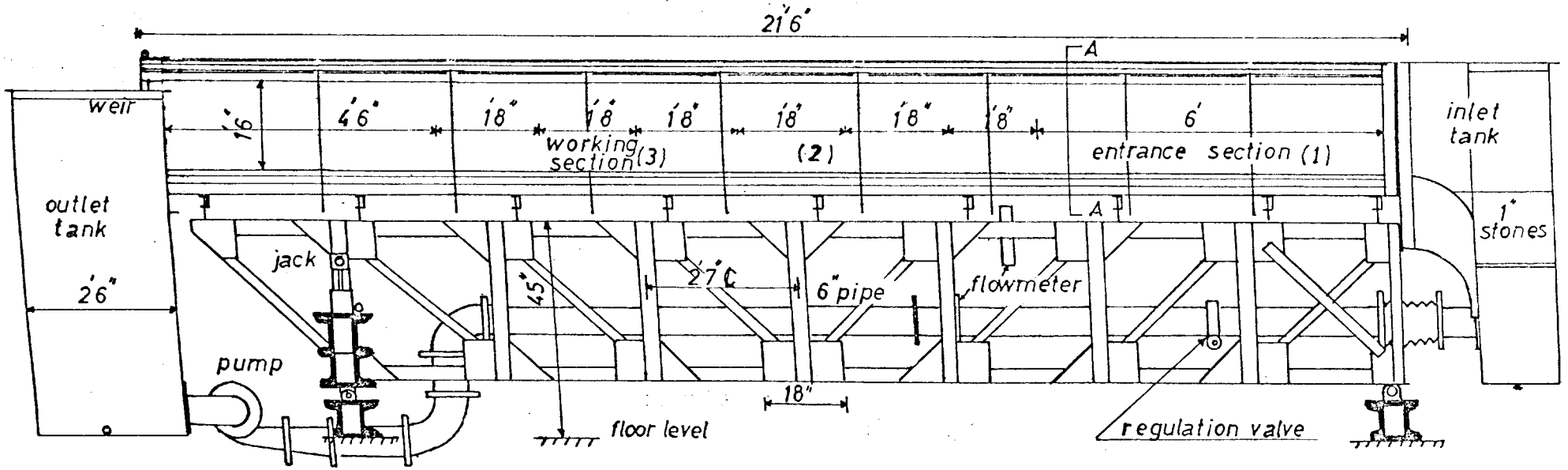

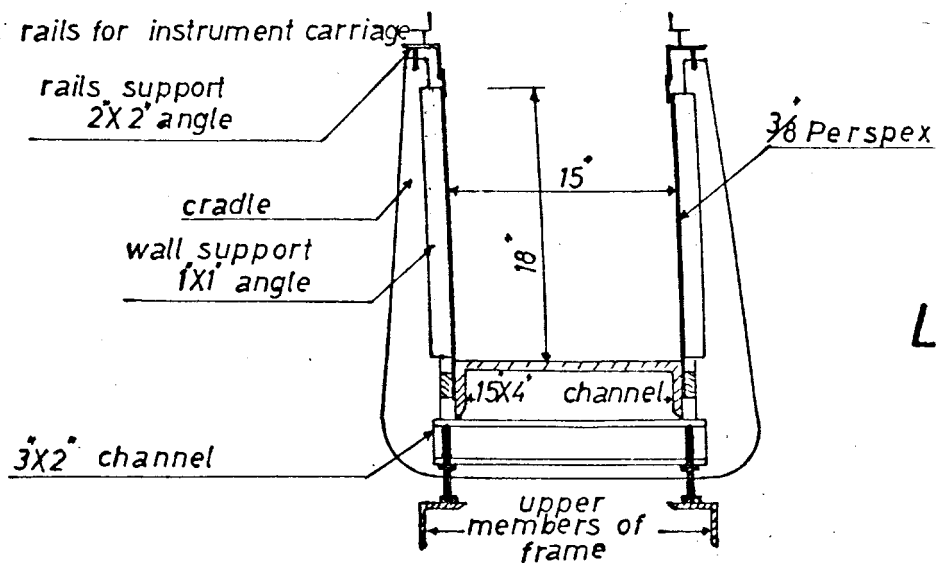

SECTIONA-A

LAYOUT OF APPARATUS

FIG 7

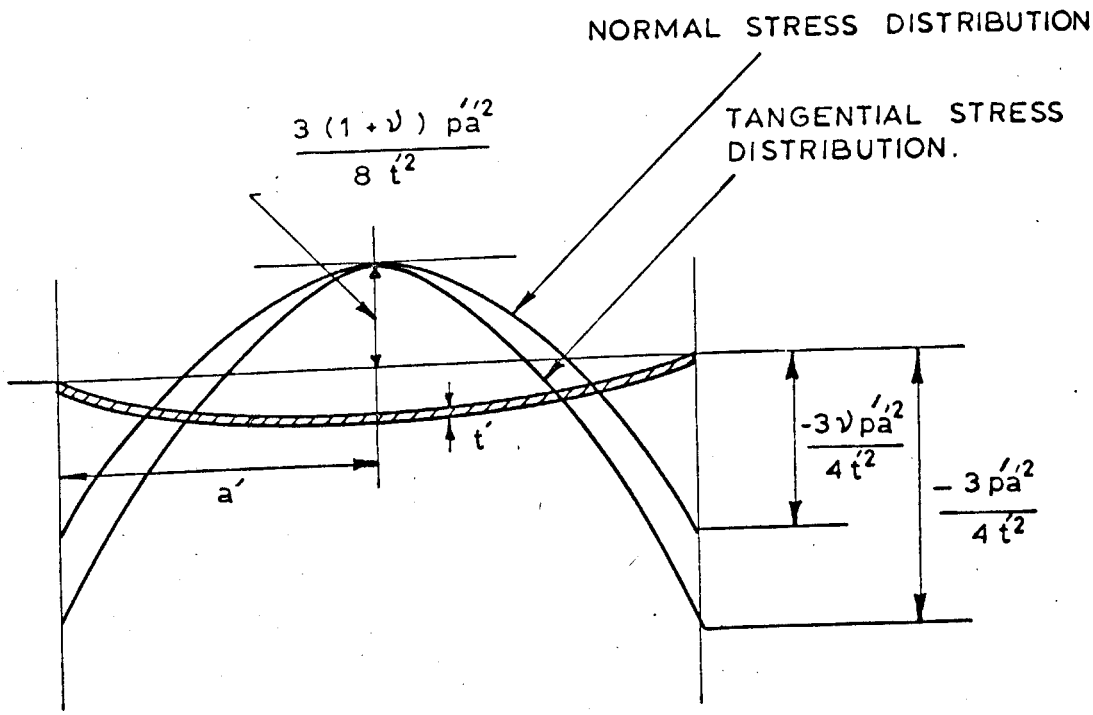

Stresses distribution in a thin circular diaphragm clamped from both edges (cross section).

FIG 8

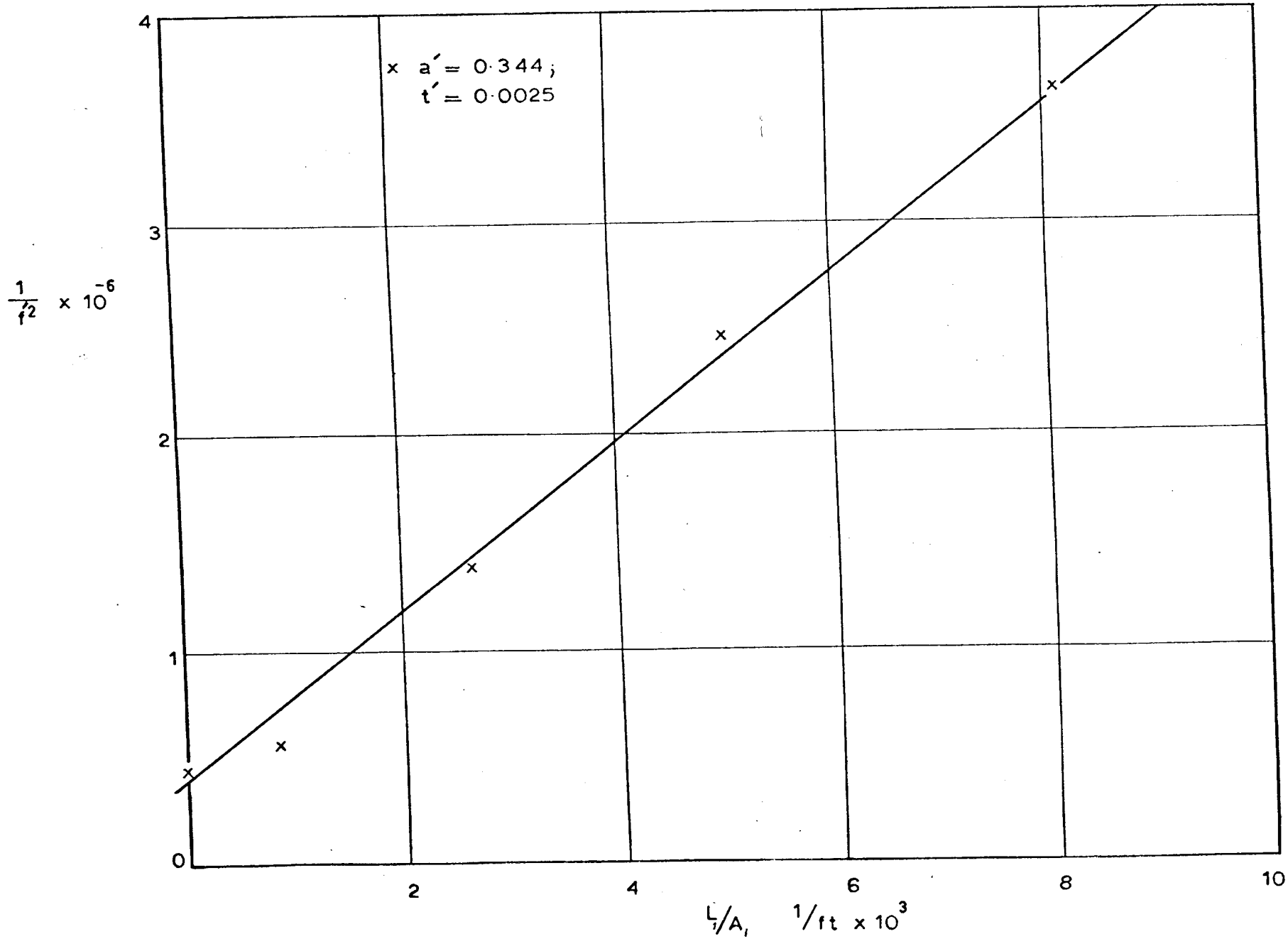

FIG 9

RELATION OF INLET PIPE TO RESONANT FREQUENCY

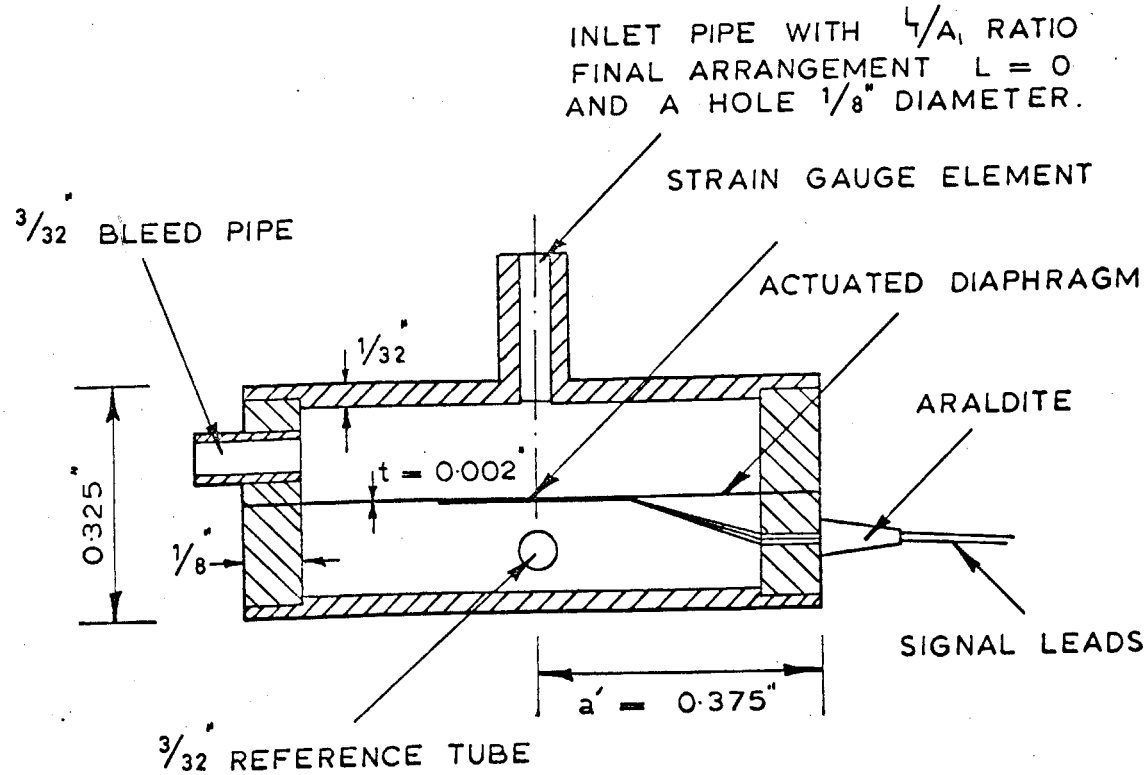

Cross section in the transducer .

FIG 10

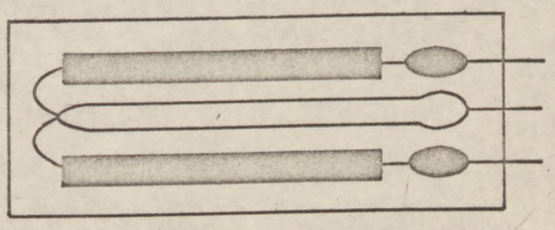

KGP-7-F1-11

GAUGE FACTOR $K' = 200$
LENGTH 7mm
WIDTH 4.5mm
MAX STRAIN 2,000 (μ STRAIN)
MAX OPERATION CURRENT 30mA
RESISTANCE 120 ohm

Strain Gauge Element.

FIG 11

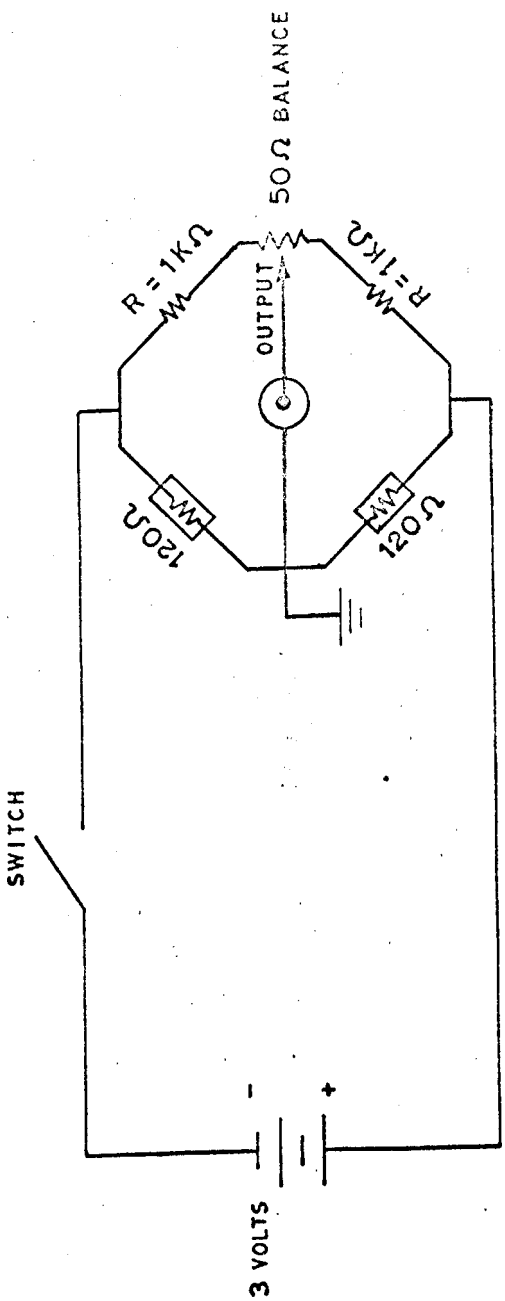

Circuit diagram of bridge

FIG 12

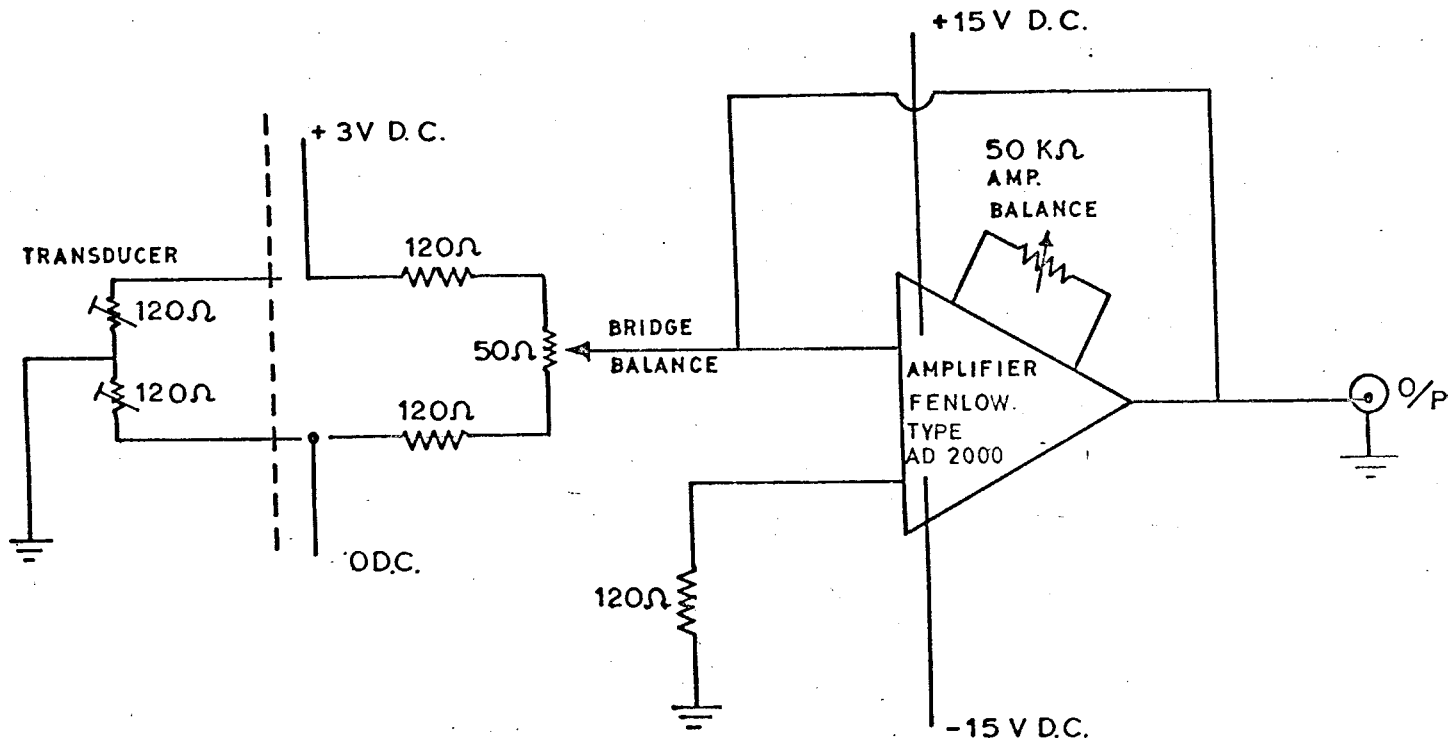

Circuit diagram of the bridge and amplifier.

FIG 13

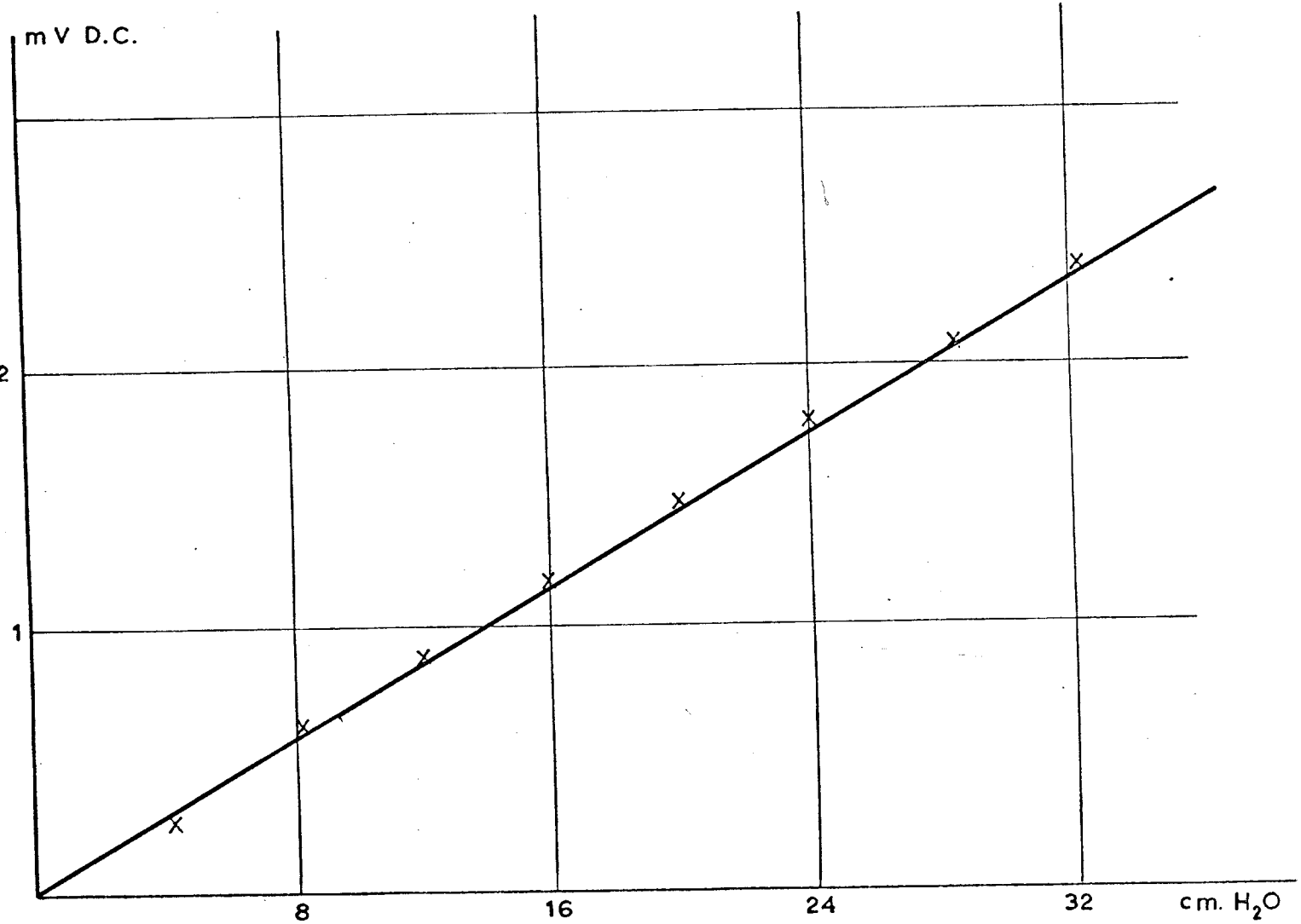

FIG 14

. Calibration curve for transducer in air .

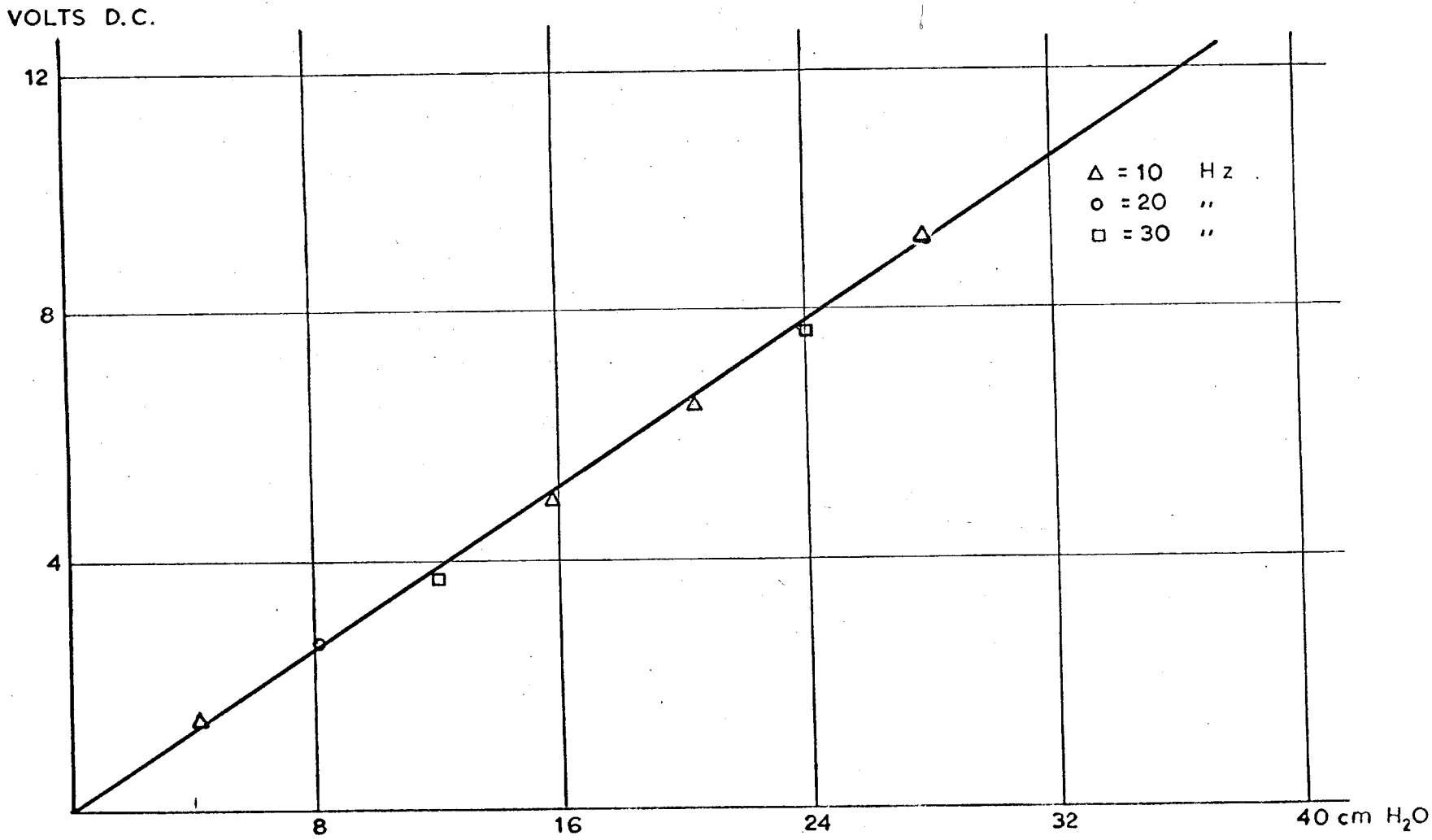

FIG 15

Calibration curve for transducer in water.

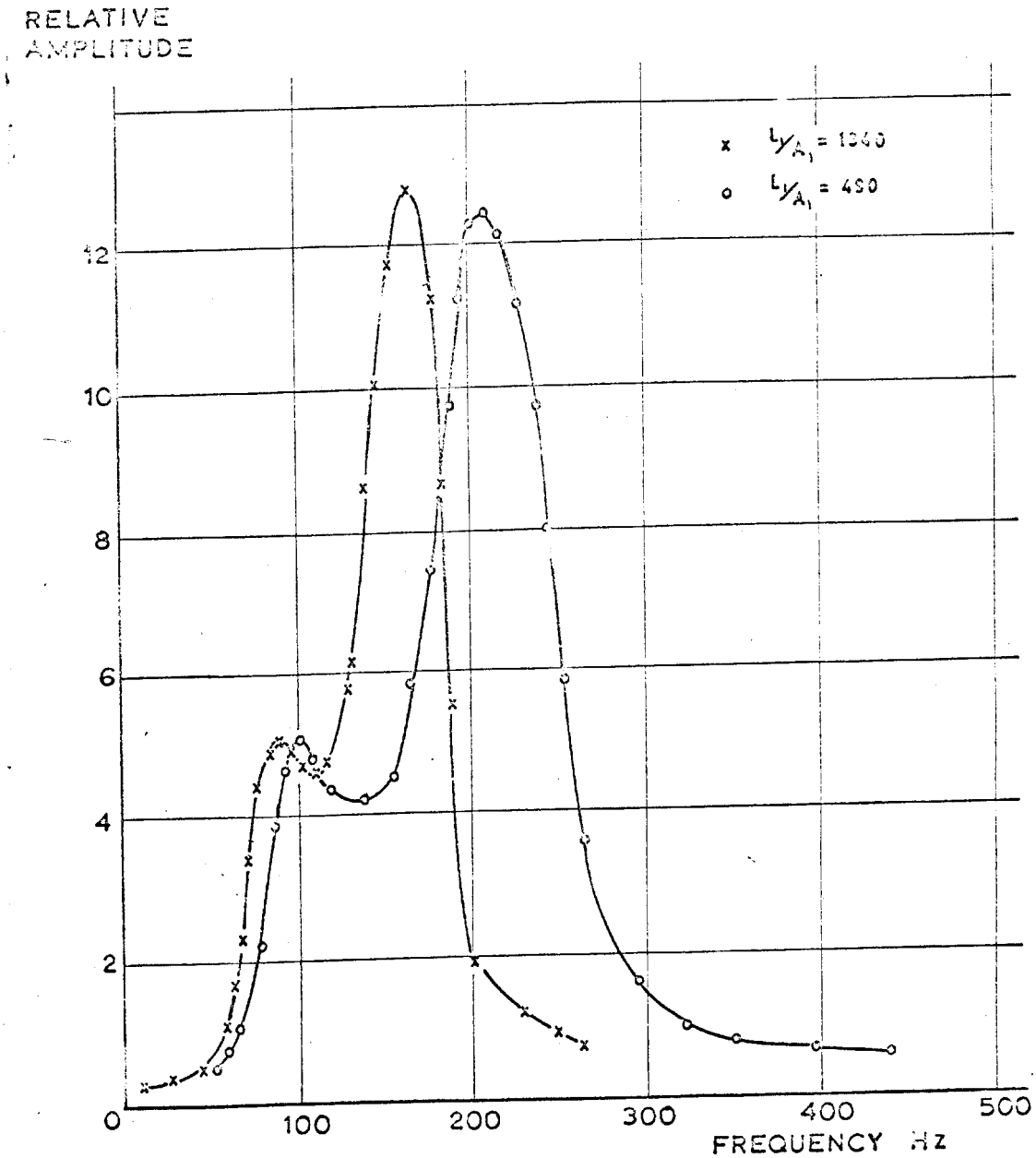

Frequency response curves.

FIG 16

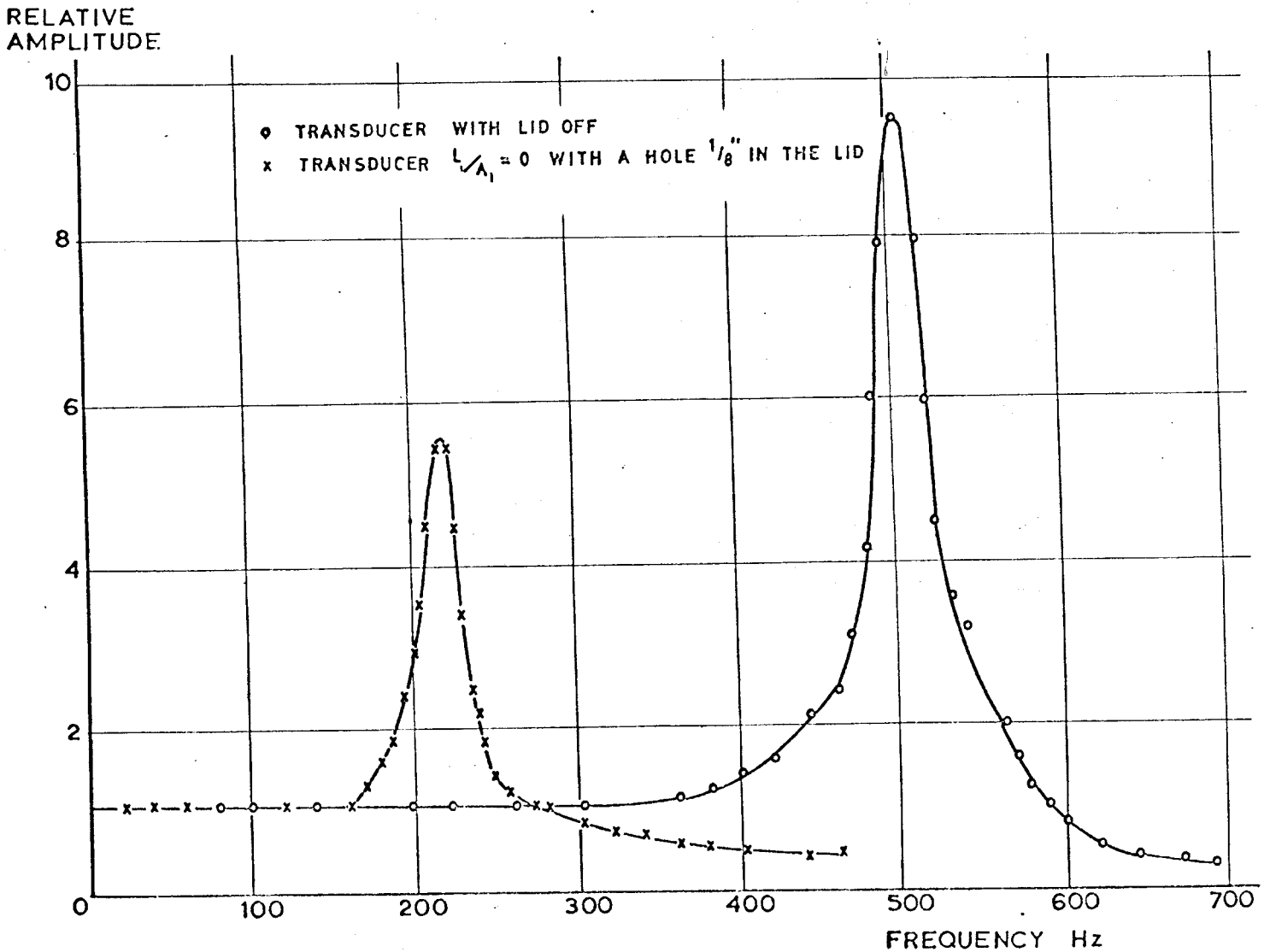

FIG 17

Frequency response curves.

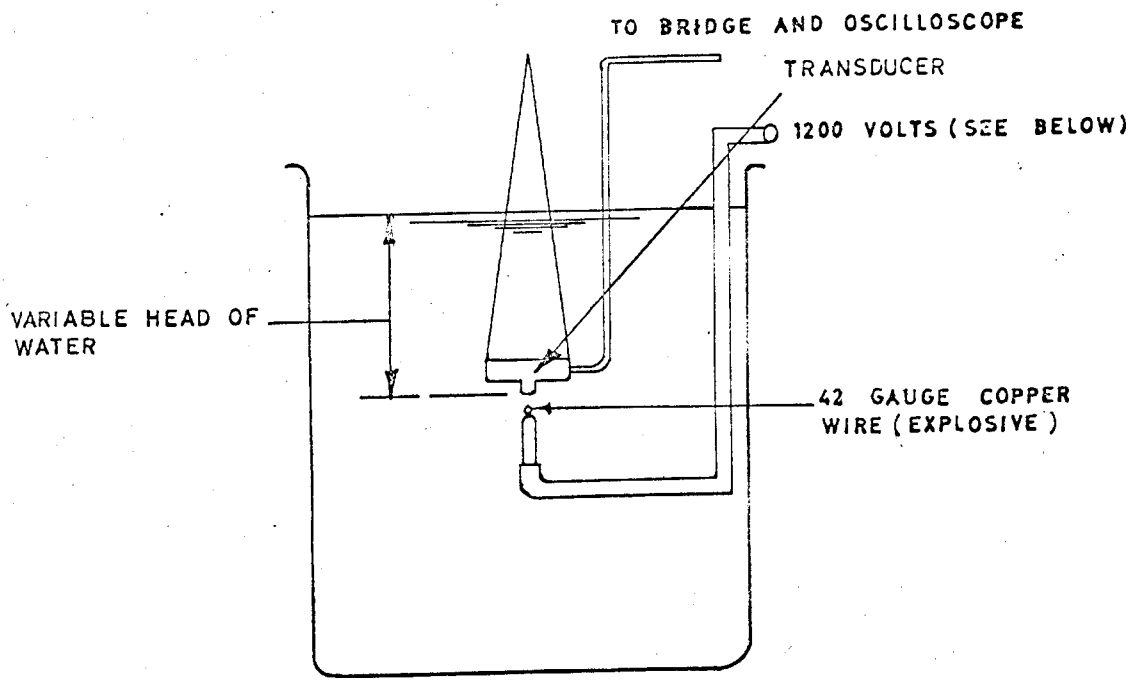

Schematic for the underwater explosion test

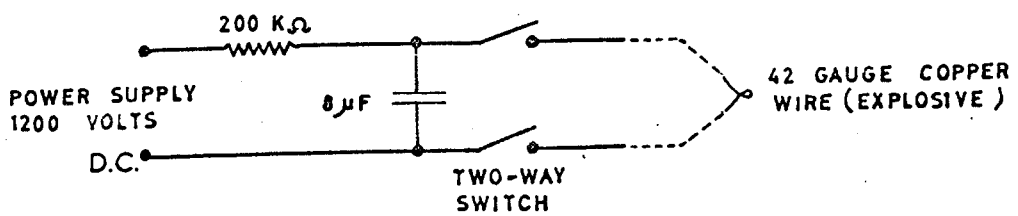

Underwater explosion test.

FIG 18

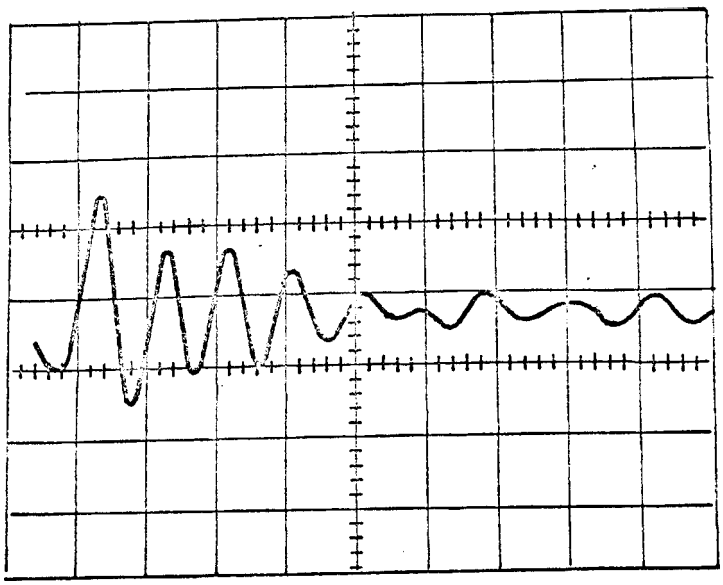

The response of the transducer to underwater explosion.
L_1/A_1 = 490 Horizontal scale 5 msec/cm
Vertical scale 5 volts/cm
$f' \simeq$ 200 Hz

FIG 19

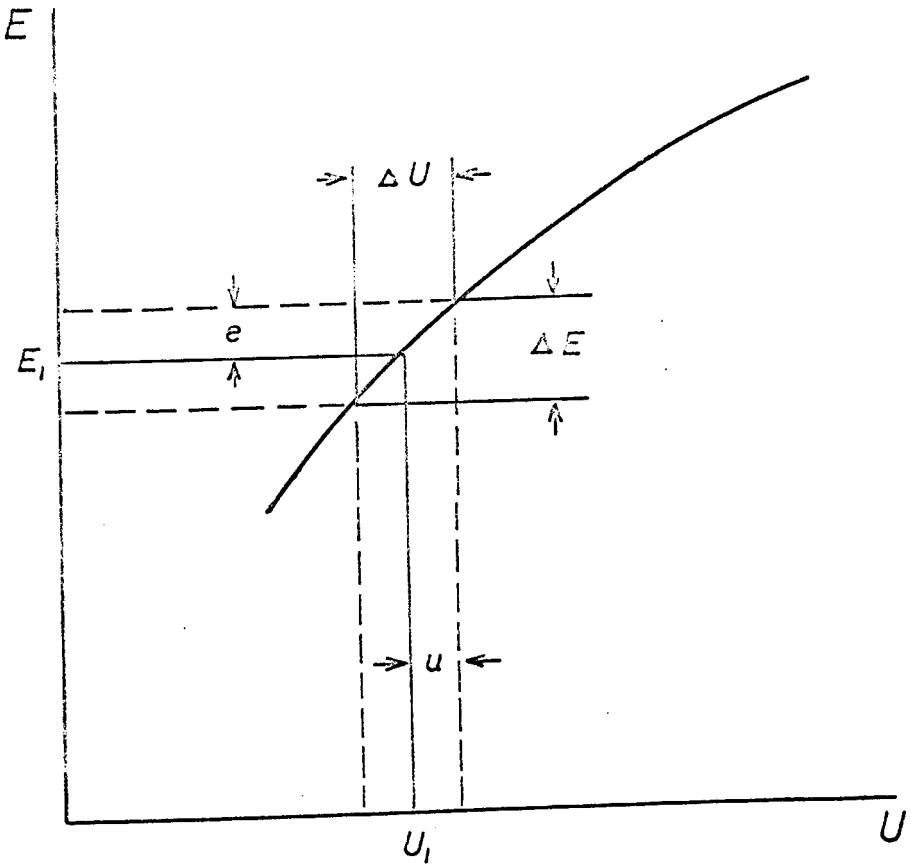

VARIATION OF VOLTAGE WITH VELOCITY

FIG 20

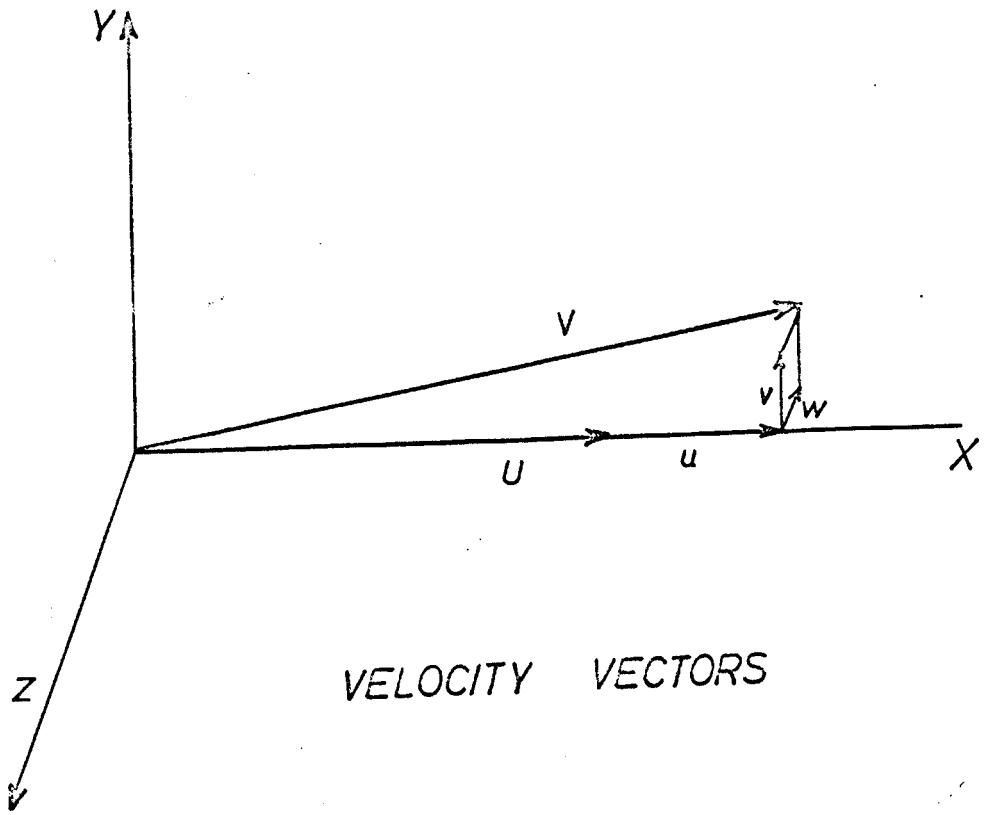

VELOCITY VECTORS

FIG 21

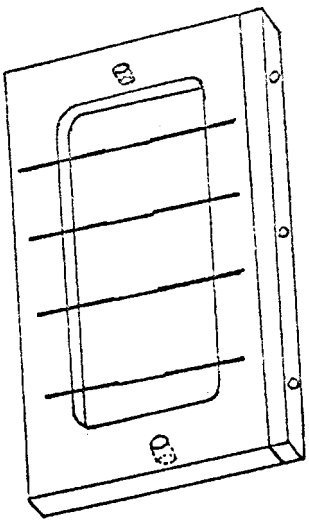

Plating Frame

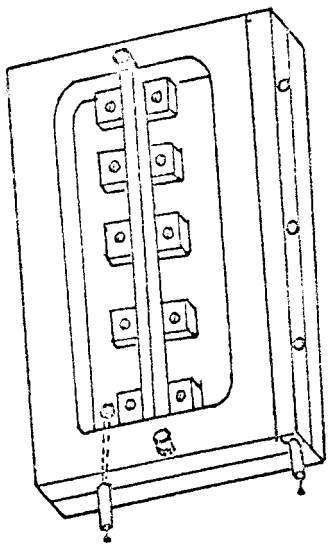

Plating Bath

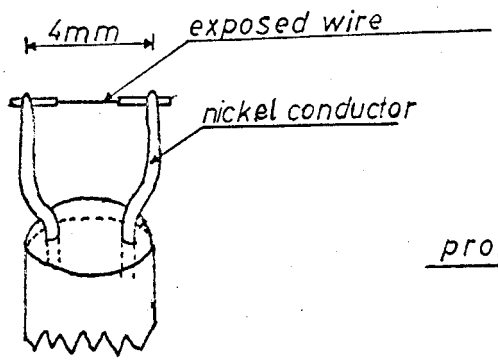

Hot-wire Probe

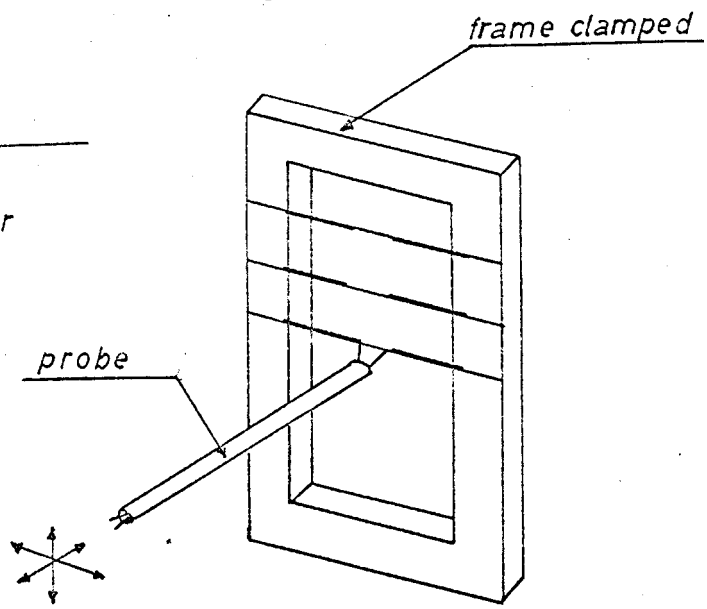

Hot-wire Manufacture

FIG 22

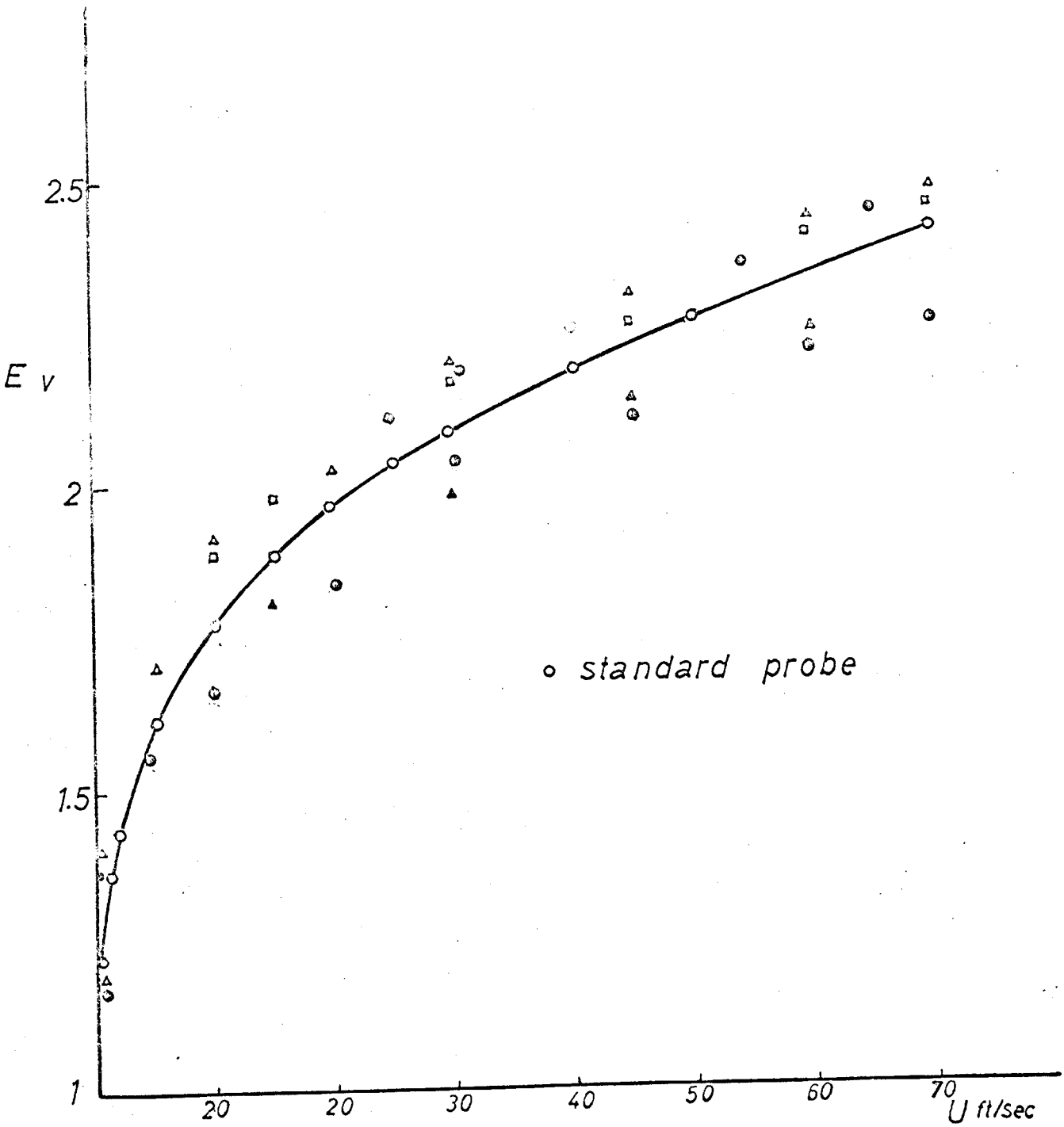

Calibration Curve of Hot-wires Used

FIG 23

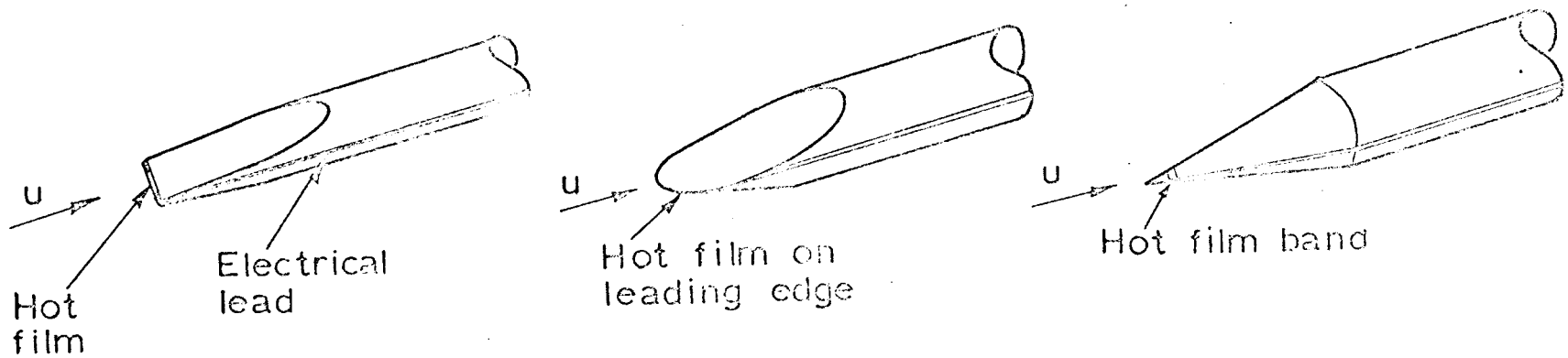

FIG 24

TYPES OF SENSORS

TEMPERATURE COMPENSATION

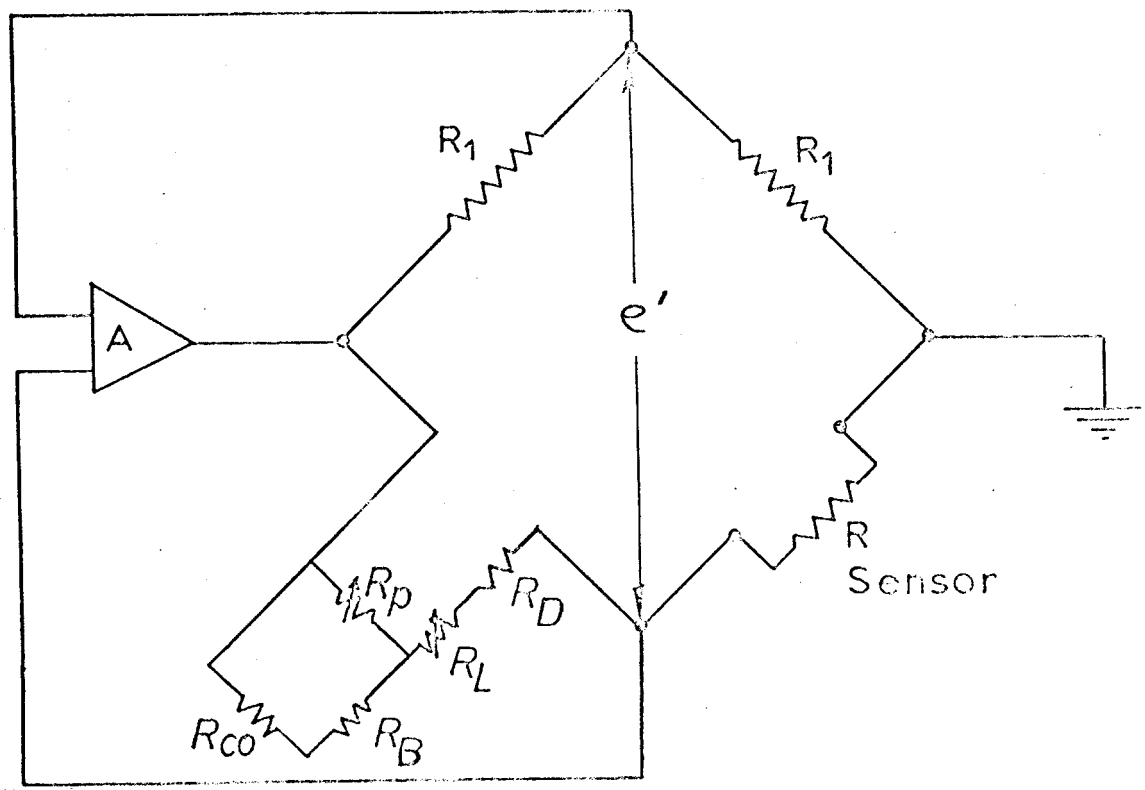

FIG 25

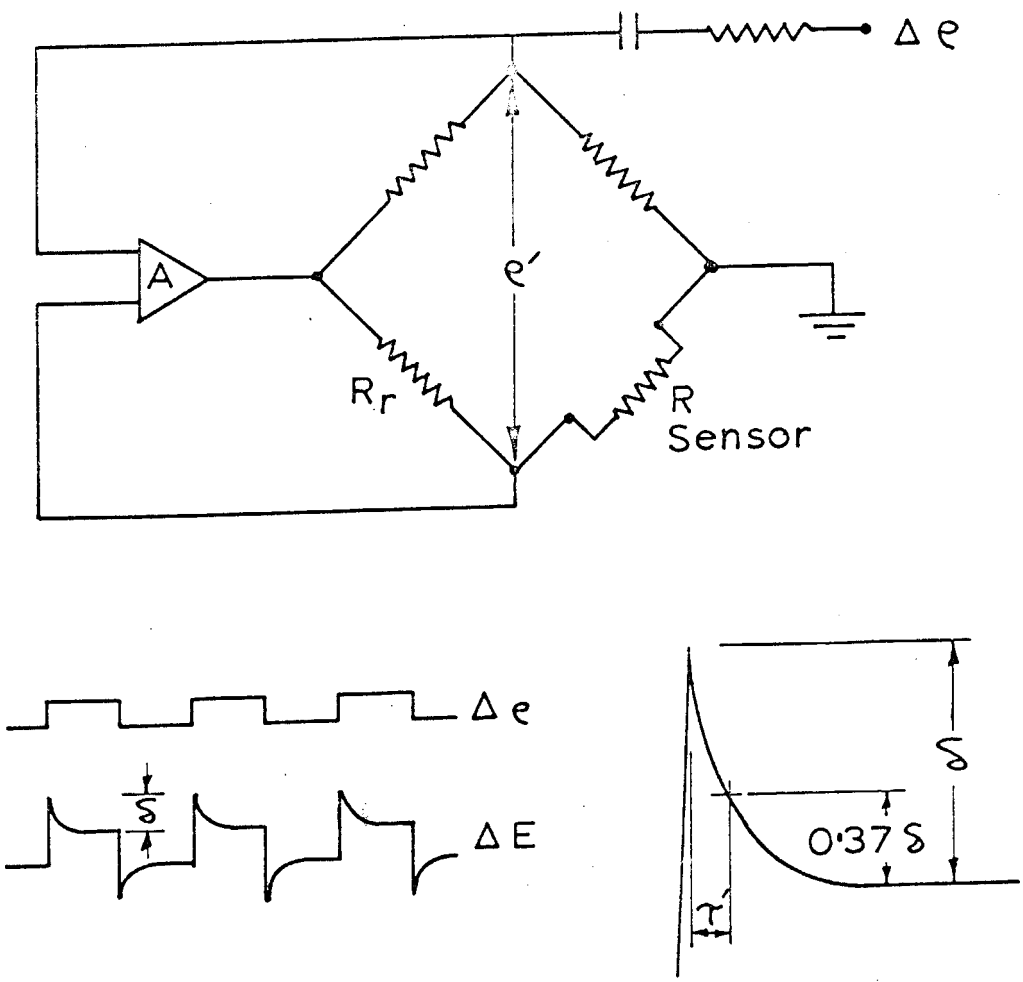

MEASUREMENT OF TIME CONSTANT

FIG 26

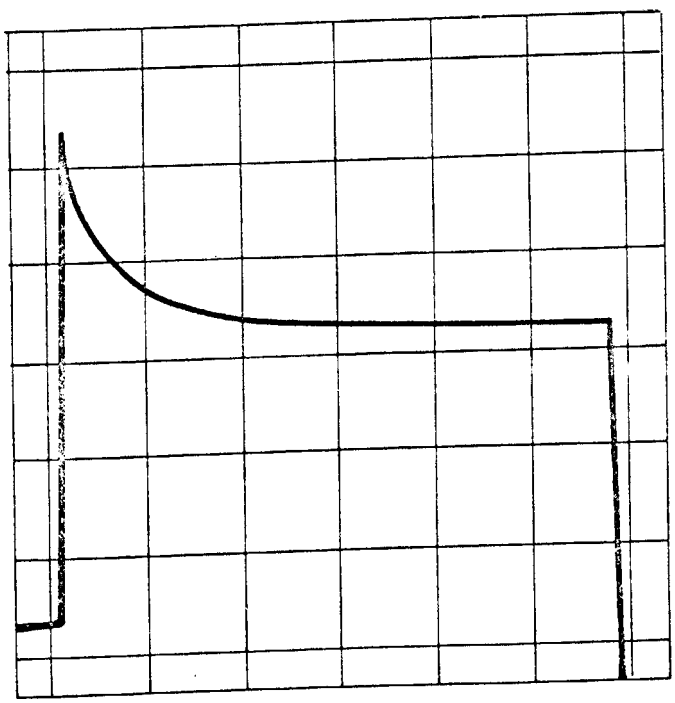

Vertical : 1 Division = 100 mV

Horizontal : 1 Division = 0·8 m sec

TIME CONSTANT DETERMINATION

FIG 27

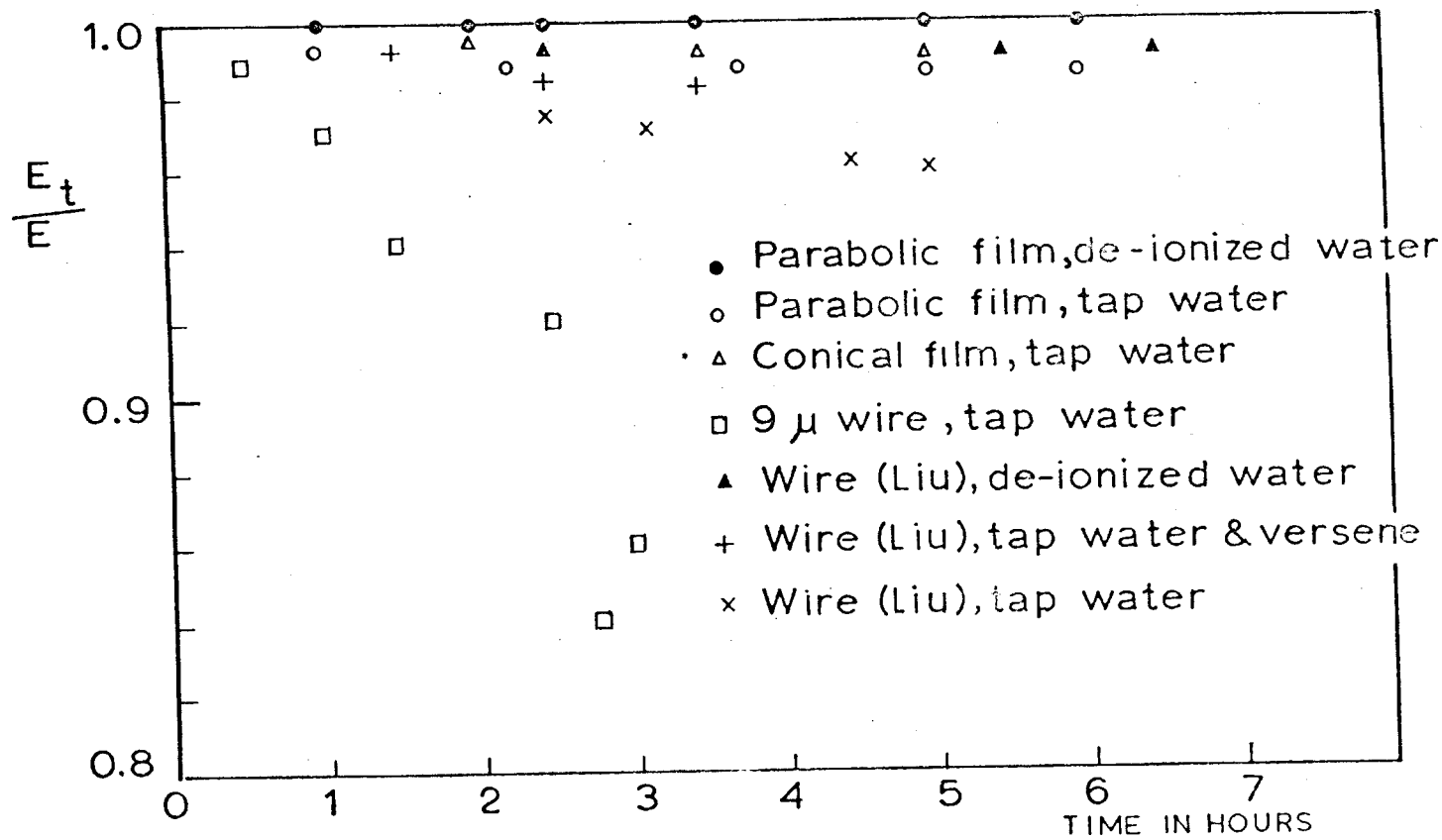

FIG 28

STABILITY MEASUREMENTS

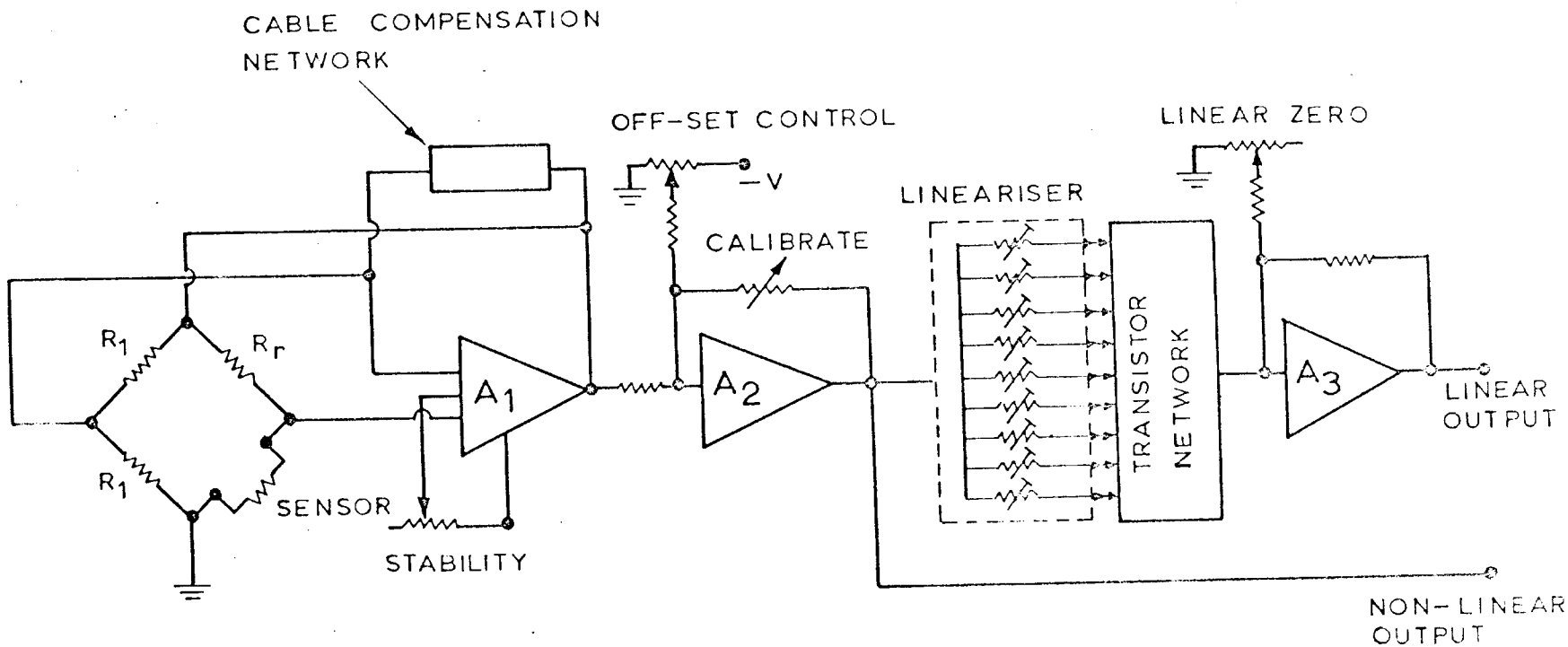

FIG 29

OUTLINE OF ANEMOMETER TYPE I.S.V.R 201

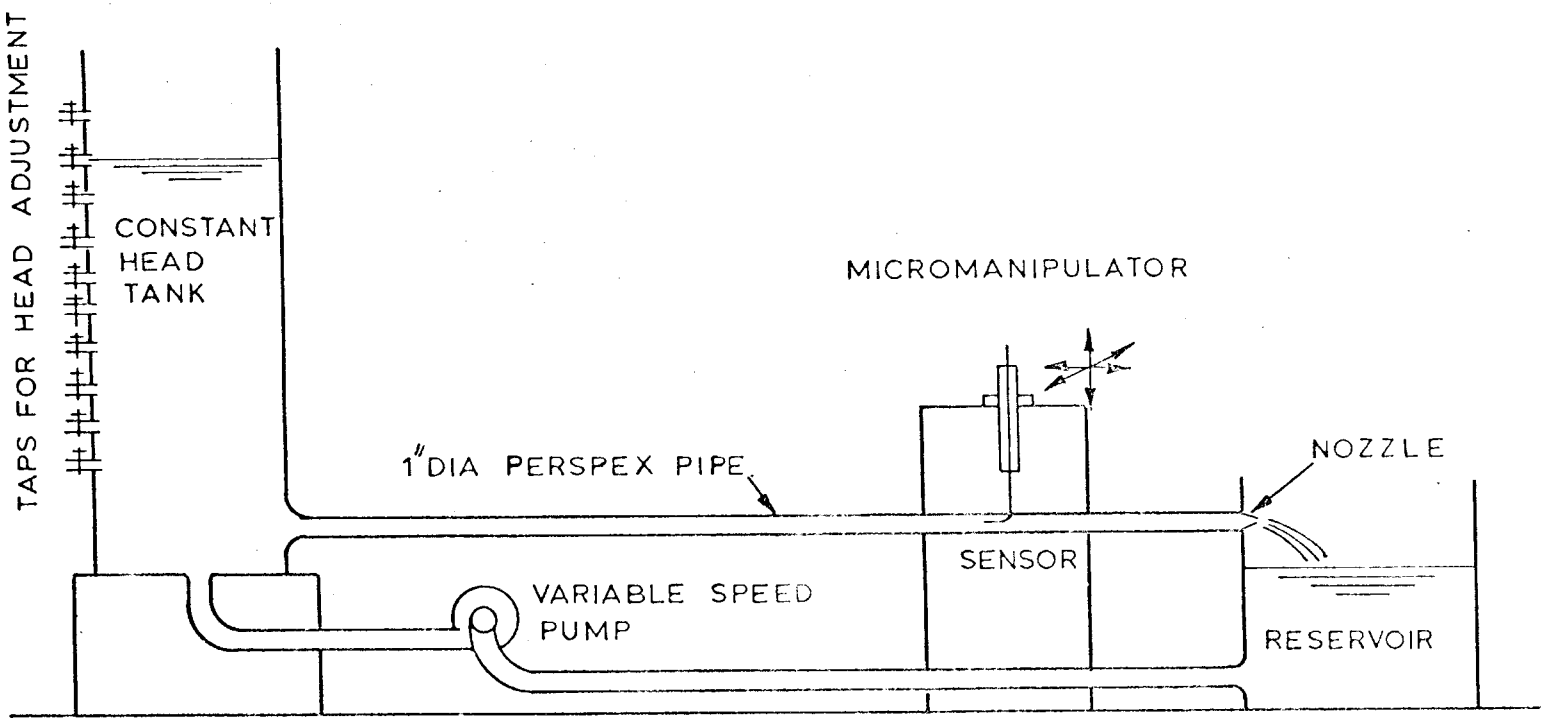

CALIBRATION DEVICE

FIG 30

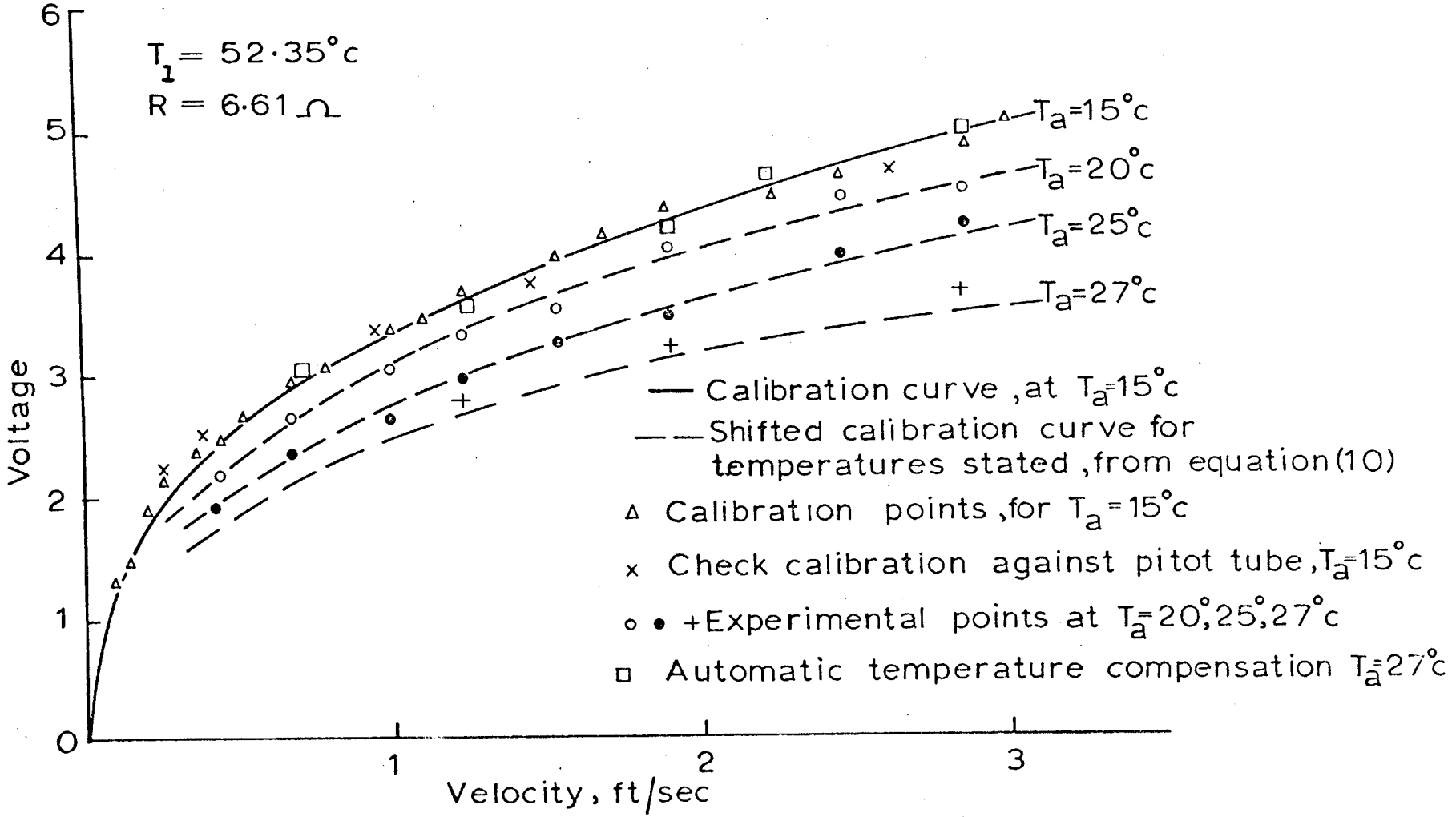

CALIBRATION CURVE FOR CONICAL SENSOR

FIG 31

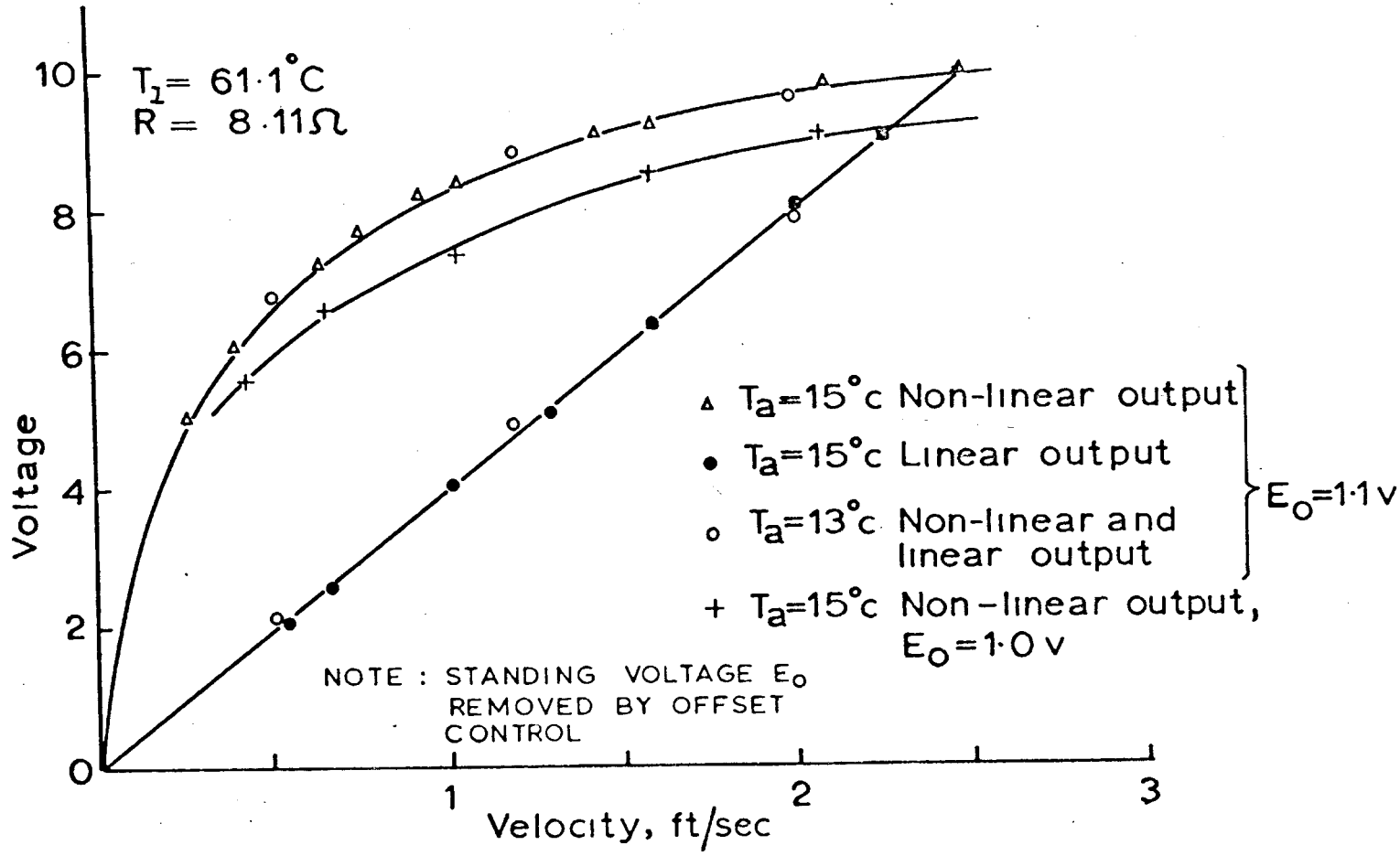

FIG 32

CALIBRATION CURVE FOR PARABOLIC SENSOR

PRESSURE DISTRIBUTION
$\bar{u}$ ft/sec
0·88
1·23
1·32
1·41
1·58
1·76
1·89
inches
6
8
10
12
4
6
10
pressure mm of water
5
4
3
2
1
0
1
2

FIG 33

SURFACE SHEAR DISTRIBUTION
$10^3 \times \tau_s$ lb/ft^2
20
16
12
8
4
$\bar{U}$ ft/sec
1.89
1.76
1.41
1.32
1.23
0.88

FIG 34

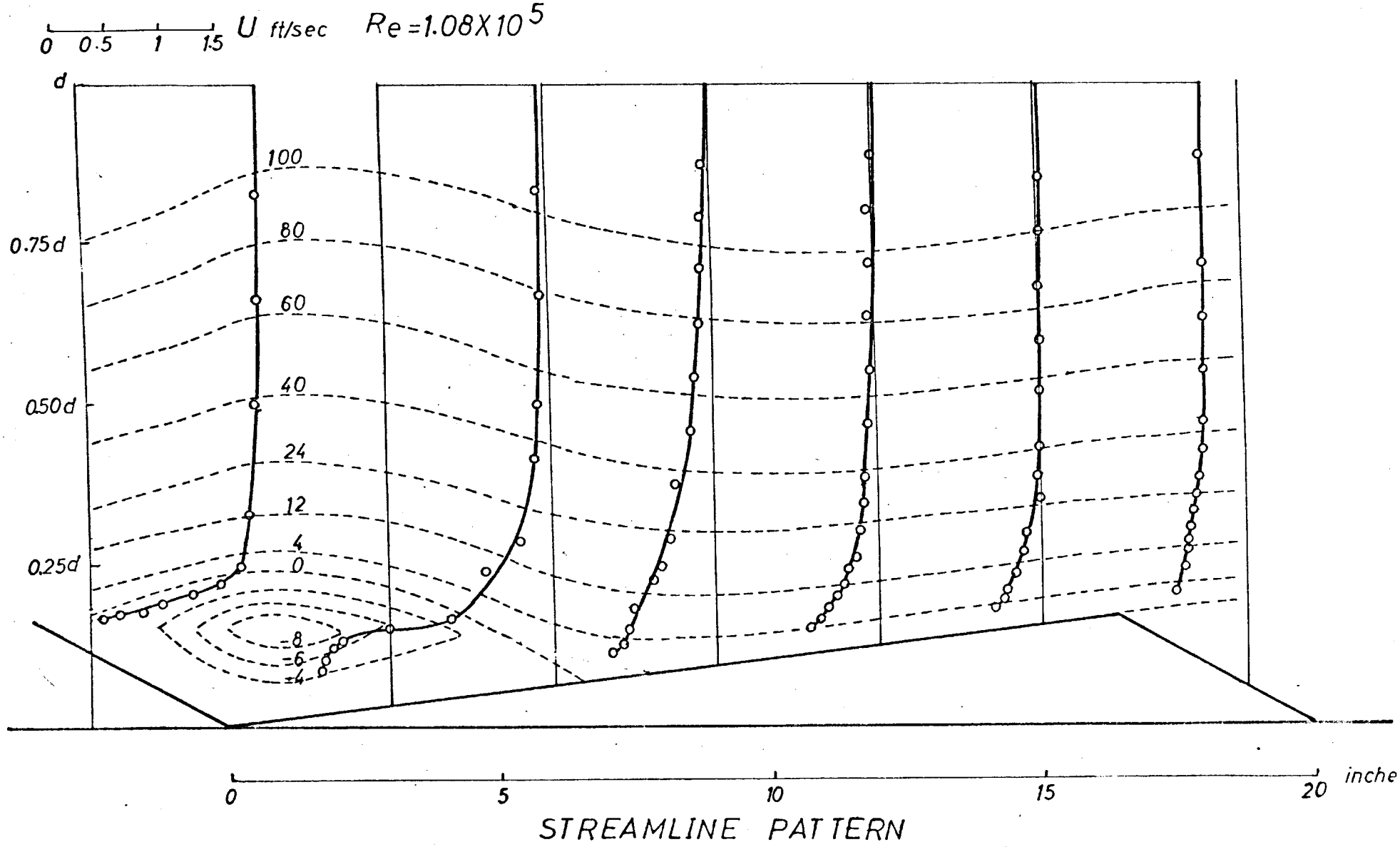

STREAMLINE PATTERN

FIG 35

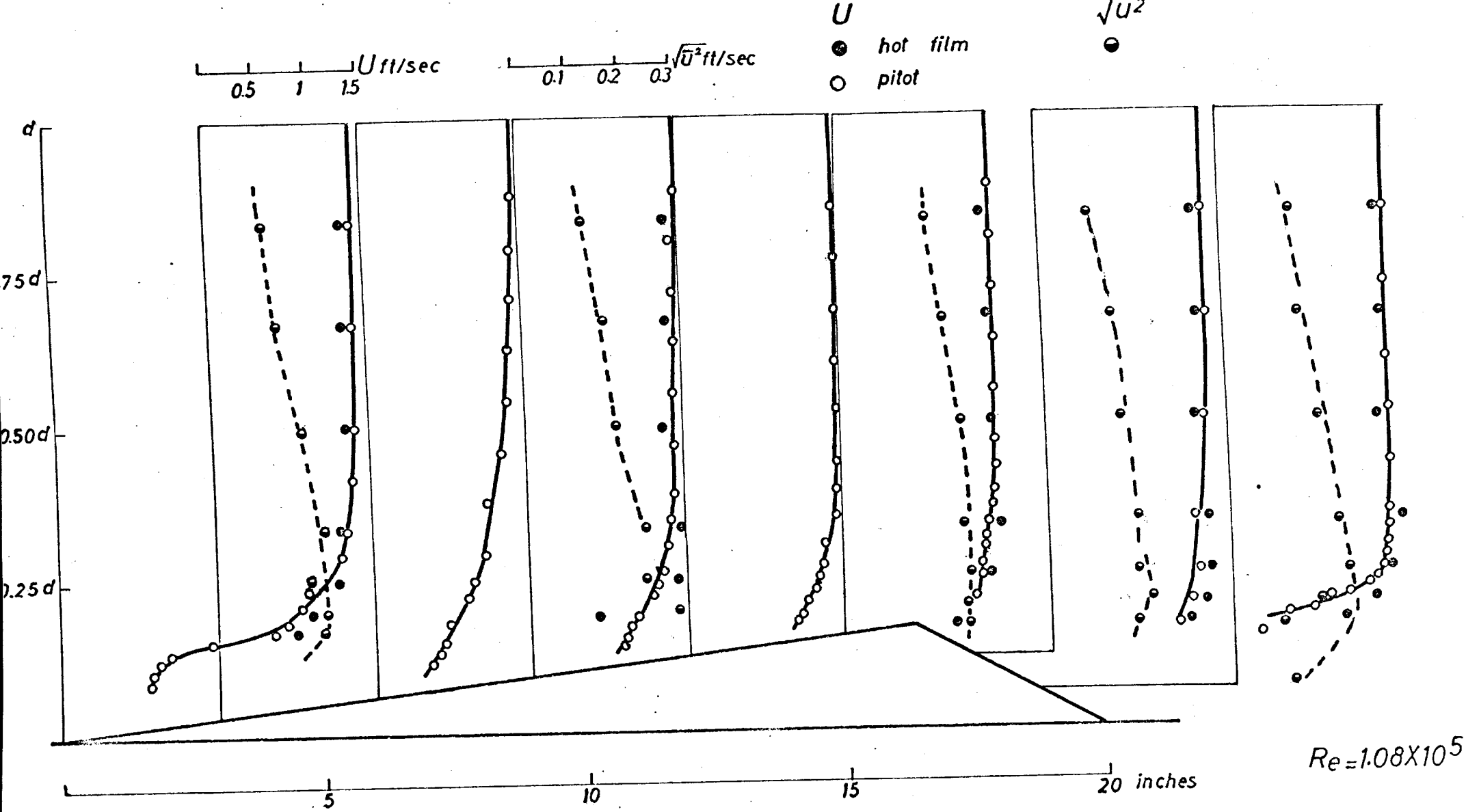

VELOCITY AND TURBULENCE DISTRIBUTION

FIG 36

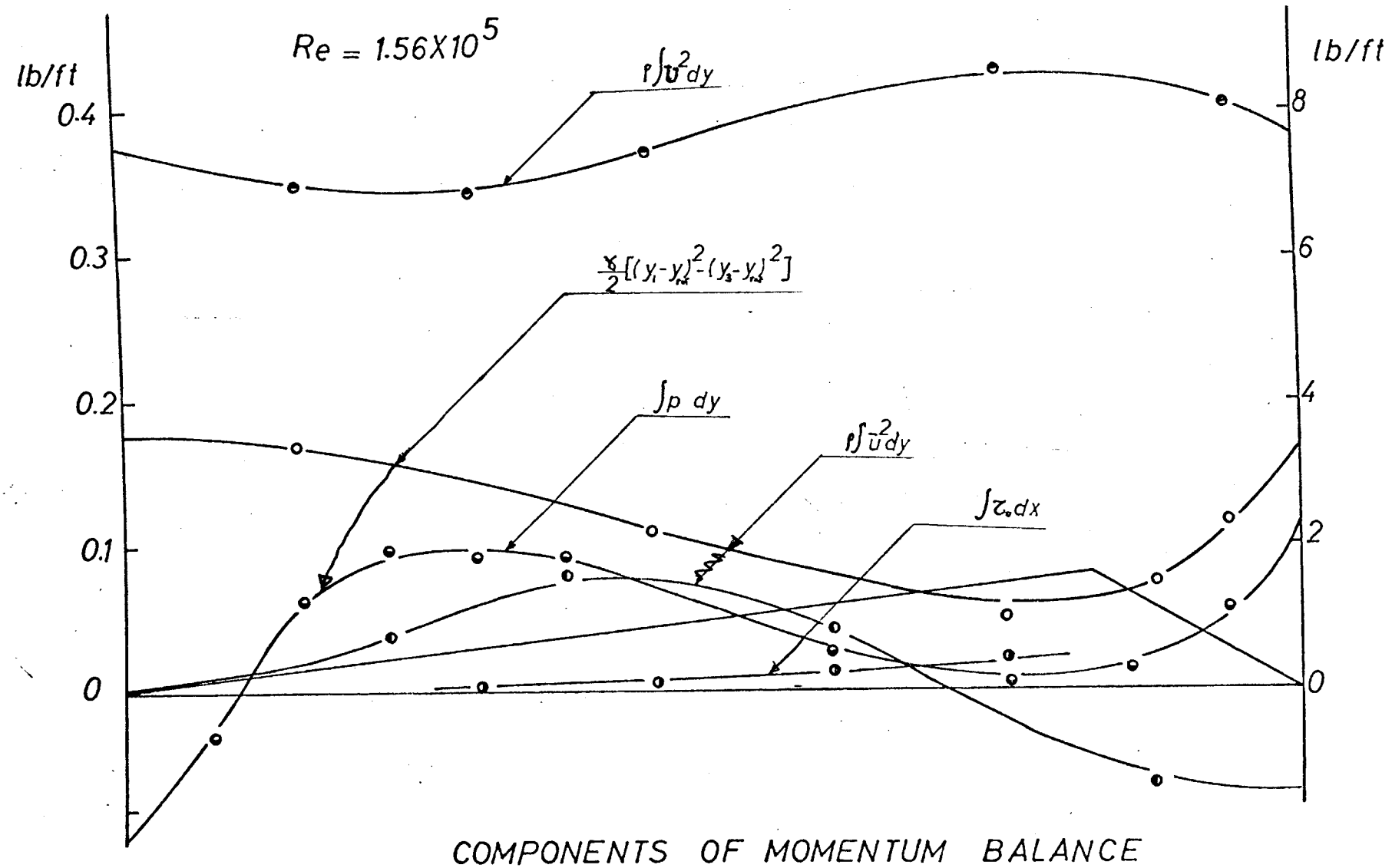

COMPONENTS OF MOMENTUM BALANCE

FIG 37

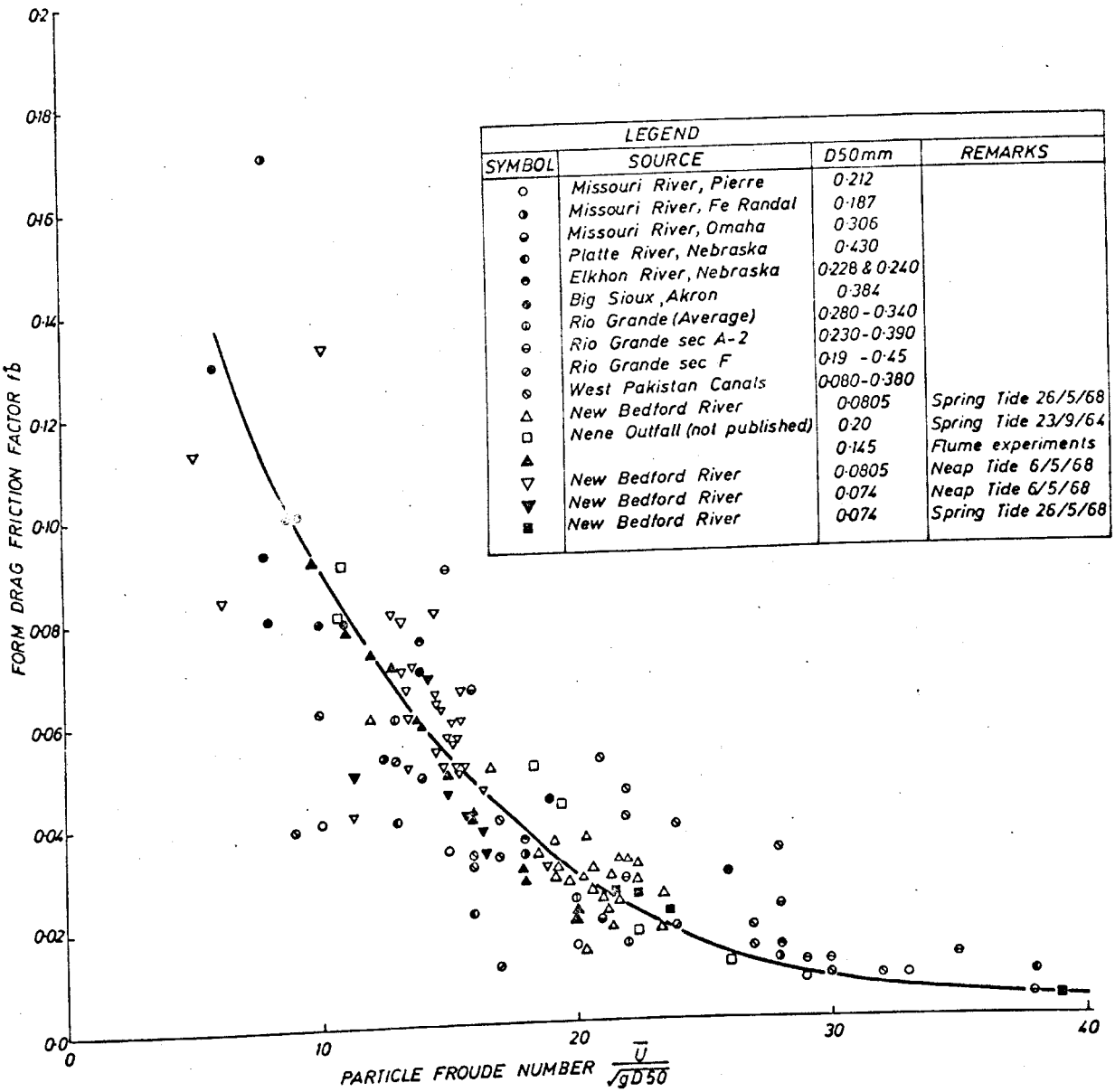

VARIATION OF FRICTION FACTOR WITH FROUDE NUMBER

FIG 38

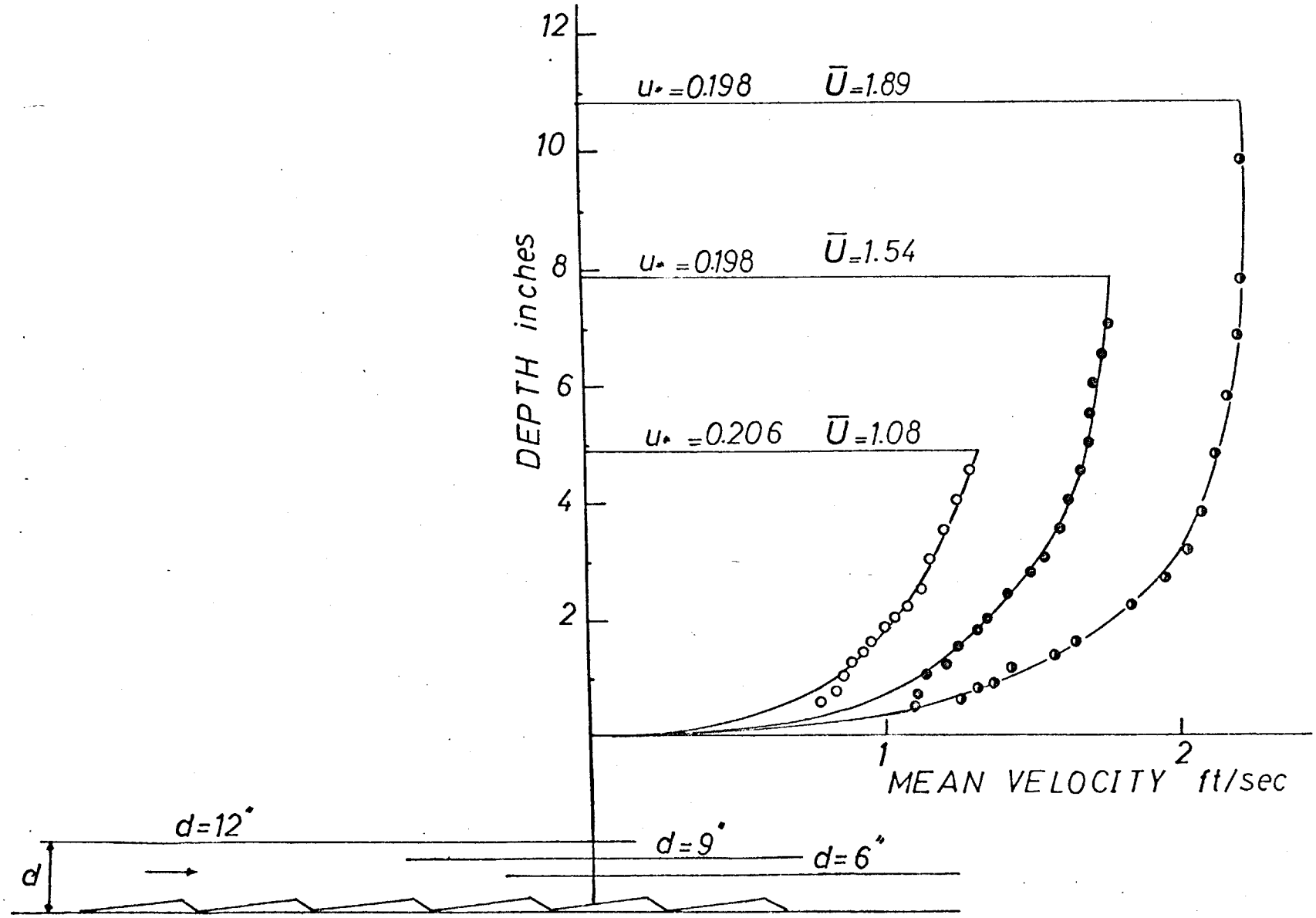

FIG 39

VARIATION OF VELOCITY DISTRIBUTION WITH DEPTH

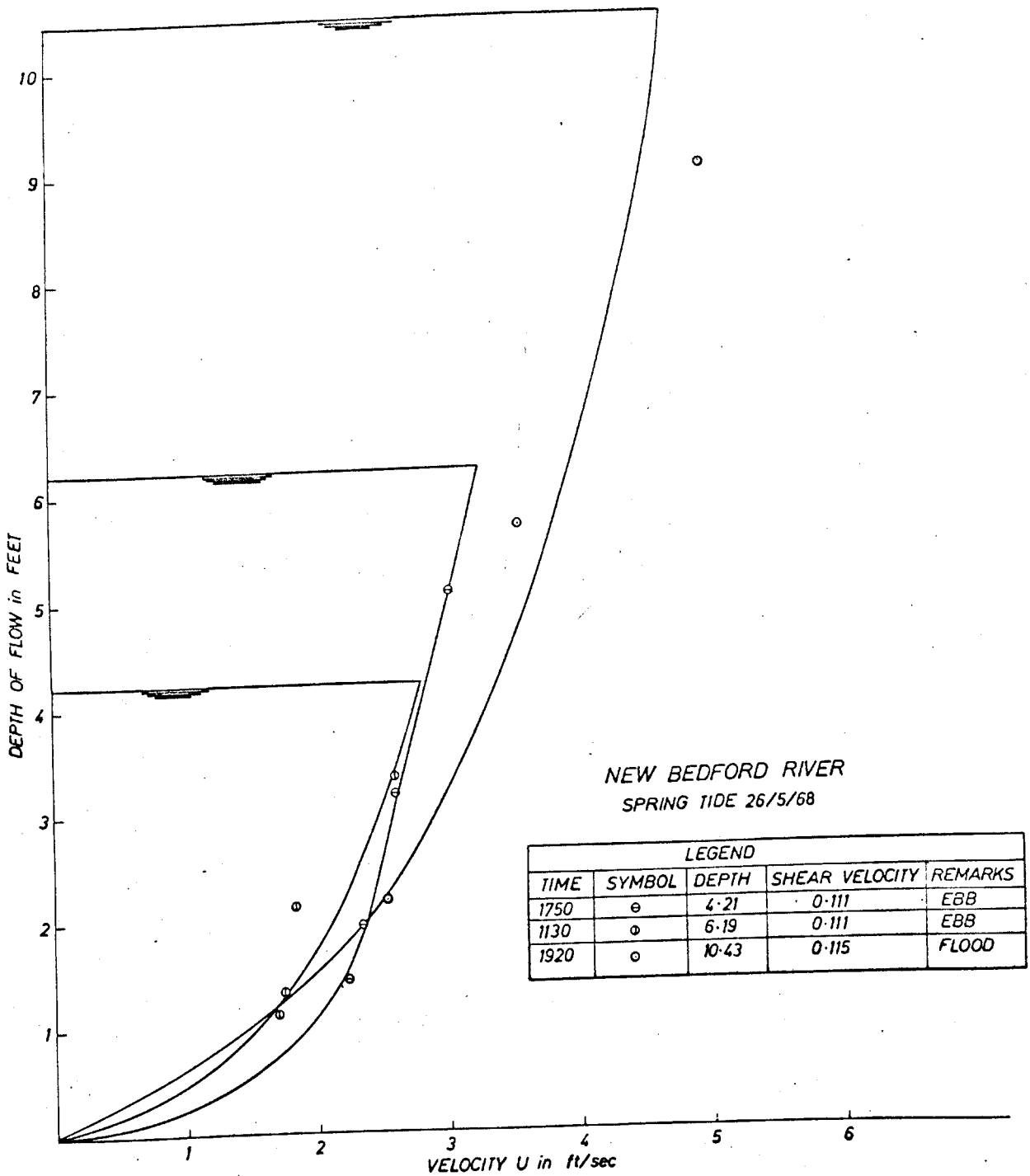

VELOCITY DISTRIBUTION

FIG 4C

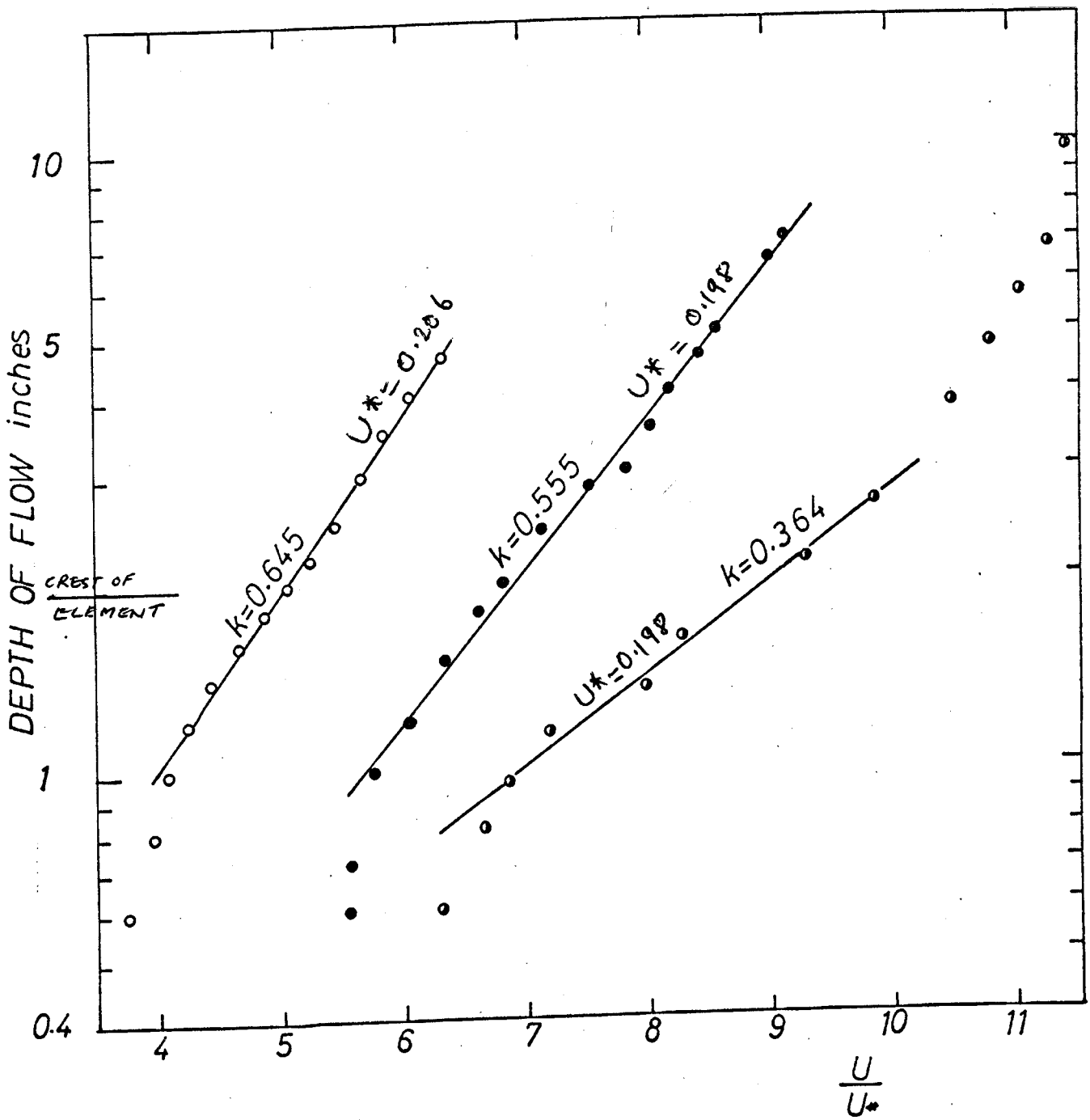

LOGARITHMIC VELOCITY DISTRIBUTION

FIG 41

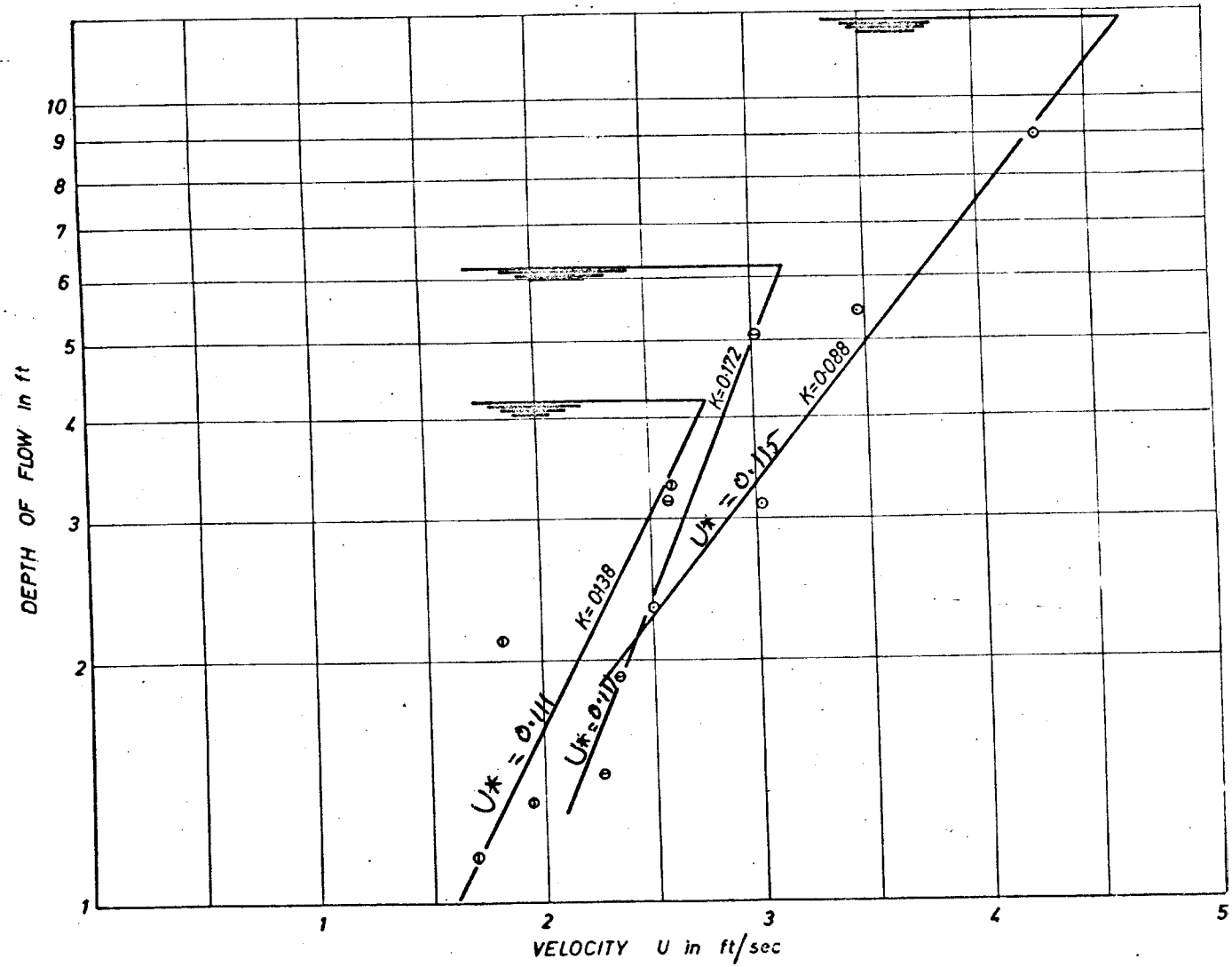

NEW BEDFORD RIVER

SPRING TIDE 26/5/68

FIG 42

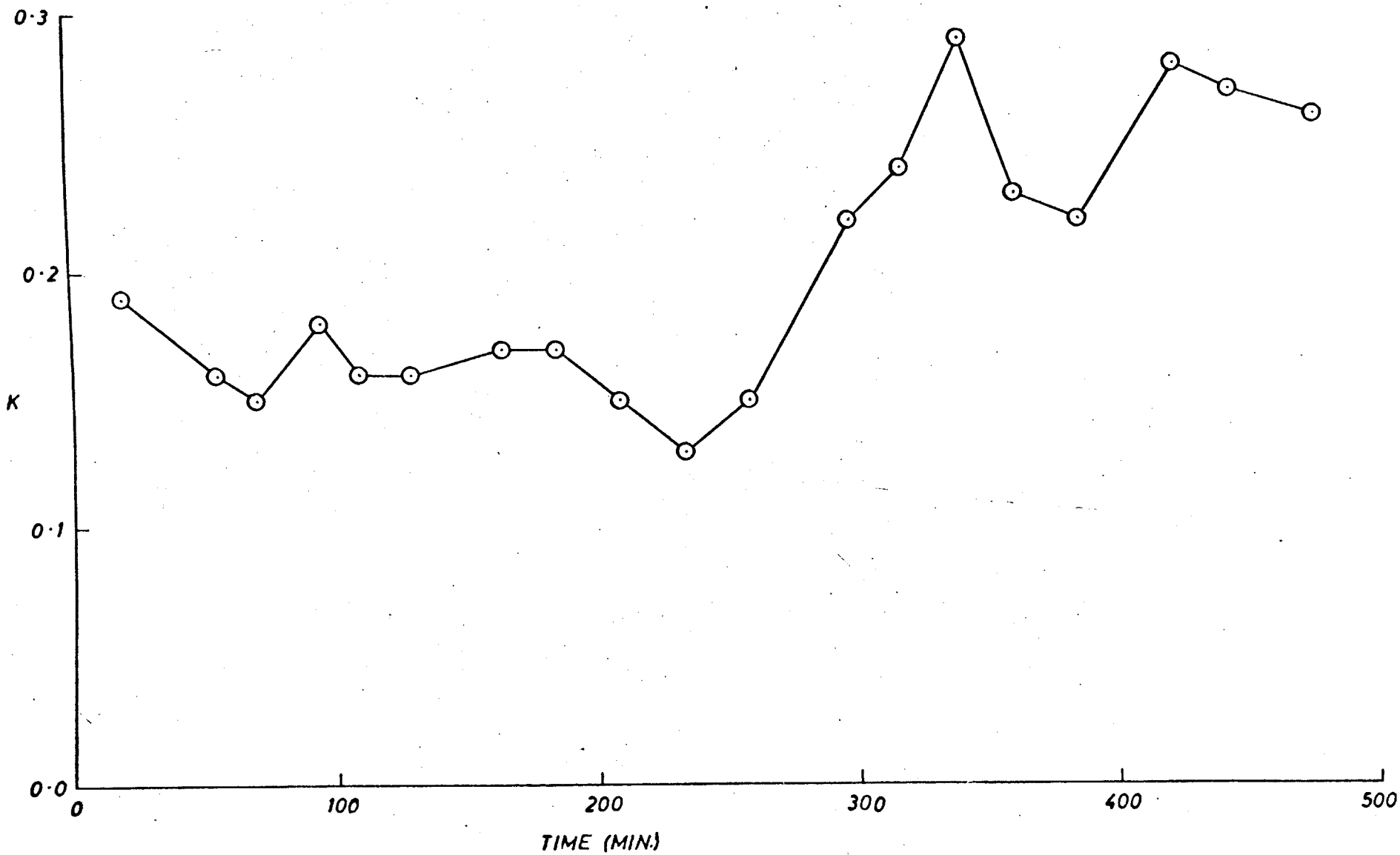

FIG 43

VARIATION OF VON KARMAN CONSTANT WITH TIME

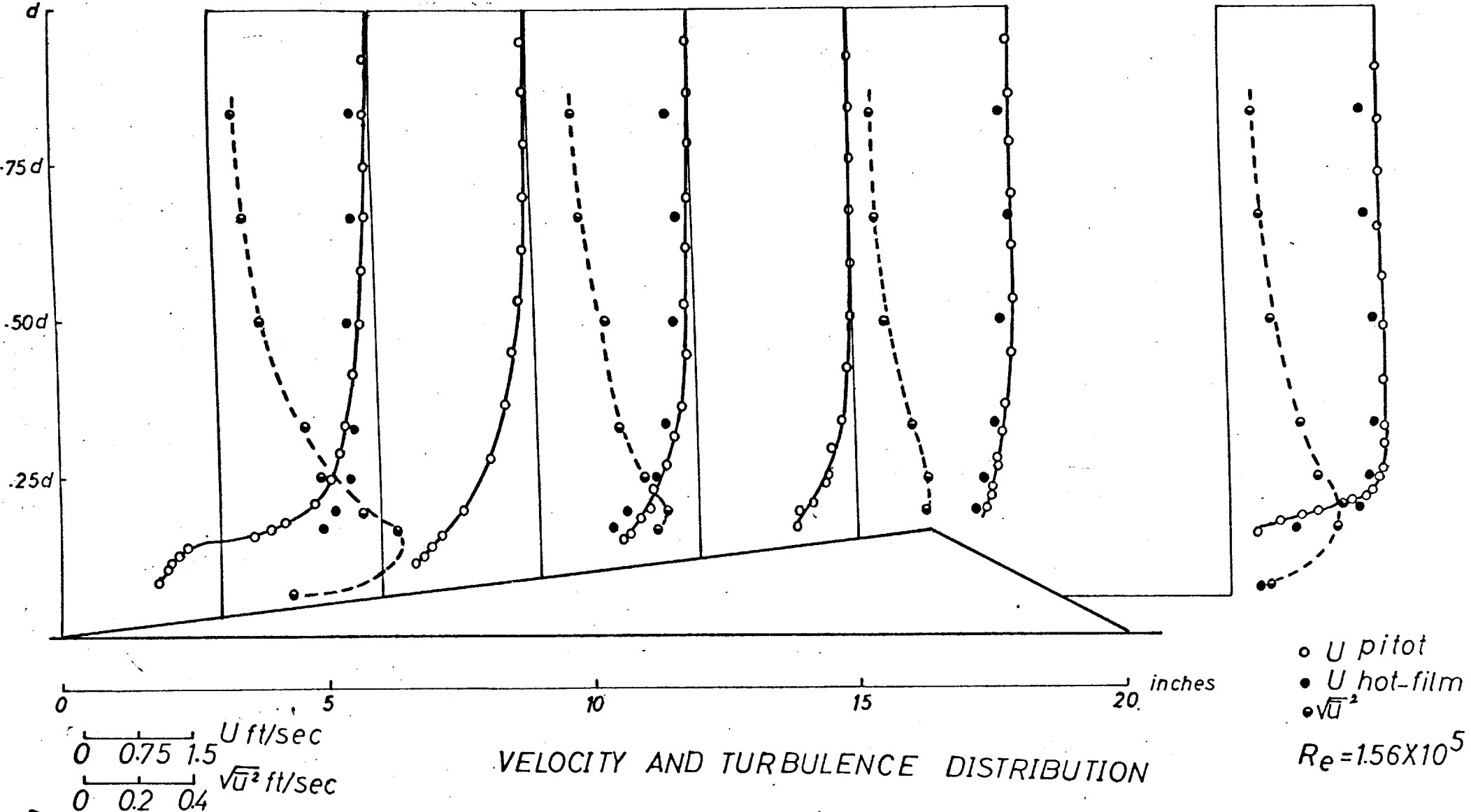
d
.75 d
.50 d
.25 d
0
5
10
15
20
inches
0 0.75 1.5 U ft/sec
0 0.2 0.4 √u² ft/sec
VELOCITY AND TURBULENCE DISTRIBUTION
U pitot
U hot-film
√u²
Re = 1.56X10⁵

FIG 44

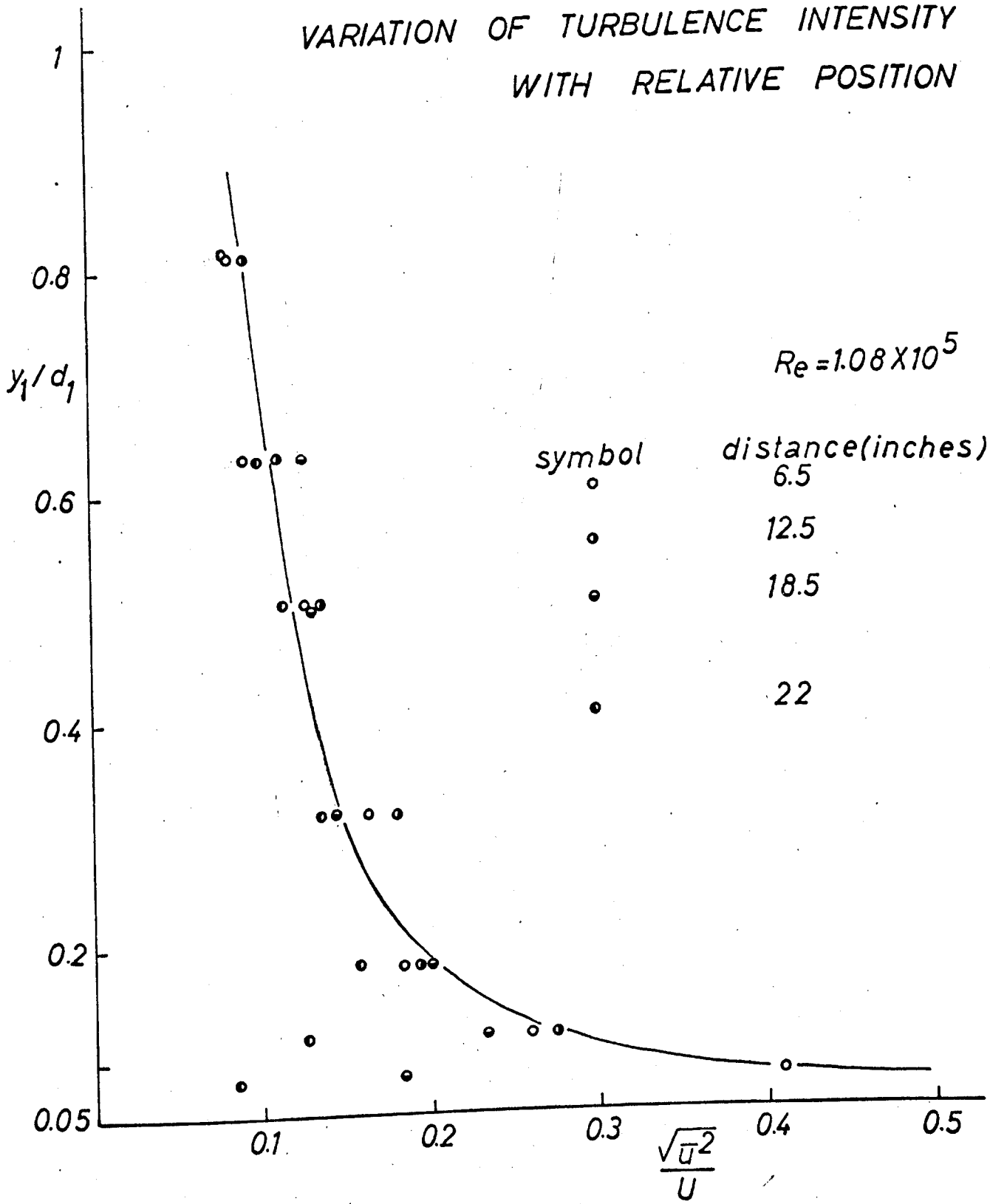
VARIATION OF TURBULENCE INTENSITY
WITH RELATIVE POSITION
$Re = 1.08 \times 10^5$
symbol
distance(inches)
6.5
12.5
18.5
22
y_1 / d_1
1
0.8
0.6
0.4
0.2
0.05
0.1
0.2
0.3
0.4
0.5
$\frac{\sqrt{\overline{u}^2}}{U}$

FIG 45

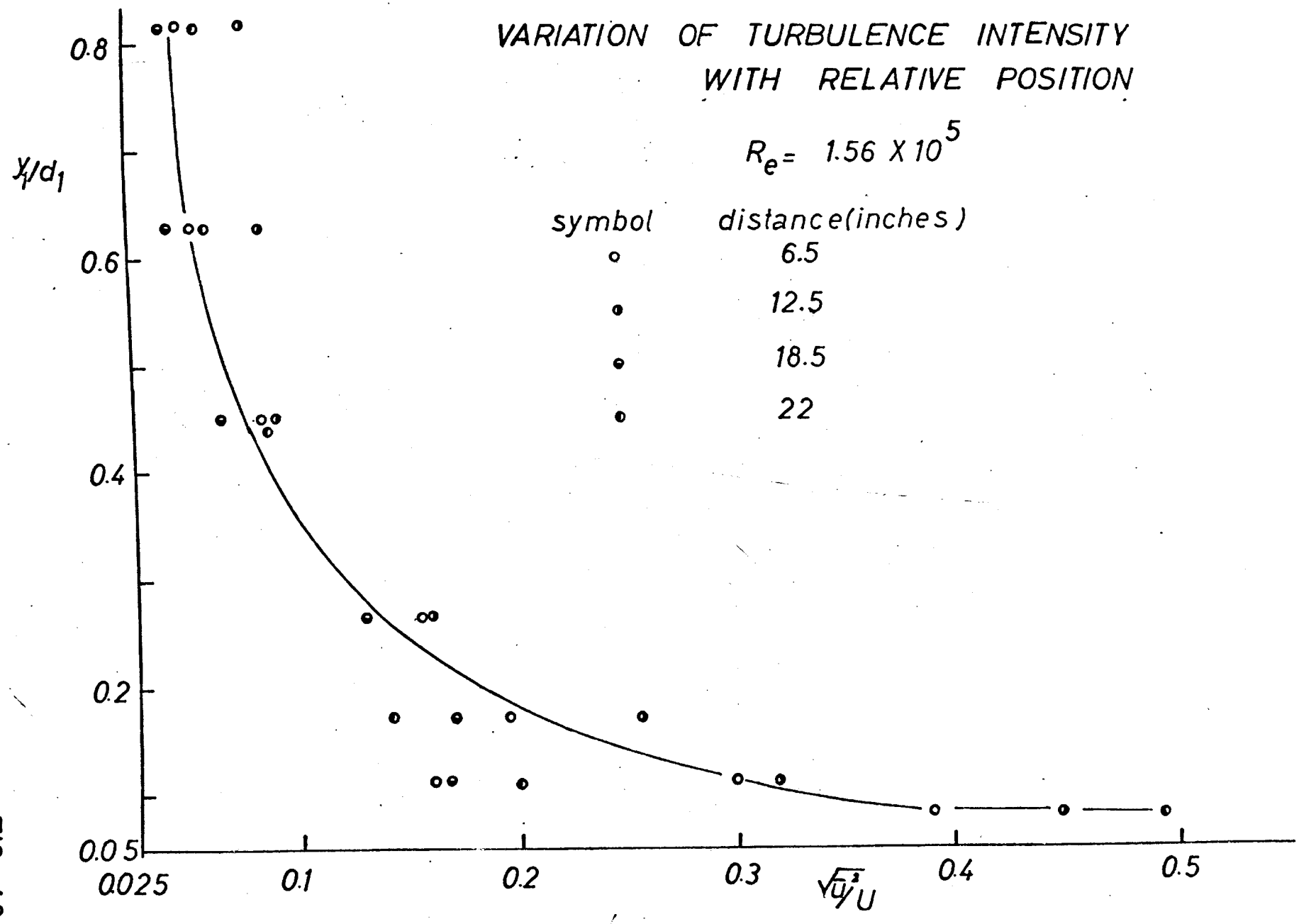
VARIATION OF TURBULENCE INTENSITY
WITH RELATIVE POSITION
$R_e = 1.56 \times 10^5$
symbol
distance(inches)
6.5
12.5
18.5
22
y_1/d_1
0.8
0.6
0.4
0.2
0.05
0.025
0.1
0.2
0.3
0.4
0.5
$\sqrt{u'^2}/U$

FIG 46

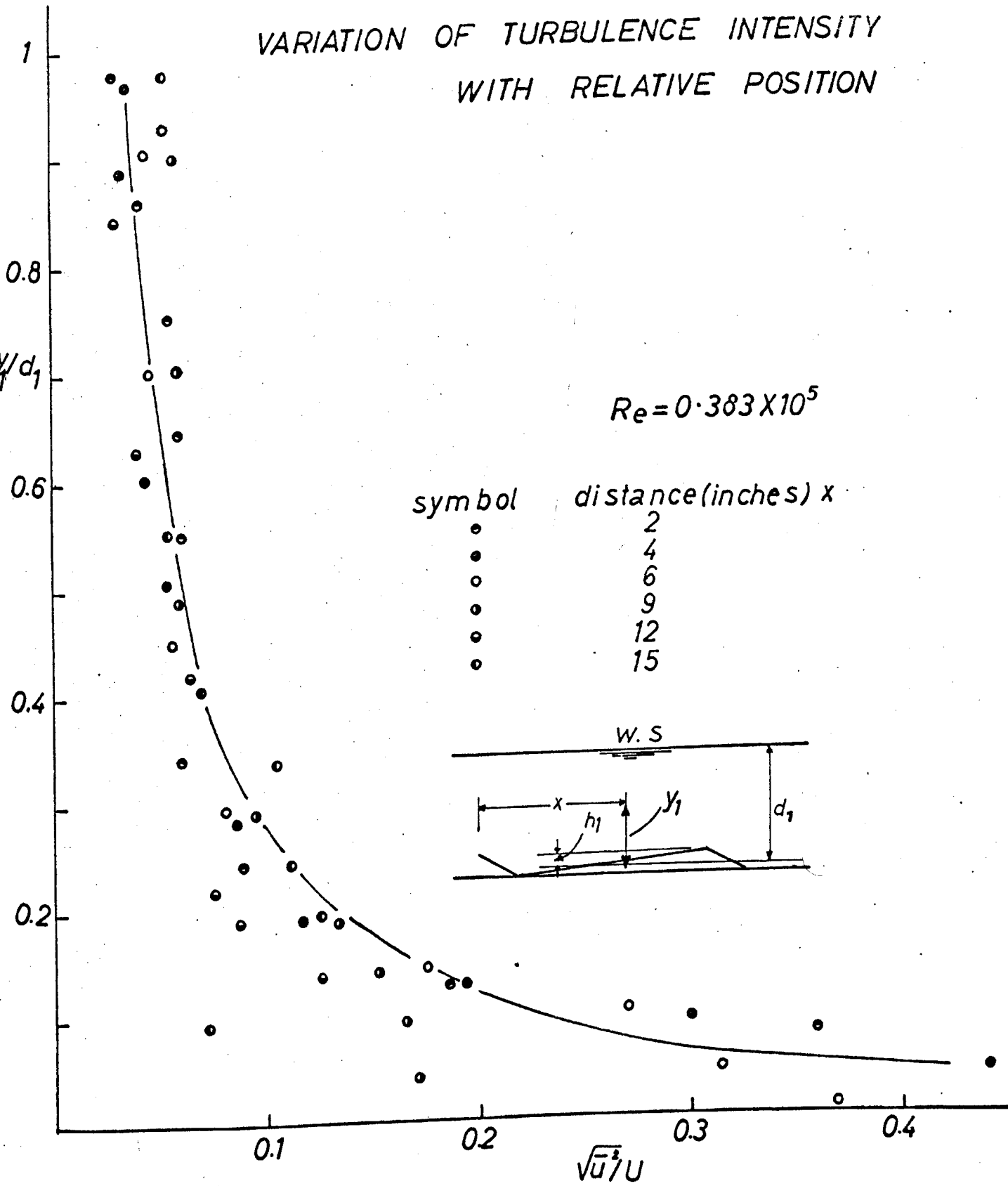
VARIATION OF TURBULENCE INTENSITY
WITH RELATIVE POSITION
Re = 0·383 X 10^5
symbol
distance (inches) x
2
4
6
9
12
15
W. S
x
y1
h1
d1
y/d1
√ū²/U
1
0.8
0.6
0.4
0.2
0.1
0.2
0.3
0.4

FIG 47

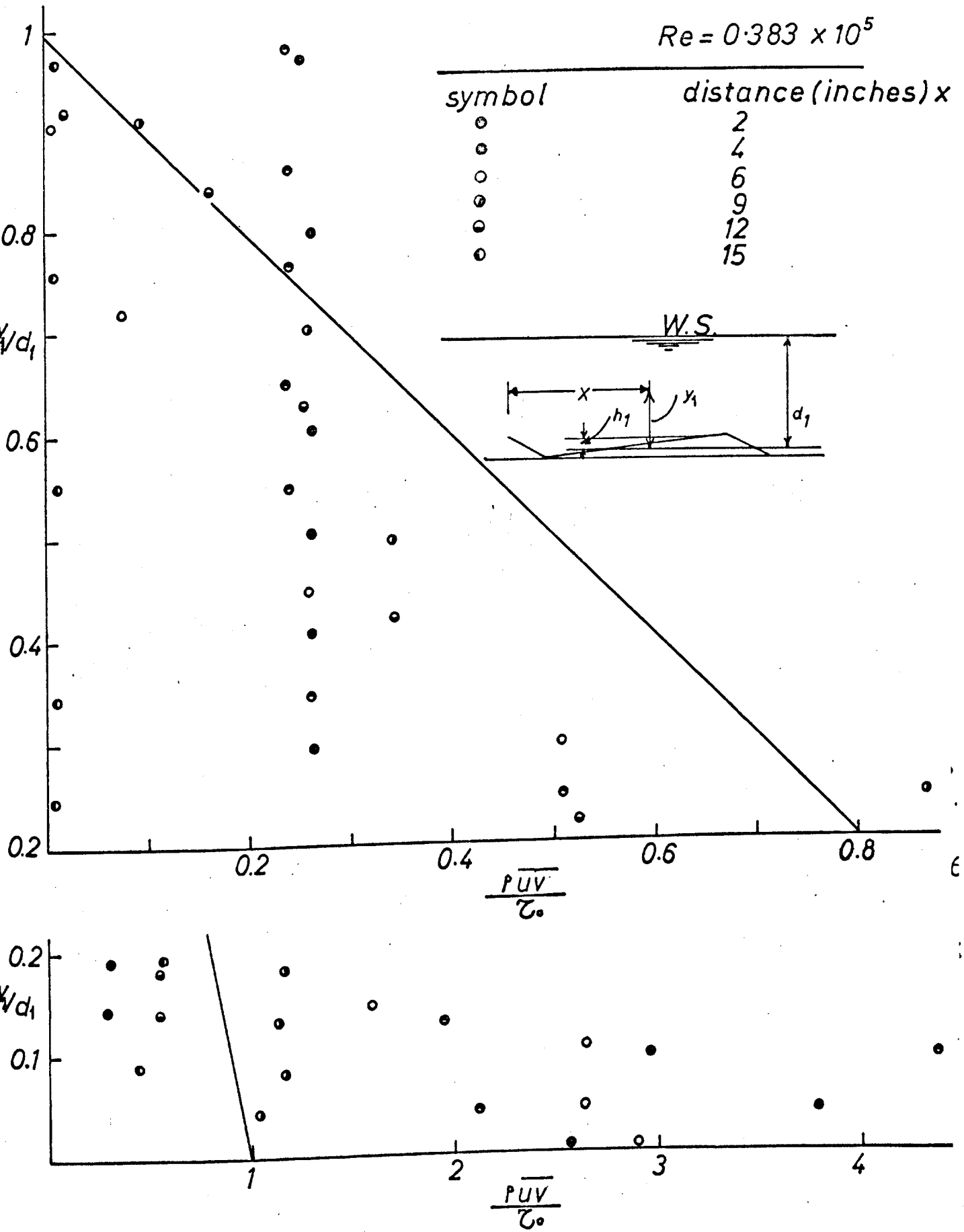

VARIATION OF SHEAR STRESS

FIG 48

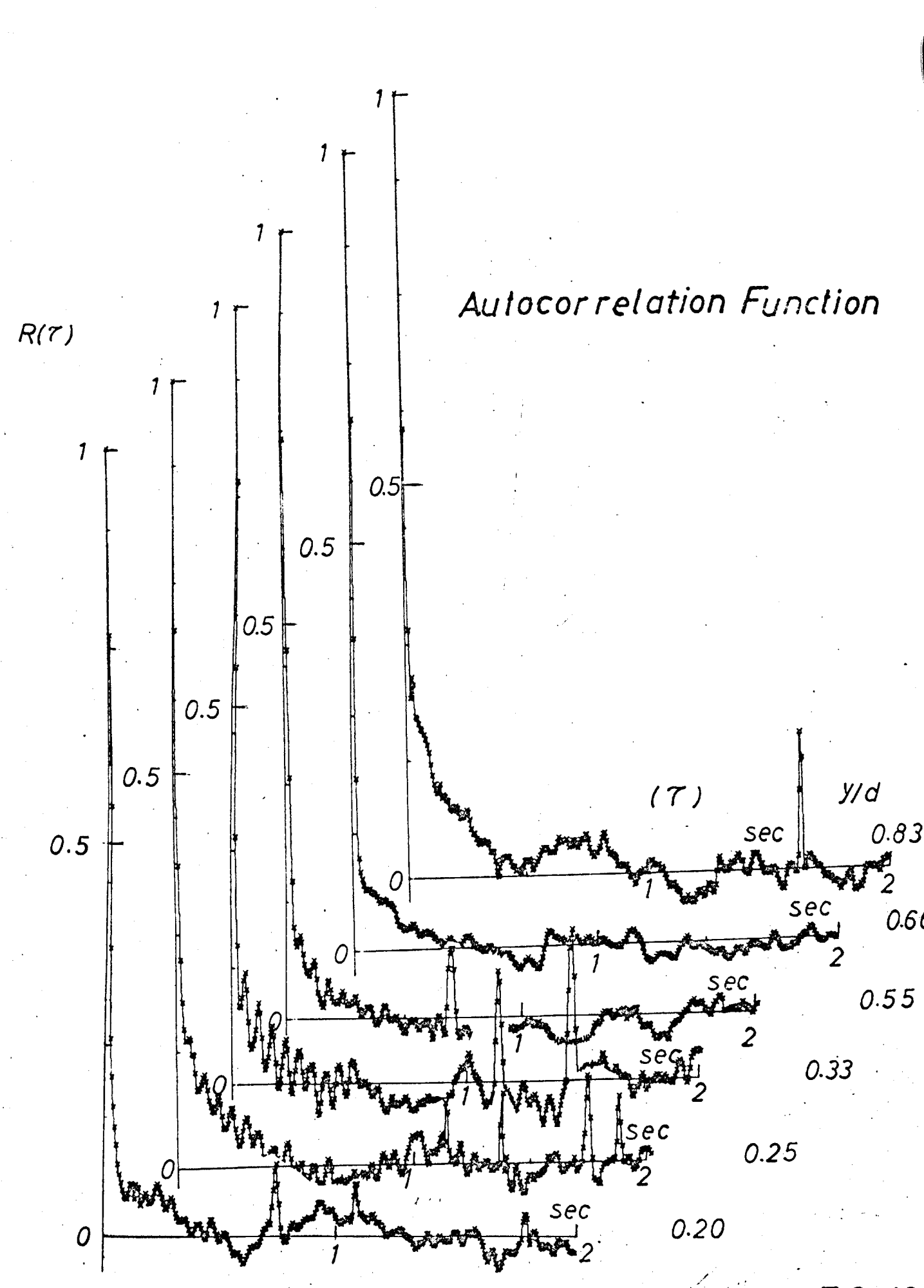
Autocorrelation Function
R(τ)
(τ)
y/d
sec
0.83
0.60
0.55
0.33
0.25
0.20
0
0.5
1
2

FIG 49

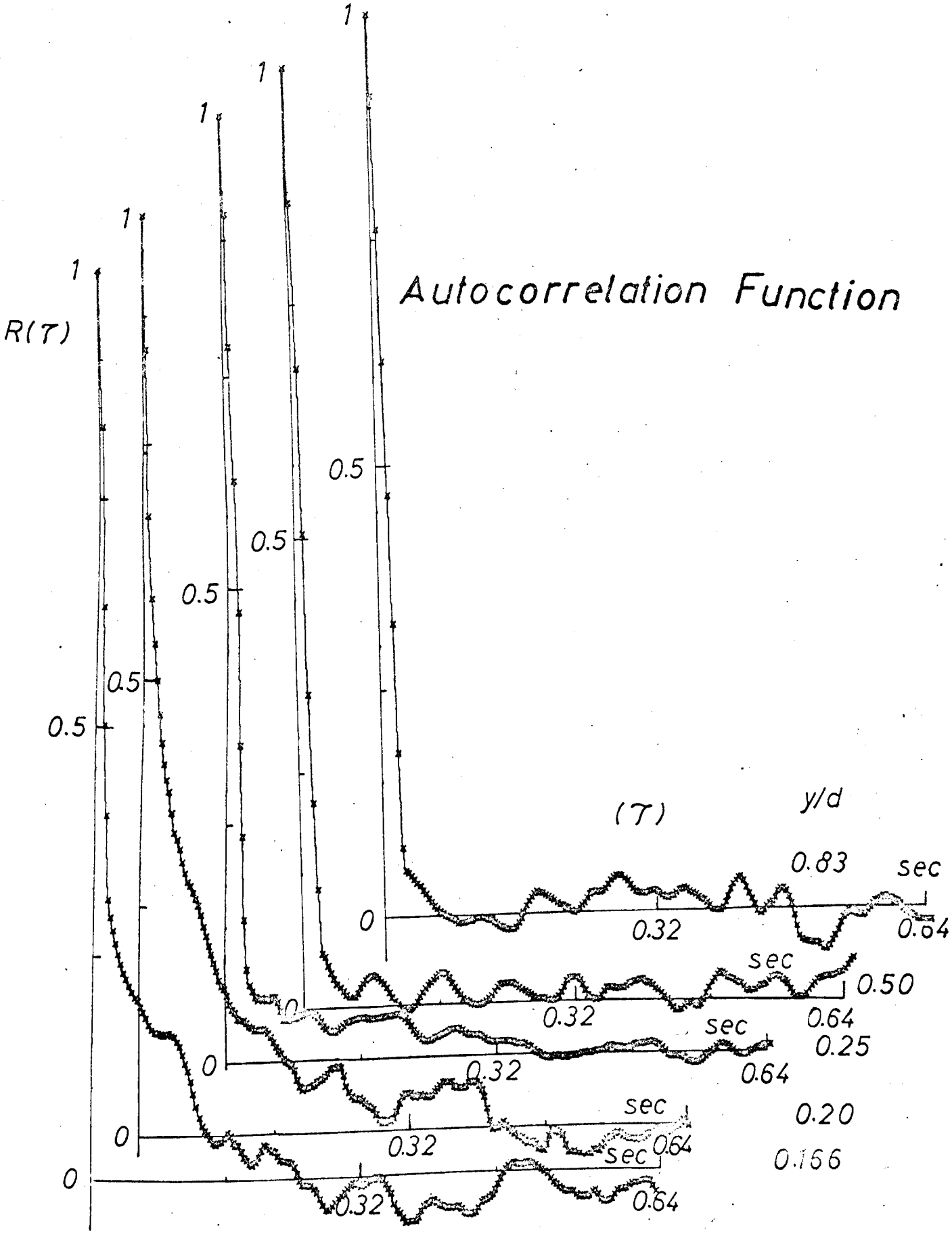
Autocorrelation Function
R(T)
(T)
y/d
0.83
sec
0.64
0.32
0.50
0.25
0.20
0.166
1
0.5
0

FIG 5

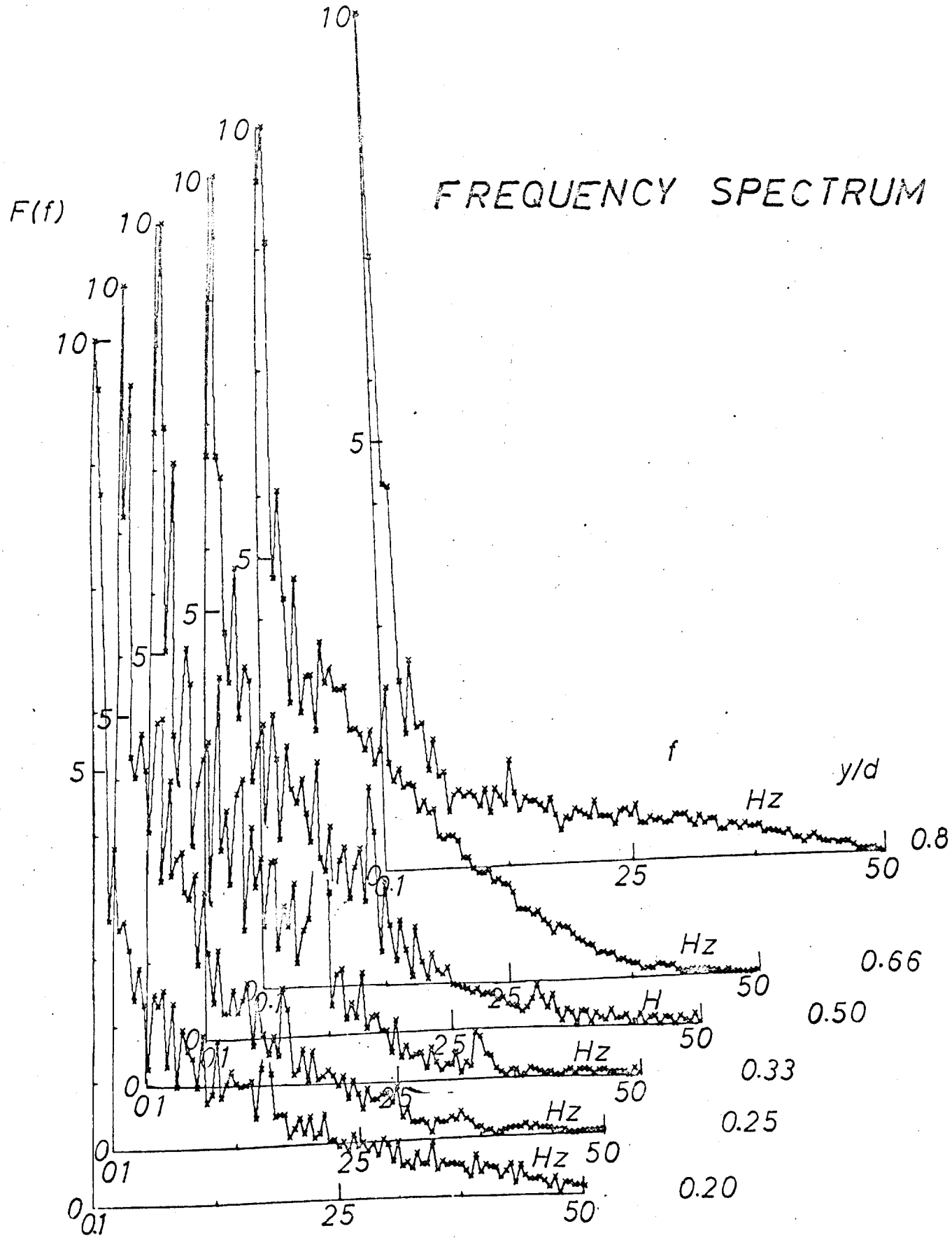
FREQUENCY SPECTRUM
F(f)
f
Hz
y/d
0.8
0.66
0.50
0.33
0.25
0.20
10
5
0
0.1
25
50

FIG 51

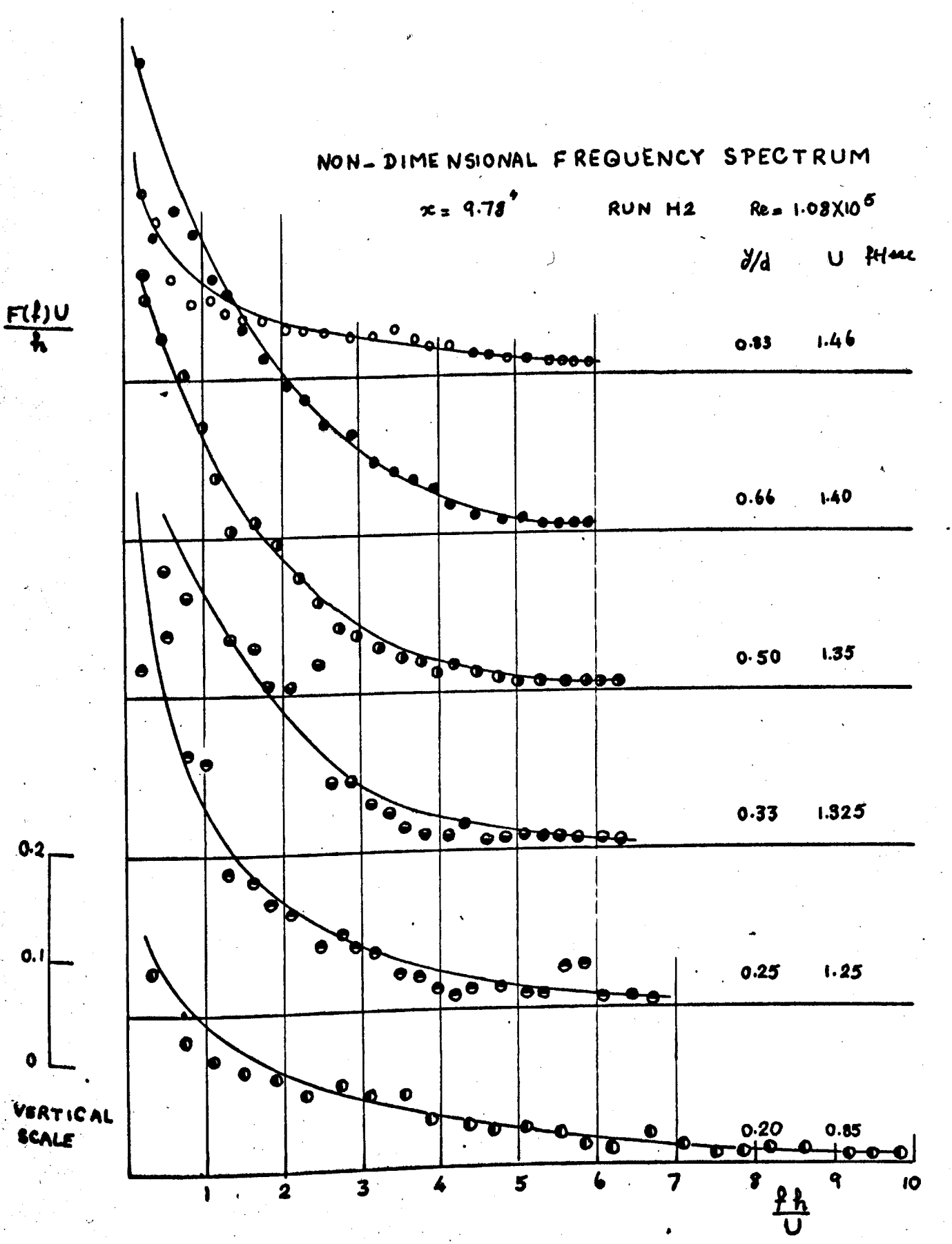
NON-DIMENSIONAL FREQUENCY SPECTRUM
x = 9.78"
RUN H2
Re = 1.08X10^6
y/d
U ft/sec
F(f)U/h
0.83
1.46
0.66
1.40
0.50
1.35
0.33
1.325
0.25
1.25
0.20
0.85
0.2
0.1
0
VERTICAL SCALE
1
2
3
4
5
6
7
8
9
10
fh/U

FIG. 51A

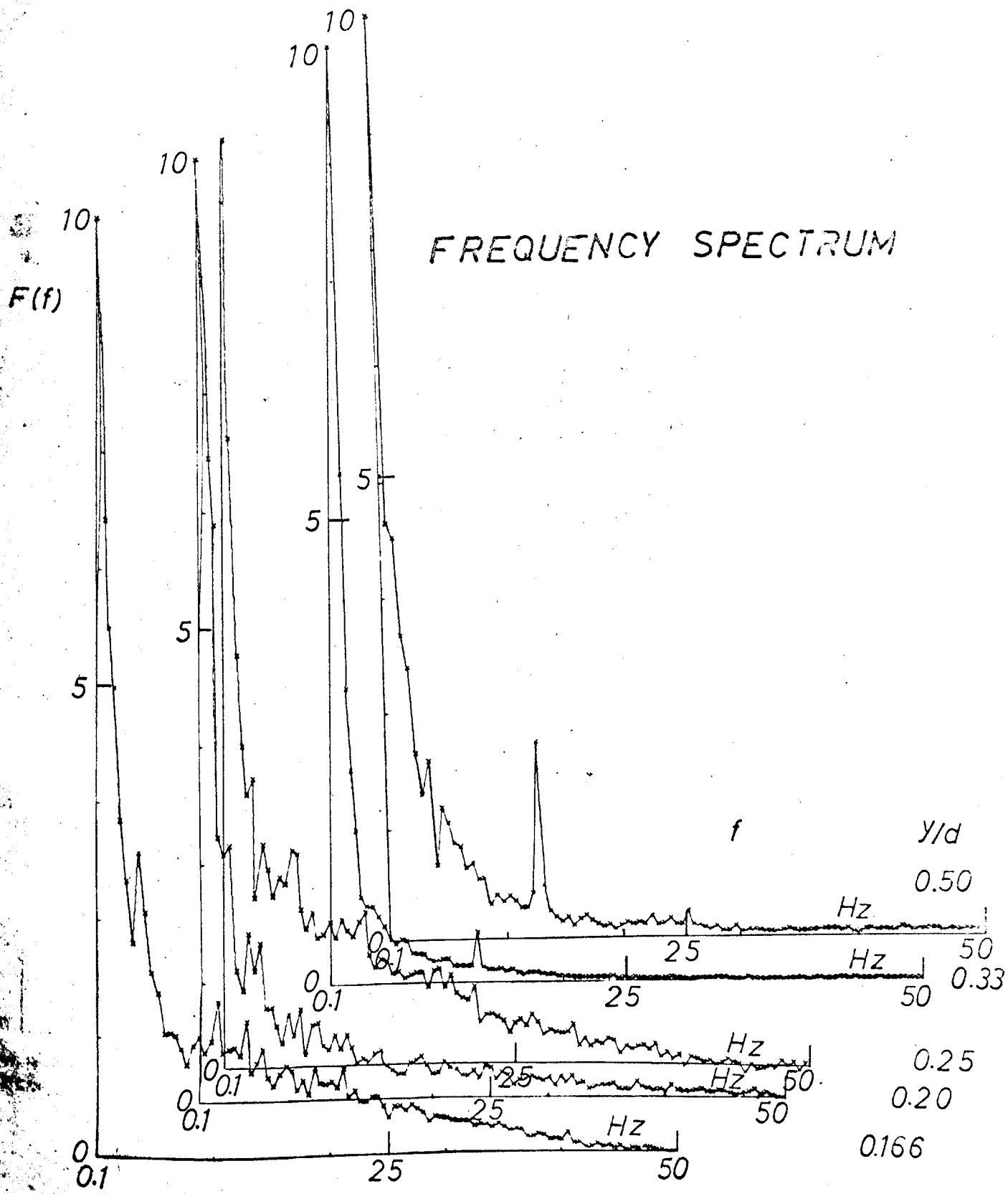
FREQUENCY SPECTRUM
F(f)
10
5
0
0.1
25
50
Hz
f
y/d
0.50
0.33
0.25
0.20
0.166

FIG 3

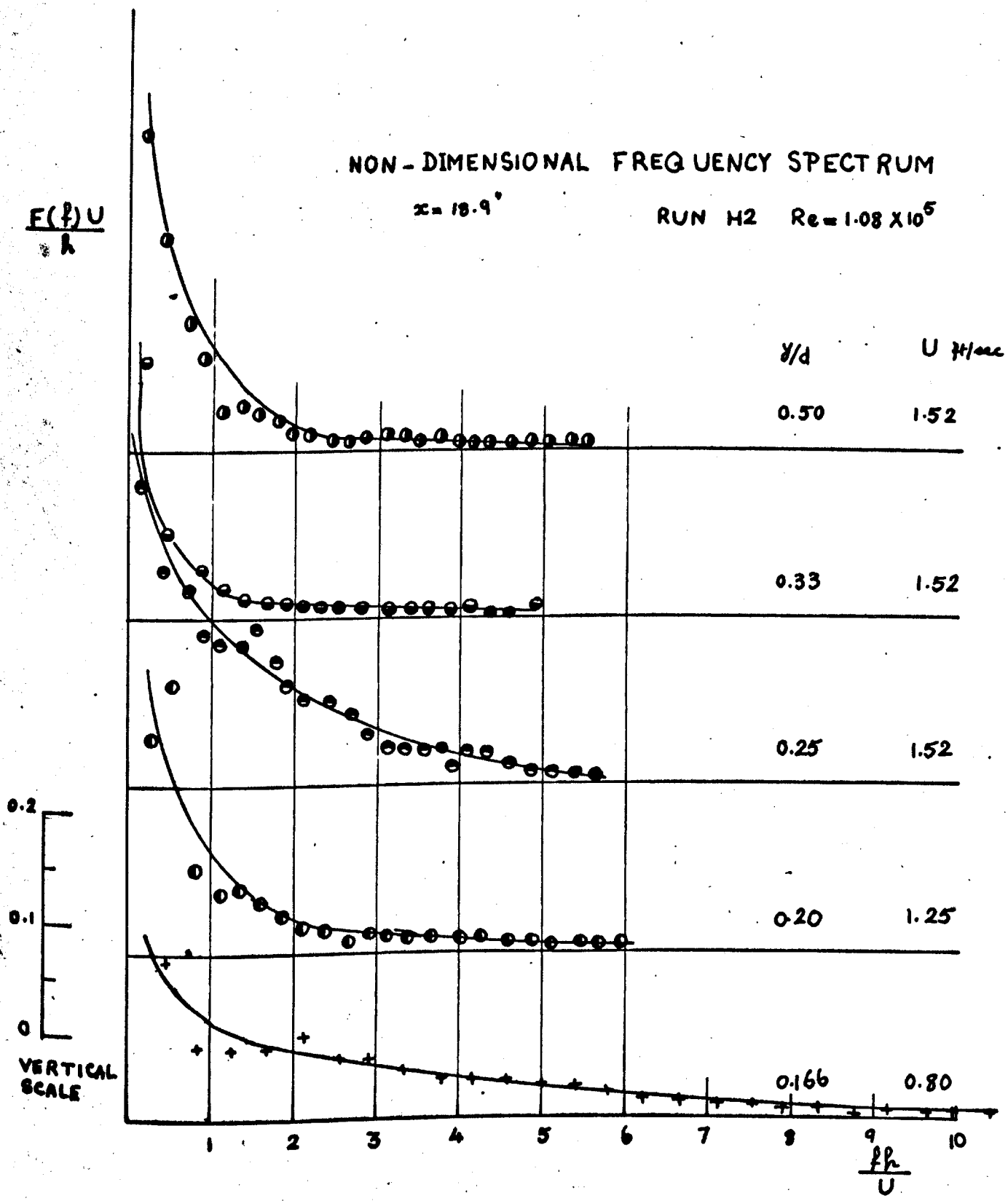
NON-DIMENSIONAL FREQUENCY SPECTRUM
x = 18.9"
RUN H2 Re = 1.08 X 10^5
E(f) U / h
y/d
U ft/sec
0.50
1.52
0.33
1.52
0.25
1.52
0.20
1.25
0.166
0.80
0.2
0.1
0
VERTICAL SCALE
1
2
3
4
5
6
7
8
9
10
fh / U

FIG 52A

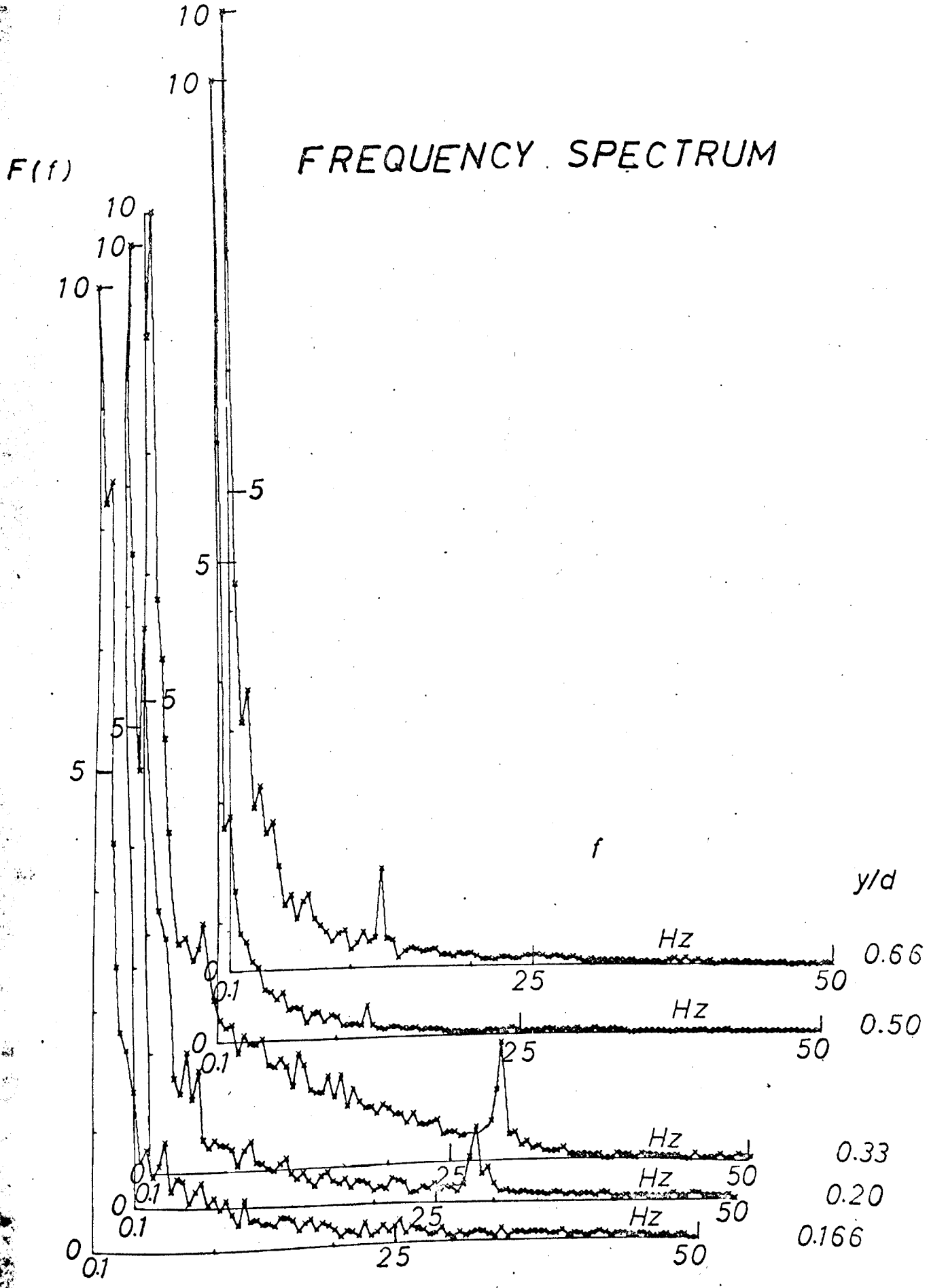
FREQUENCY SPECTRUM
F(f)
10
10
5
5
f
y/d
Hz
0.1
25
50
0.66
0.50
0.33
0.20
0.166
0

FIG 5.

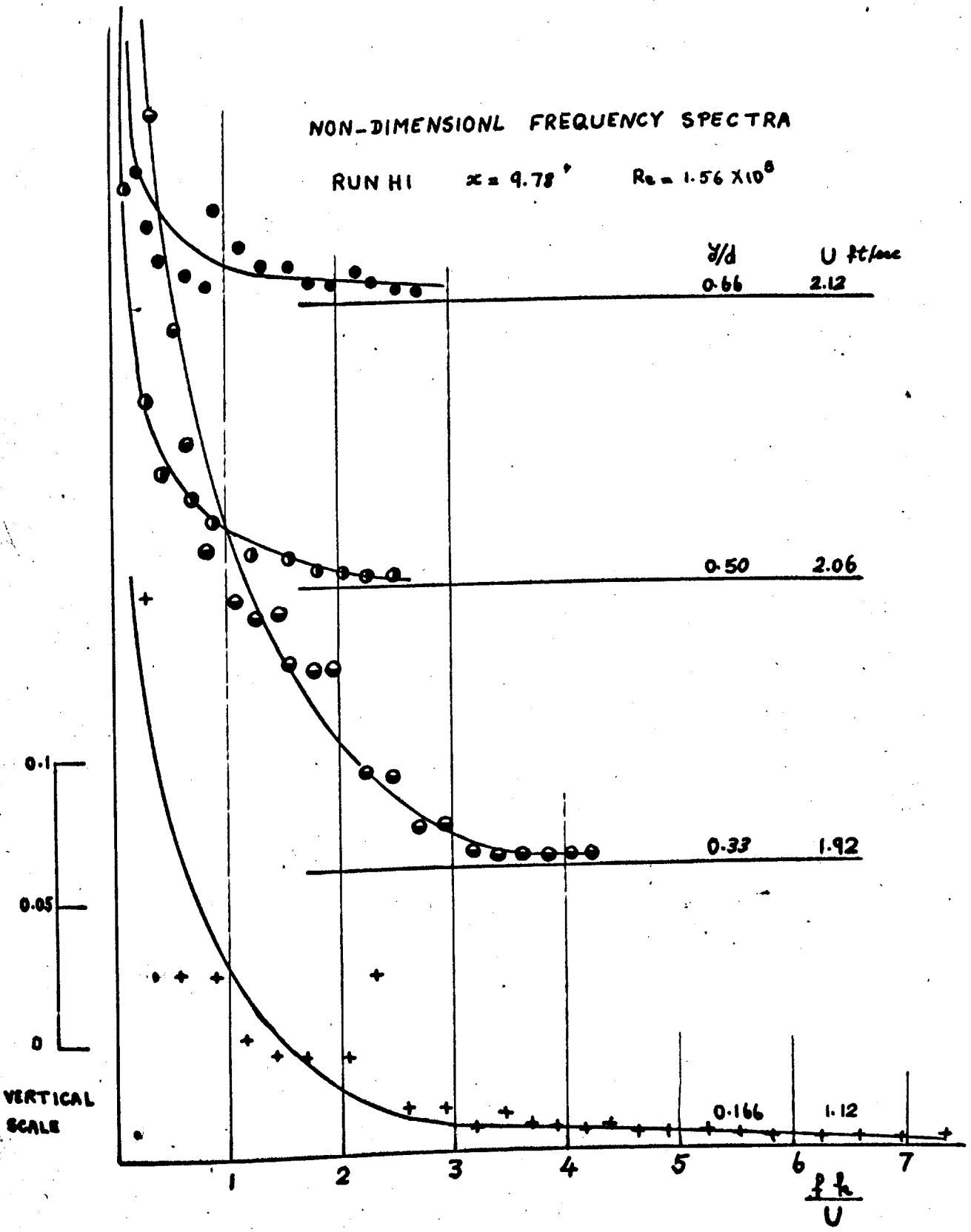
NON-DIMENSIONL FREQUENCY SPECTRA
RUN H1 x = 9.78' Re = 1.56 X10^6
y/d U ft/sec
0.66 2.12
0.50 2.06
0.33 1.92
0.166 1.12
0.1
0.05
0
VERTICAL SCALE
1
2
3
4
5
6
7
f k / U

FIG 53A

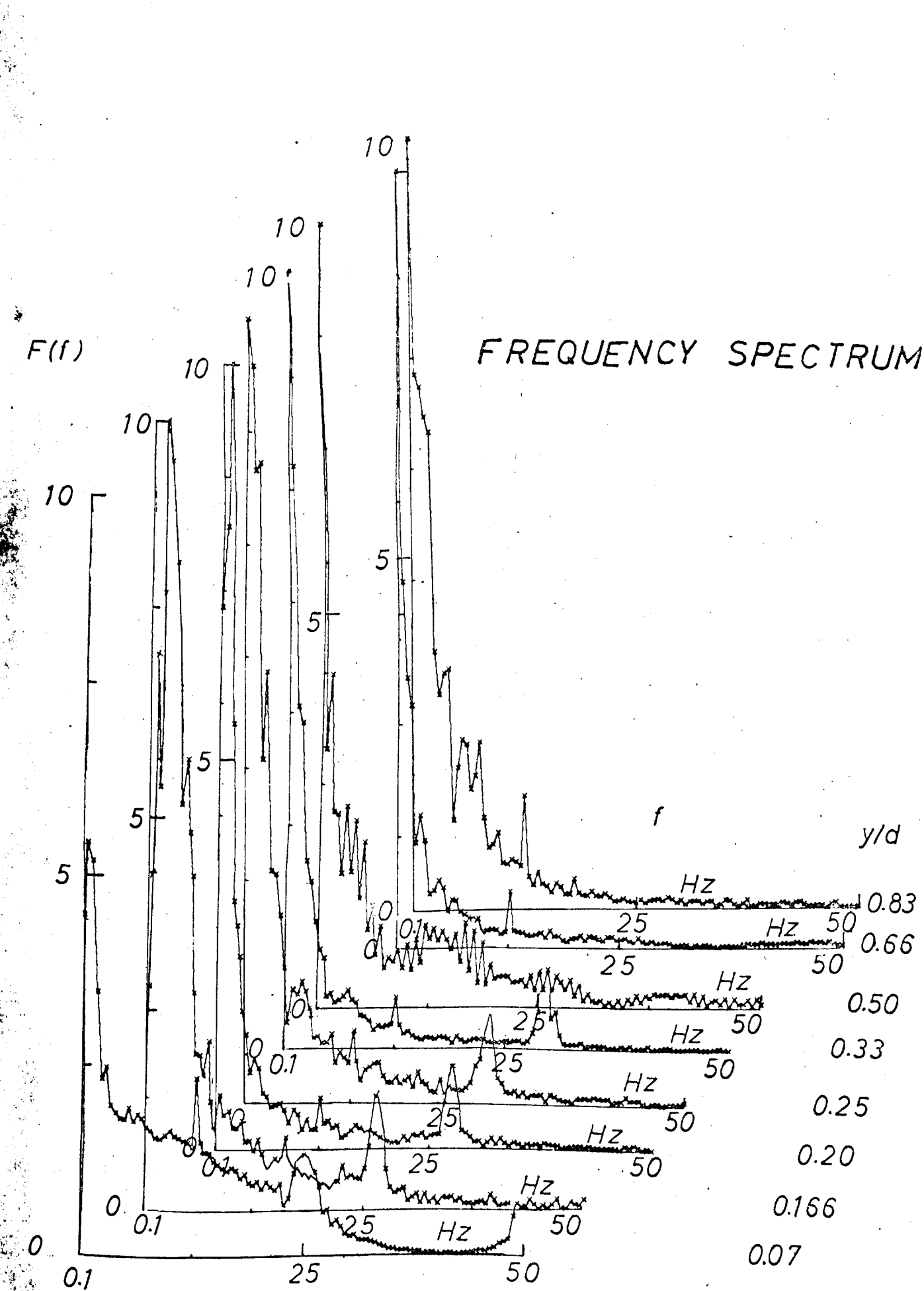
F(f)
FREQUENCY SPECTRUM
f
y/d
10
5
0
0.1
25
50
Hz
0.83
0.66
0.50
0.33
0.25
0.20
0.166
0.07

FIG 5

FLOW CONDITIONS FOR THE FREQUENCY SPECTRA SHOWN

IN FIGS. 51, 52, 53 AND 54.

y/d	Local velocity at y/d ft/sec.			
	Run H2		Run H1	
	Fig.51 x_1=9.78"	Fig.52 x_1=18.90"	Fig.53 x_1=9.78"	Fig.54 x_1=18.90"
0.07				0.375
0.166	0.78	0.80	1.12	1.72
0.20	0.85	1.25	1.39	2.05
0.25	1.25	1.52	1.65	2.08
0.33	1.325	1.52	1.92	2.08
0.50	1.39	1.52	2.06	2.08
0.66	1.48	1.52	2.12	2.08
0.83	1.49	1.52	2.17	2.08

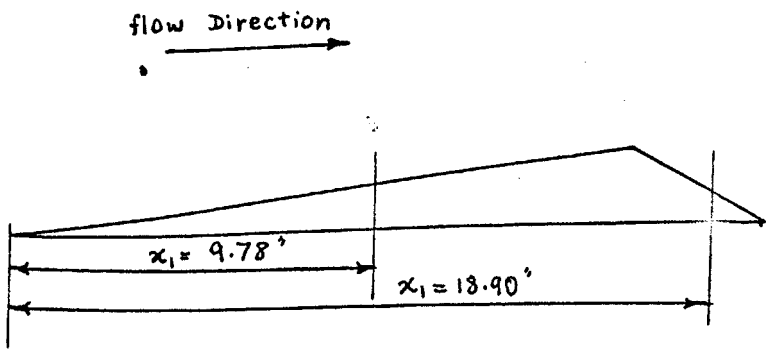

FIG 55

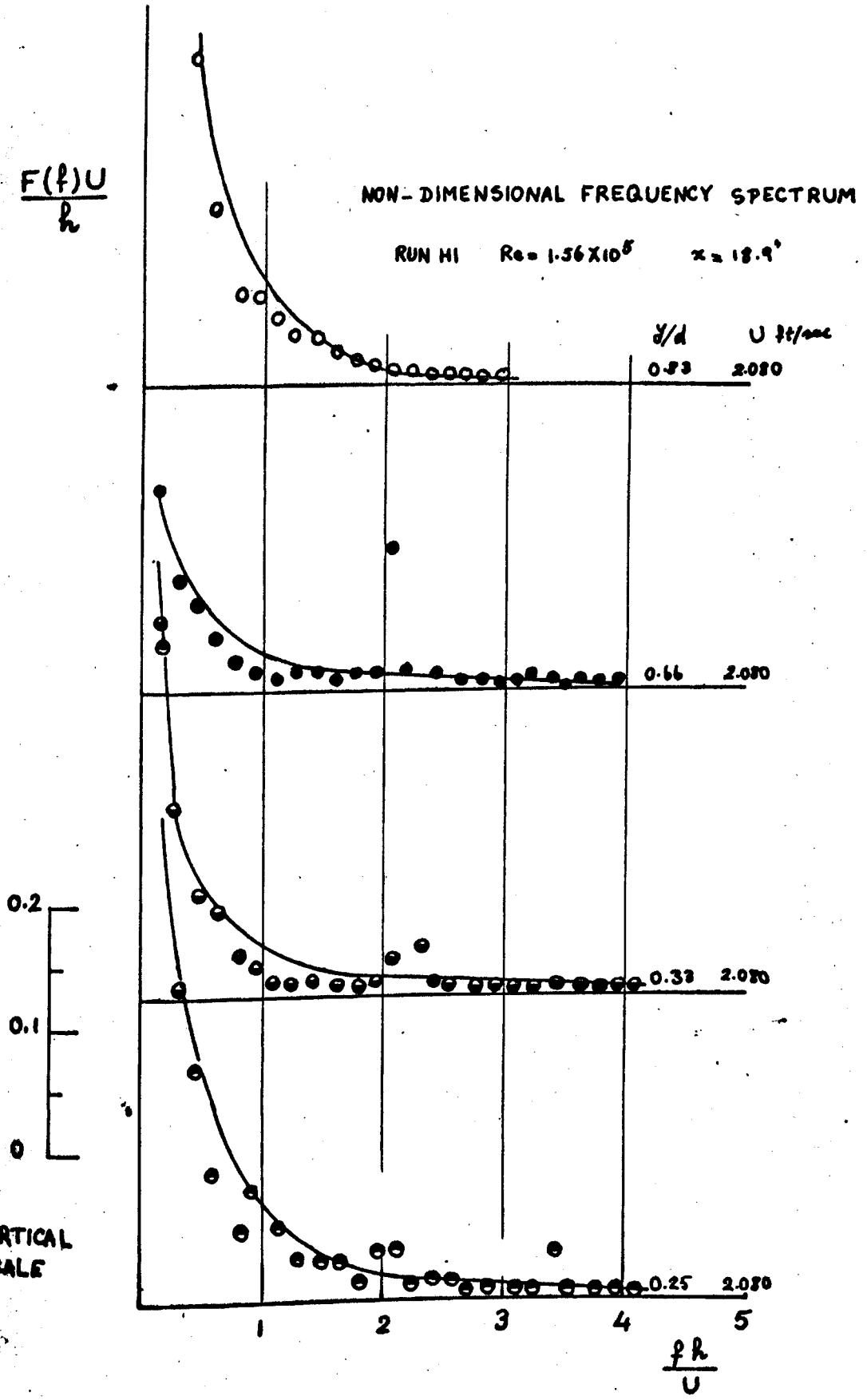
F(f)U / h
NON-DIMENSIONAL FREQUENCY SPECTRUM
RUN H1 Re = 1.56 X 10^6 x = 18.9'
y/d U ft/sec
0.83 2.080
0.66 2.080
0.33 2.080
0.25 2.080
0.2
0.1
0
VERTICAL SCALE
1
2
3
4
5
fh / U

FIG 56

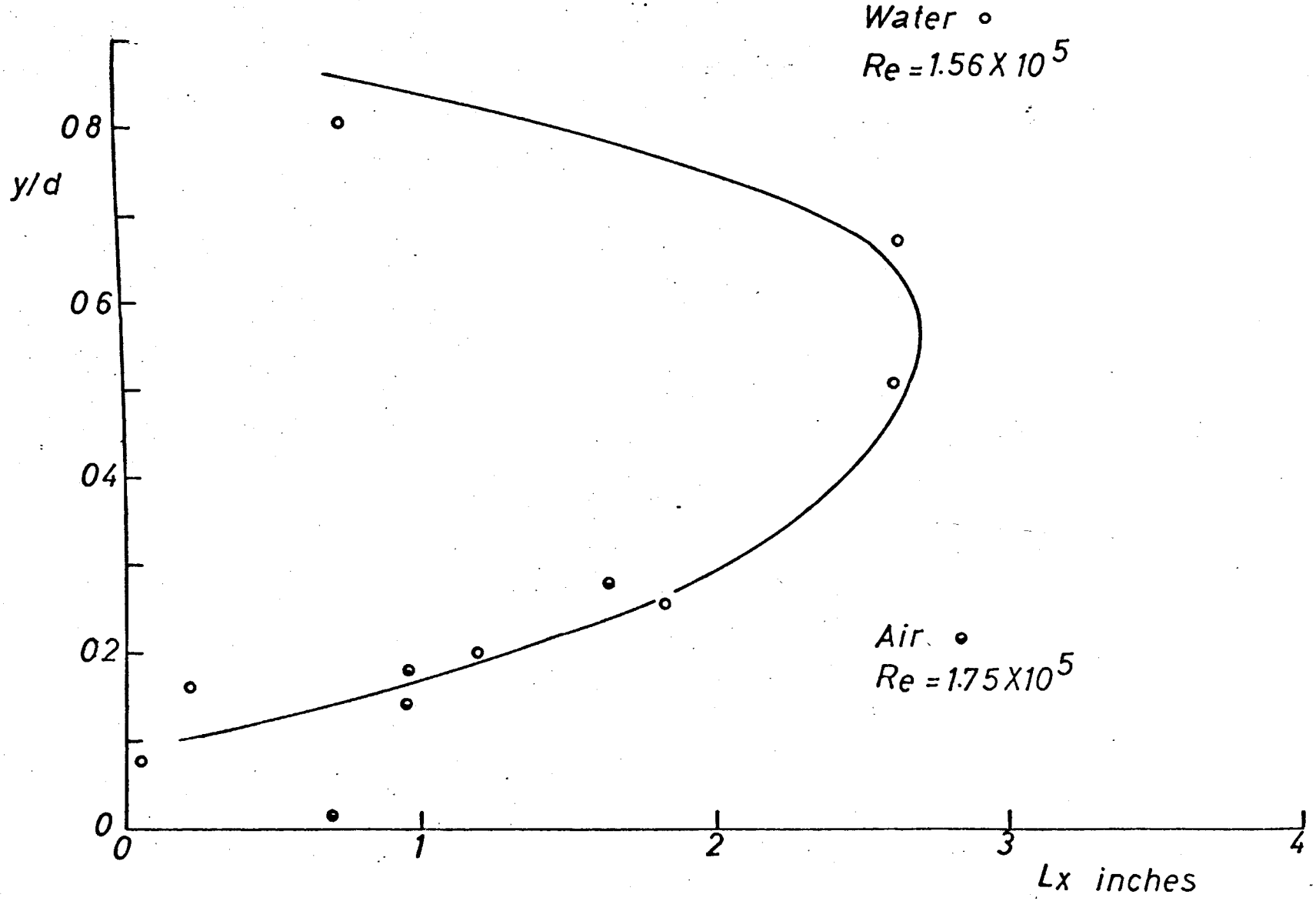

FIG 57

VARIATION OF MACROSCALE

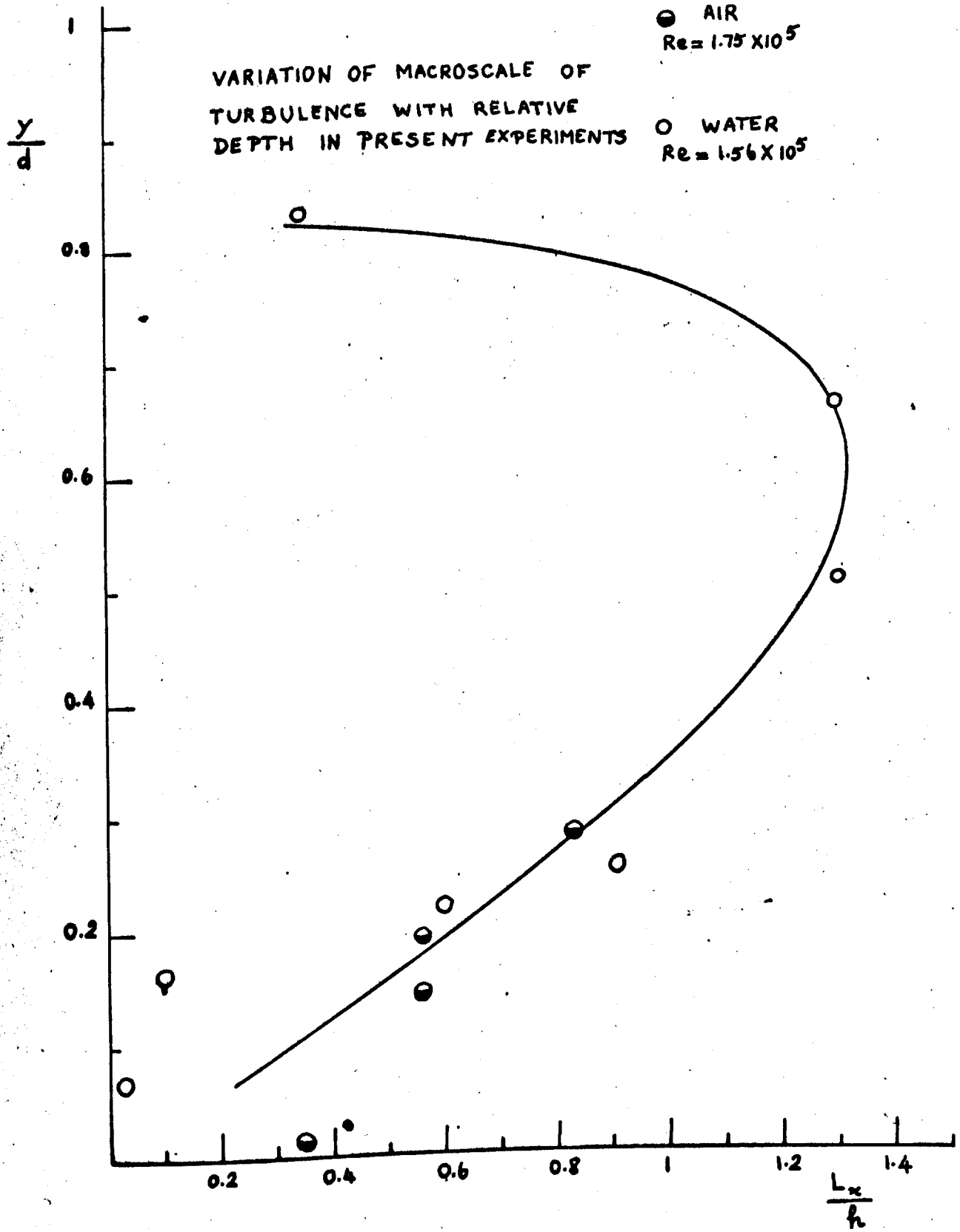
VARIATION OF MACROSCALE OF TURBULENCE WITH RELATIVE DEPTH IN PRESENT EXPERIMENTS
AIR
Re = 1.75 X 10^5
WATER
Re = 1.56 X 10^5
y/d
1
0.8
0.6
0.4
0.2
0.2
0.4
0.6
0.8
1
1.2
1.4
Lx/h

FIG 57A

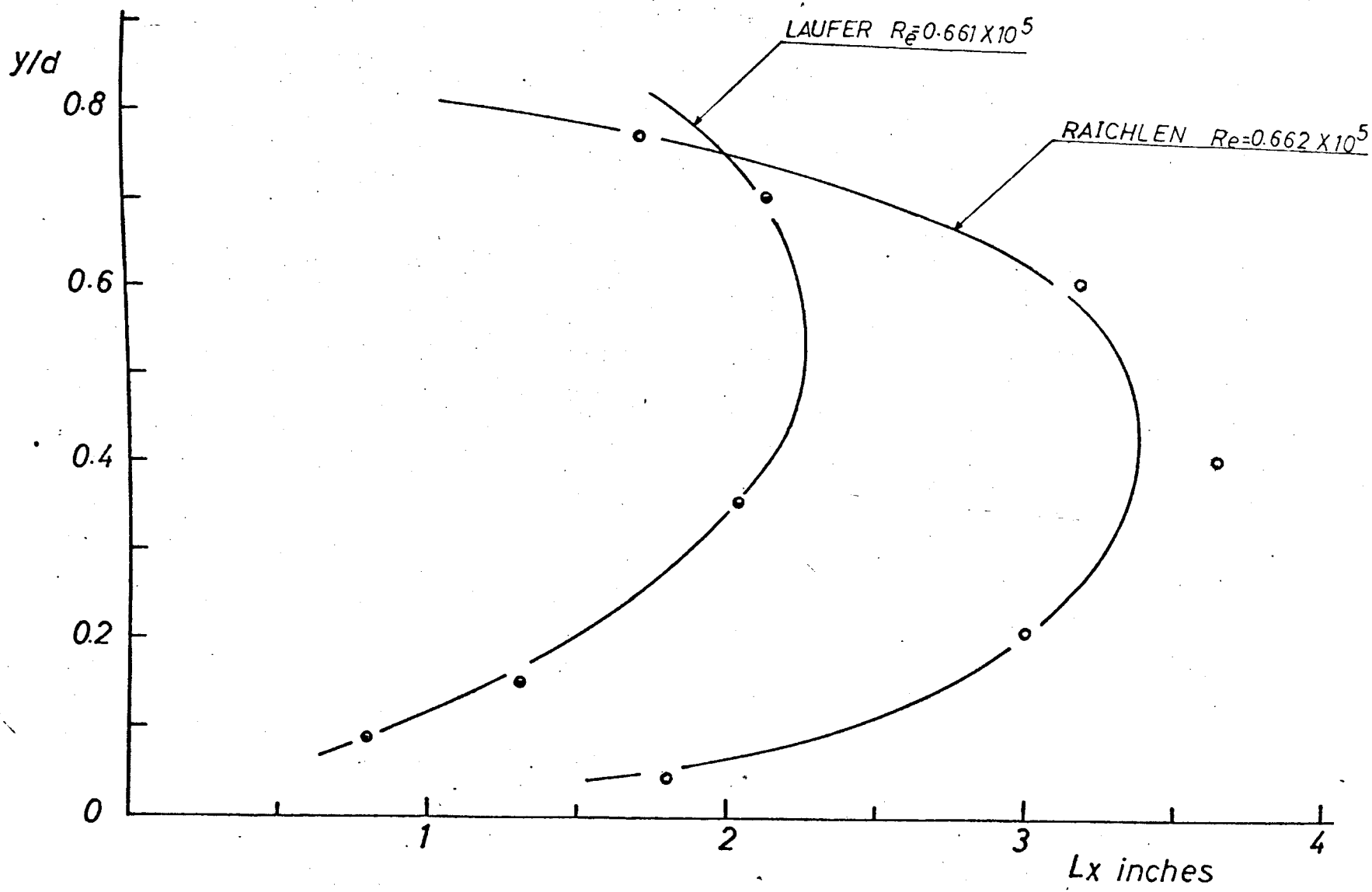

FIG 58

VARIATION OF MACROSCALE (comparison)

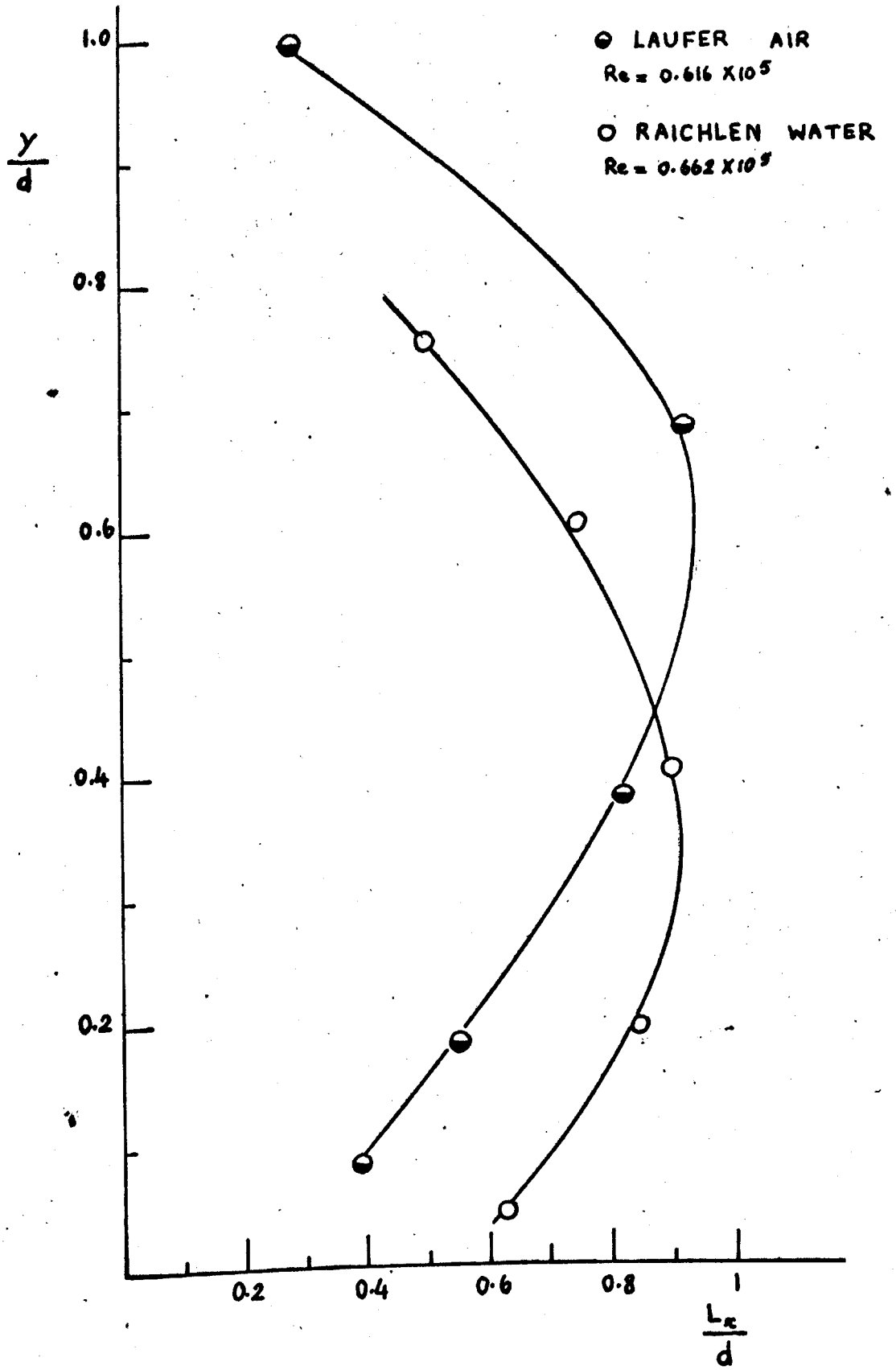

VARIATION OF TURBULENT MACROSCALE WTH RELATIVE DEPTH

FIG. 58A

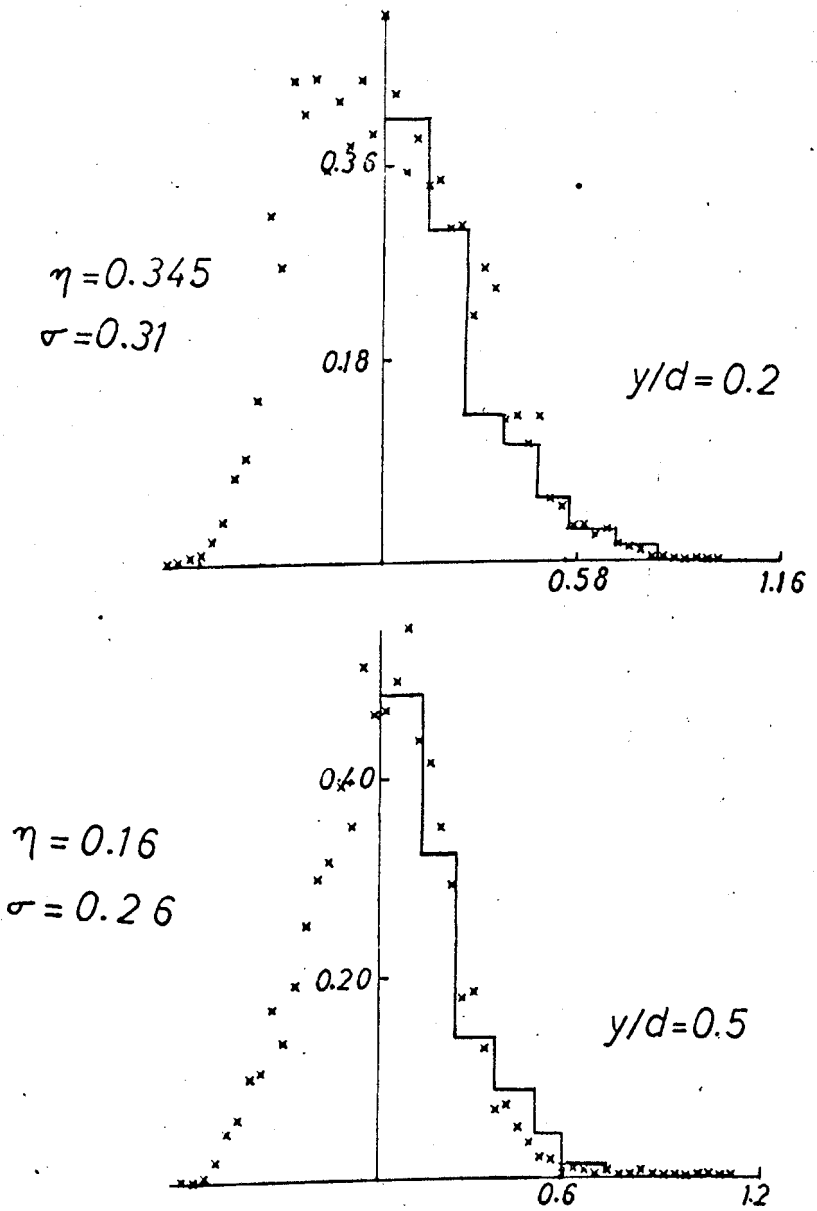
η = 0.345
σ = 0.31
0.36
0.18
y/d = 0.2
0.58
1.16
η = 0.16
σ = 0.26
0.40
0.20
y/d = 0.5
0.6
1.2
η = 0.184
σ = 0.22
0.48
0.24
y/d = 0.66
0.52
1.04
PROBABILITY DENSITY FUNCTION

FIG. 59

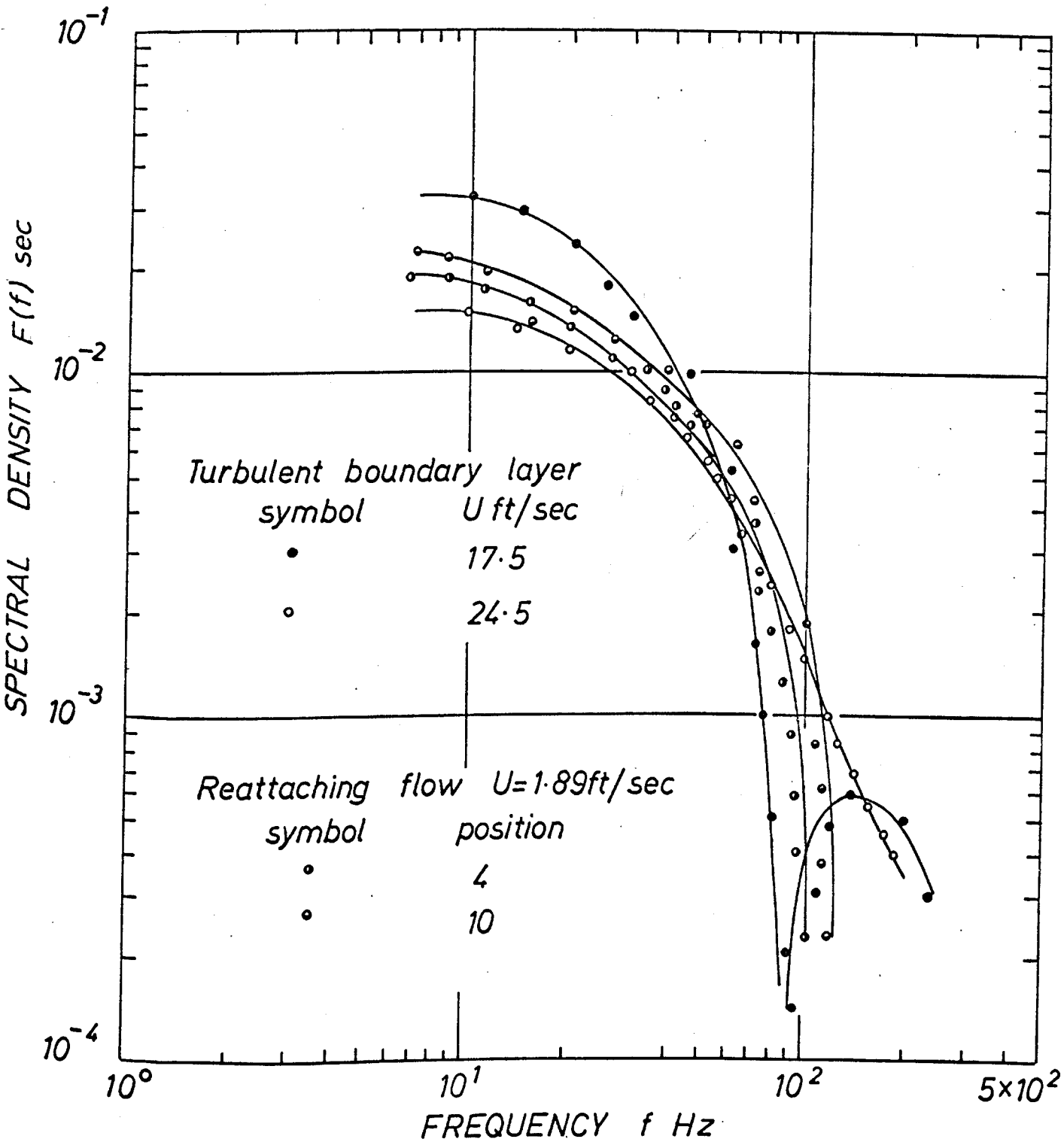

FREQUENCY SPECTRUM

FIG 60

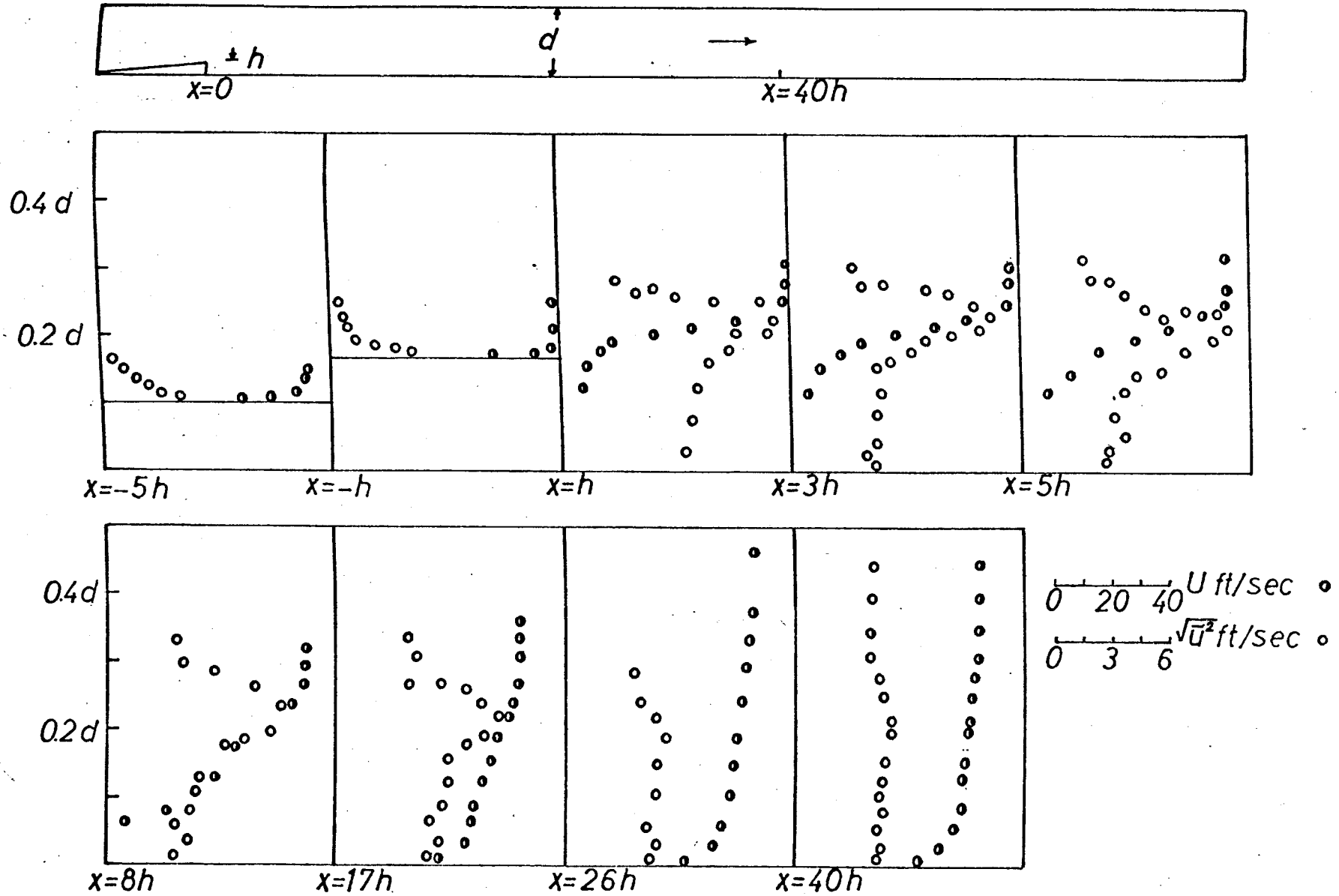

FIG 61

VELOCITY AND TURBULENCE OVER ADVERSE SLOPE

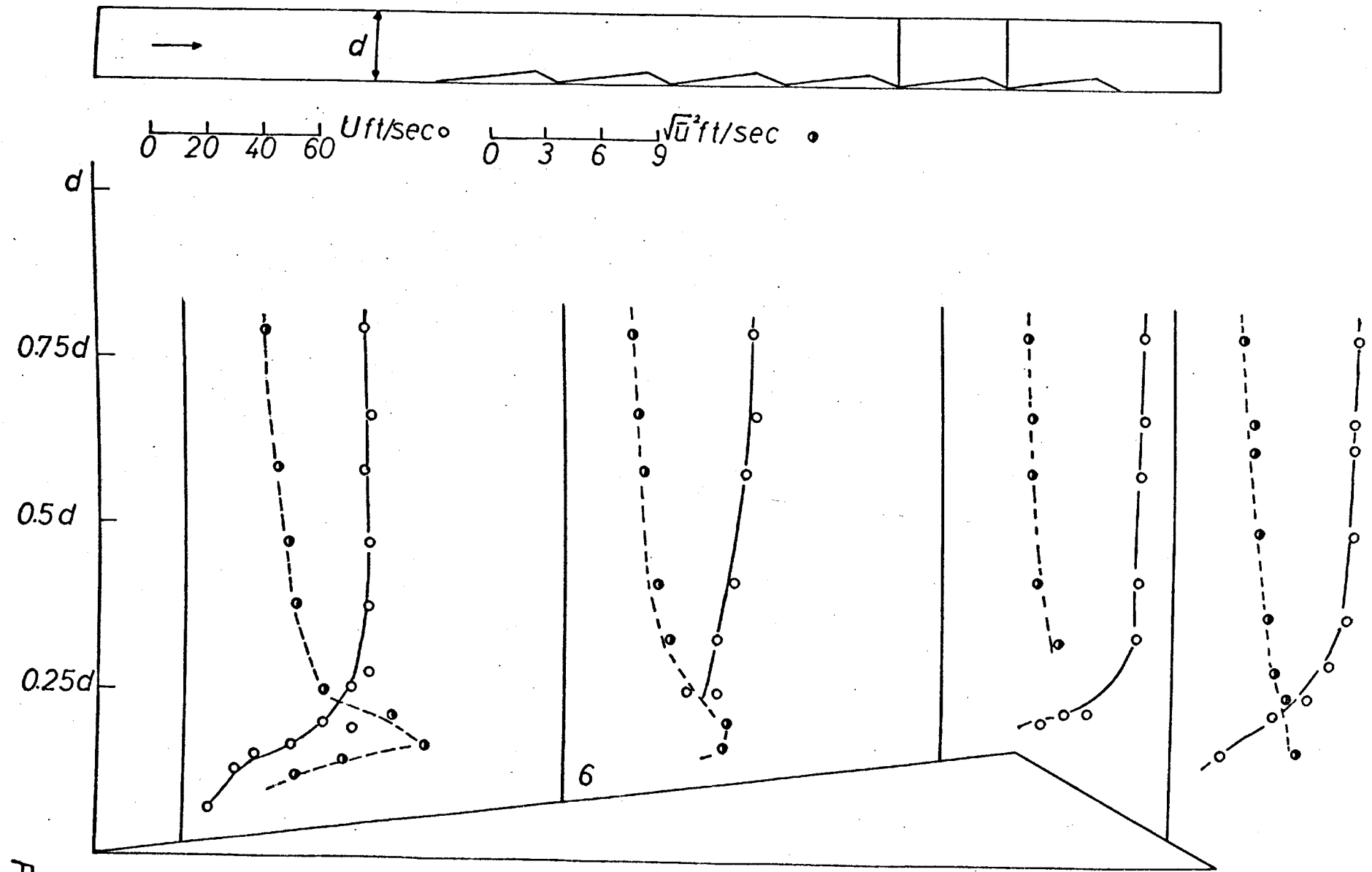

FIG 62 VELOCITY AND TURBULENCE

AUTOCORRELATION FUNCTION

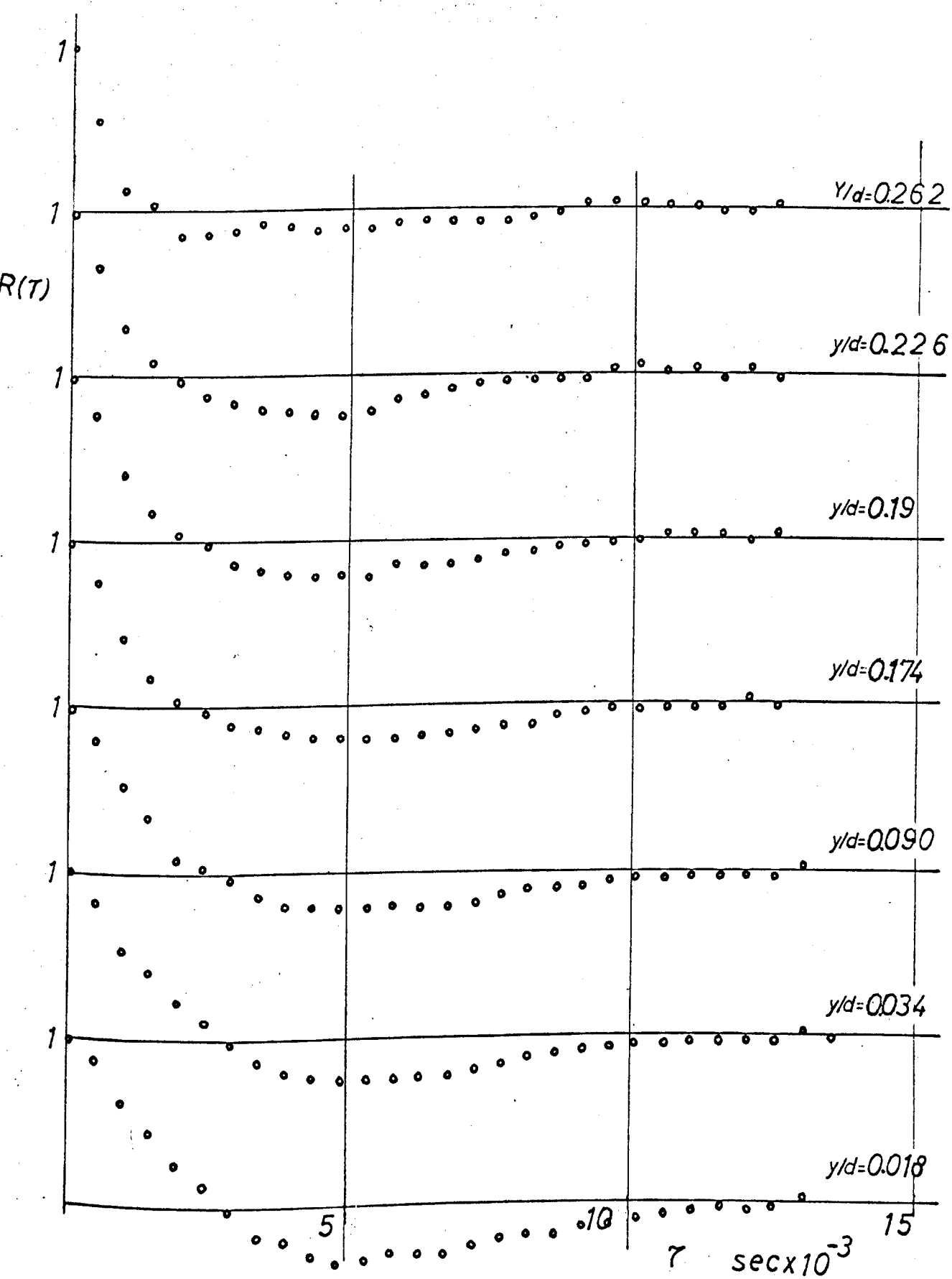

FIG 63

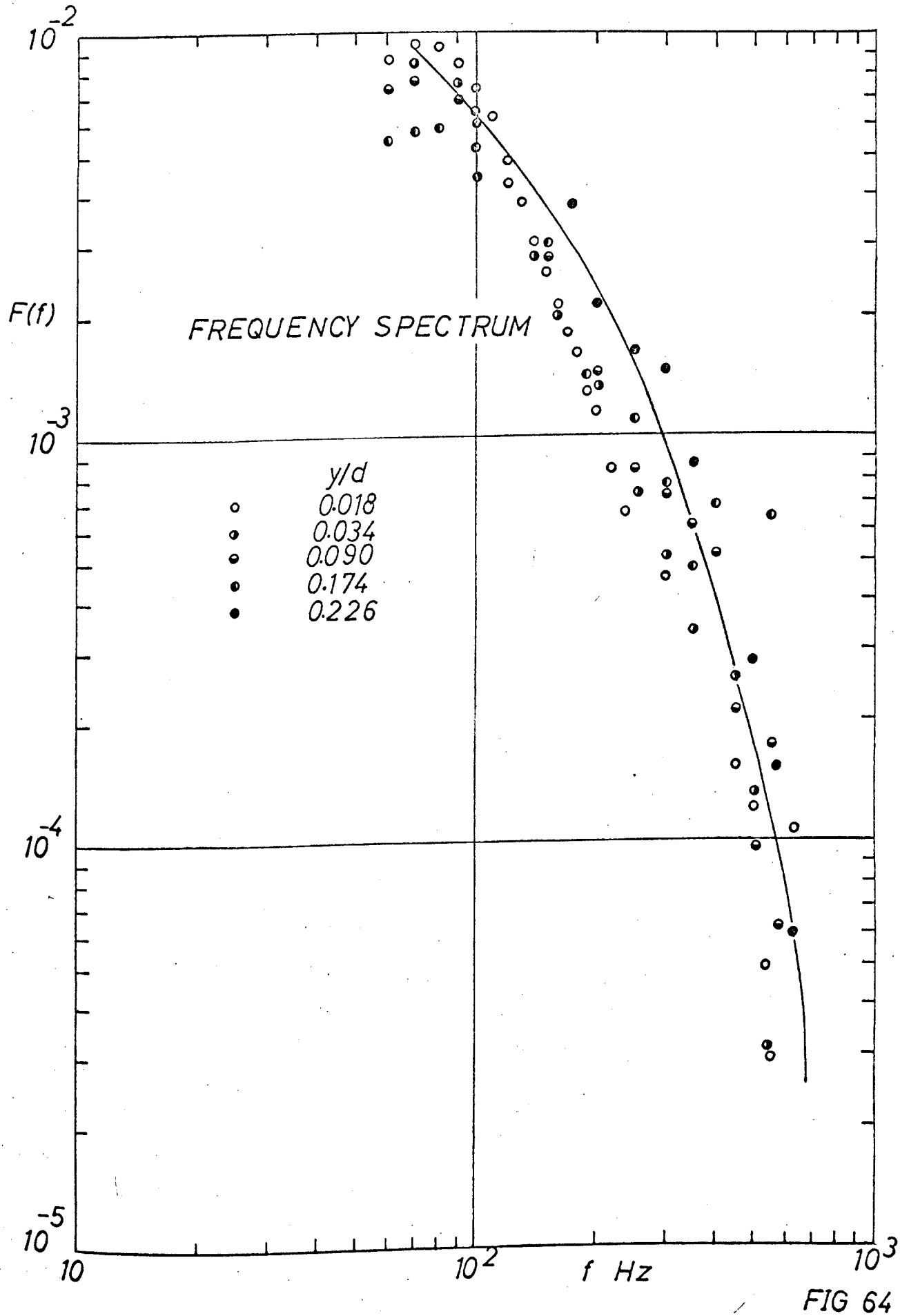
FREQUENCY SPECTRUM
F(f)
f Hz
y/d
0.018
0.034
0.090
0.174
0.226
10^-2
10^-3
10^-4
10^-5
10
10^2
10^3

FIG 64

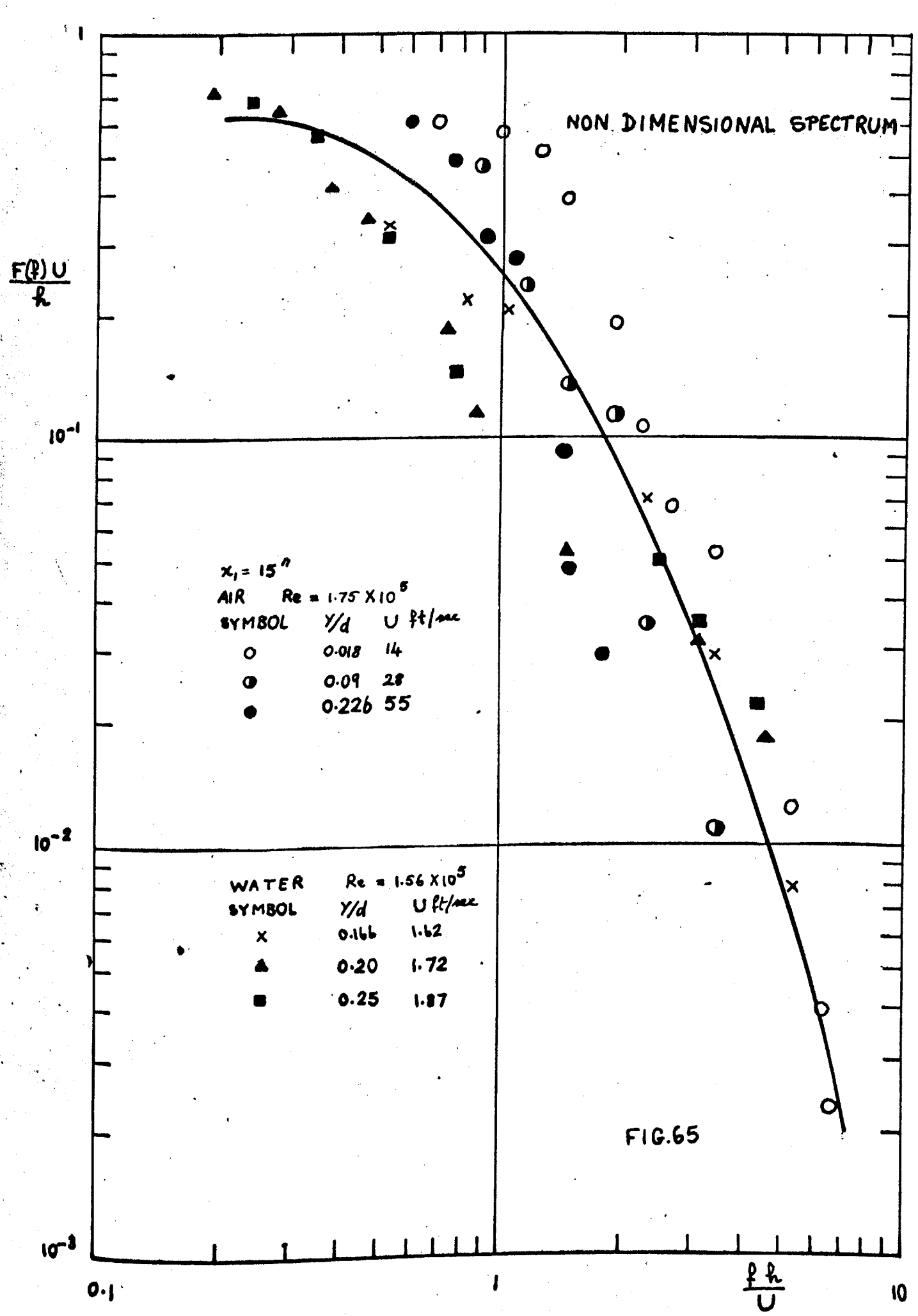
NON DIMENSIONAL SPECTRUM
F(f) U / h
1
10⁻¹
10⁻²
10⁻³
0.1
1
10
f h / U
x₁ = 15"
AIR Re = 1.75 X 10⁵
SYMBOL Y/d U ft/sec
○ 0.018 14
◑ 0.09 28
● 0.226 55
WATER Re = 1.56 X 10⁵
SYMBOL Y/d U ft/sec
× 0.166 1.62
▲ 0.20 1.72
■ 0.25 1.87

FIG.65

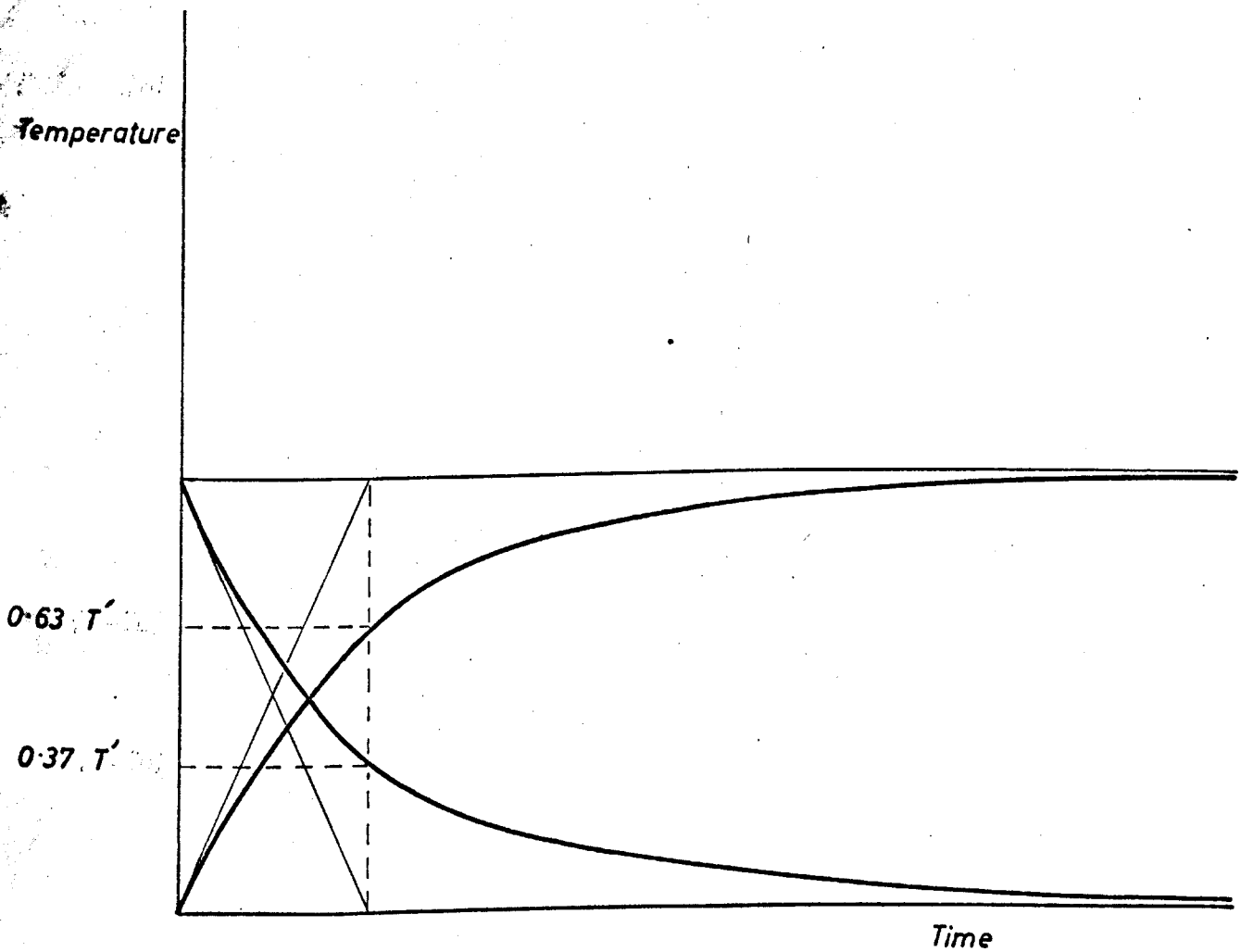

VARIATION OF DIFFERENTIAL TEMPERATURE WITH TIME

FIG 66